AD-A179 028 PRESSURE STUDIES OF PROTEIN DYNAMICS(U) ILLINOIS UNIV AT URBANA DEPT OF PHYSICS H FRAUENFELDER ET AL. 20 FEB 87 N00014-86-K-0270 1/1

UNCLASSIFIED F/G 6/1 NL

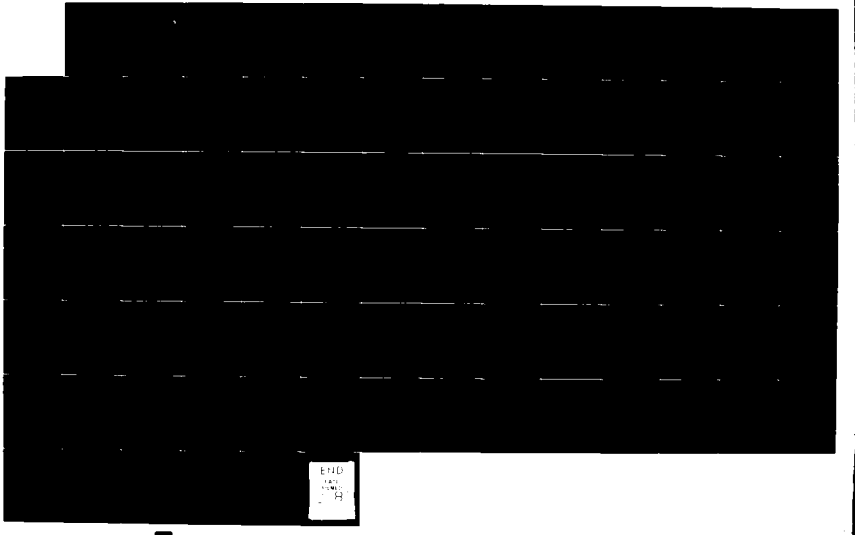

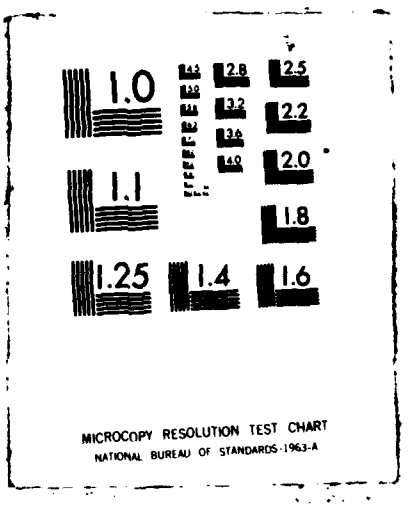
1.0
1.1
1.25
1.4
1.6
2.8
3.2
3.6
4.0
2.5
2.2
2.0
1.8
MICROCOPY RESOLUTION TEST CHART
NATIONAL BUREAU OF STANDARDS-1963-A

SECURITY CLASSIFICATION OF THIS PAGE

REPORT DOCUMENTATION PAGE

1a. [illegible]	1b. RESTRICTIVE MARKINGS: NA
2a. SECUR / 2b. DECLA — **AD-A179 028**	3. DISTRIBUTION/AVAILABILITY OF REPORT: Distribution Unlimited
4. PERFORMING ORGANIZATION REPORT NUMBER(S): NA	5. MONITORING ORGANIZATION REPORT NUMBER(S): NA
6a. NAME OF PERFORMING ORGANIZATION: University of Illinois; 6b. OFFICE SYMBOL (If applicable): NA	7a. NAME OF MONITORING ORGANIZATION: Office of Naval Research
6c. ADDRESS (City, State, and ZIP Code): Department of Physics, University of Illinois at Urbana-Champaign, 1110 W. Green St., Urbana, IL 61801	7b. ADDRESS (City, State, and ZIP Code): 800 North Quincy Street, Arlington, VA 22217-5000
8a. NAME OF FUNDING/SPONSORING ORGANIZATION: Office of Naval Research; 8b. OFFICE SYMBOL (If applicable): ONR	9. PROCUREMENT INSTRUMENT IDENTIFICATION NUMBER: N00014-86-K-0270
8c. ADDRESS (City, State, and ZIP Code): 800 North Quincy Street, Arlington, VA 22217-5000	10. SOURCE OF FUNDING NUMBERS: PROGRAM ELEMENT NO. 61153N; PROJECT NO. RR04106; TASK NO. 4413015; WORK UNIT ACCESSION NO.

11. TITLE (Include Security Classification): (U) Pressure Studies of Protein Dynamics

12. PERSONAL AUTHOR(S): Hans Frauenfelder and Robert D. Young

13a. TYPE OF REPORT	13b. TIME COVERED	14. DATE OF REPORT (Year, Month, Day)	15. PAGE COUNT
Technical	FROM 3/1/86 TO 2/28/87	2-20-87	

16. SUPPLEMENTARY NOTATION: Supplements the Annual rept.

17. COSATI CODES		
FIELD	GROUP	SUB-GROUP
08		

18. SUBJECT TERMS (Continue on reverse if necessary and identify by block number): Keywords: Protein dynamics, pressure, myoglobin, hierarchy of substates, proteinquake, flash photolysis, spectroscopic markers, ligand binding.

19. ABSTRACT (Continue on reverse if necessary and identify by block number)

In this research we extend and deepen our investigations of the relation between dynamic structure and function of proteins. We study protein dynamics by observing the phenomena induced by flash photolysis using near ultraviolet, optical, and infrared spectroscopies over wide ranges in temperature (60-300K), time (50ns-1ks), and, most importantly for this grant, pressure (0.1-200MPa). Initially we study a simple biomolecular reaction - carbon monoxide binding to myoglobin. Our previous work over wide ranges in temperature and time has been crucial to developing models of protein dynamics. Pressure effects are less well explored, an imbalance we intend to correct since studies over wide ranges of both temperature and pressure can probe protein states which are not accessible by varying only temperature or pressure. Recently we developed a hierarchical model of protein dynamics which promises to contribute to understanding both biomolecular reactions and the physics of amorphous solids and glasses. The combined pressure and temperature experiments will test various features of the hierarchical model including the glass-like properties of proteins.

20. DISTRIBUTION/AVAILABILITY OF ABSTRACT	21. ABSTRACT SECURITY CLASSIFICATION
☒ UNCLASSIFIED/UNLIMITED ☐ SAME AS RPT. ☐ DTIC USERS	(U)

22a. NAME OF RESPONSIBLE INDIVIDUAL	22b. TELEPHONE (Include Area Code)	22c. OFFICE SYMBOL
Dr. E. Schmell	(202) 696-4038	ONR

DD FORM 1473, 84 MAR — 83 APR edition may be used until exhausted. All other editions are obsolete. SECURITY CLASSIFICATION OF THIS PAGE

DTIC FILE COPY

A

DTIC ELECTE MAR 31 1987 S D

Grant # N00014-86-K-0270

PRESSURE STUDIES OF PROTEIN DYNAMICS

Hans Frauenfelder and Robert D. Young

Department of Physics, University of Illinois at Urbana-Champaign

Technical Report to Office of Naval Research

The following reprints and preprints are included in this Technical Report which supplements our Annual Report on the above named grant. The following reprints and preprints were not neccessarily supported by this grant but are related to the research under the grant. Preprints which were supported at least inpart by the present grant are indicated by an asterisk.

1. J. Hill, M. Cole, D. Dlott, J. Kauffman, J. McDonald, P. Steinbach, J. Berendzen, and H. Frauenfelder. Chemical Reaction in a Glassy Matrix. Dynamics of Ligand Binding to Protoheme in Glycerol:Water. Proceedings of the Fifth OSA Topical Meeting, Ultrafast Phenomena V, Springer Series in Chemical Physics, Ed. G. R. Fleming and A. E. Siegman (Springer, 1986).

* 2. R. D. Young. Pressure Studies of Largescale Protein Motions. Proceedings of the EBSA Workshop on Structure, Function, and Dynamics of Biomolecules, Springer Verlag, in press.

3. H. Frauenfelder and R. D. Young. Protein Dynamics and Ligand Binding. Comm. Mol. Cell Bioph. 3, 347-372 (1986).

* 4. A. Ansari, J. Berendzen, D. Braunstein, B. Cowen, H. Frauenfelder, M. K. Hong, I. E. T. Iben, J. B. Johnson, P. Ormos, T. Sauke, R. Scholl, A. Schulte, P. Steinbach, J. Vittitow, and R. D. Young. Binding and Relaxations in the Myoglobin Pocket. Biophysical Chemistry, submitted.

Chemical Reaction in a Glassy Matrix: Dynamics of Ligand Binding to Protoheme in Glycerol:Water

J.R. Hill[1], *M.J. Cote*[1], *D.D. Dlott*[1], *J.F. Kauffman*[1], *J.D. McDonald*[1], *P.J. Steinbach*[2], *J.R. Berendzen*[2], *and H. Frauenfelder*[2]

[1]School of Chemical Sciences, University of Illinois at Urbana-Champaign, Urbana, IL 61801, USA

[2]Department of Physics, University of Illinois at Urbana-Champaign, Urbana, IL 61801, USA

A fundamental understanding of condensed phase chemical reaction dynamics can be obtained from the study of biomolecules, particularly heme and hemeproteins. The complexity of these systems gives rise to a rich variety of phenomena, allowing many aspects of condensed matter reactions to be examined. The rate theories and puzzles of hemeprotein kinetics have recently been discussed by Frauenfelder and Wolynes [1]. In this work we present new experiments on ligand binding to protoheme (Fe:protoporphyrin-IX) in a glassy matrix. We have studied the rebinding of carbon monoxide after photodissociation over a wide range of time [5ps-10ms] and temperature [300K-70K]. The significance of our results is that (1) the influence of friction and nonadiabaticity on a condensed phase reaction can be directly investigated, (2) the influence of an inhomogeneous glassy matrix (glycerol-water 75:25) on the reaction can be studied, and (3) meaningful comparison between protoheme and hemeprotein kinetics isolates the role of the protein relaxation in the reaction.

Temperature-dependent ligand rebinding to protoheme was studied with μs resolution by Alberding et al. [2]. We extended the results to the ps timescale using conventional pump-probe methods with 565 nm dye laser pulses (10μJ, 3ps, FWHM, 80Hz). Figure 1 shows a log-log plot of the time-resolved absorbance change (proportional to N(t), the fraction of protoheme molecules that have not rebound CO at time t) at 300K and 260K. The slow process (Process S) involves binding of CO that have escaped their initial solvent cage by diffusion. This solvent process is exponential in time with a pseudo-first-order rate coefficient that depends on [CO]. As T is decreased, the fraction of CO molecules that escape the cage decreases until it is below 0.01 at 240K [2], well above the glass transition T_c = 173K. Subtraction of the 260K Process S data (solid circles from [2]) yields a nonexponential decay (Process I), the solid rectangles in Fig. 1. The relative fraction of ligands that rebind via Process I increases as T decreases from 300K to 240K. Process I is nonexponential at all temperatures up to 300K.

As T is decreased below 240K, process S vanishes, the rate of process I decreases in a manner consistent with [2], and a new process, I*, is observed. The amplitude of I* increases with further decrease in T until it dominates I. Figure 2 shows the rebinding data at 140K (open rectangles), the temperature at which processes I and I* have equal amplitudes. Subtraction of process I, which is known to have the form of a power-law decay, reveals that process I* (open circles) decays exponentially with a 15 ps lifetime. As T is decreased from 220 to 70K, the rate of process I* decreases linearly with T.

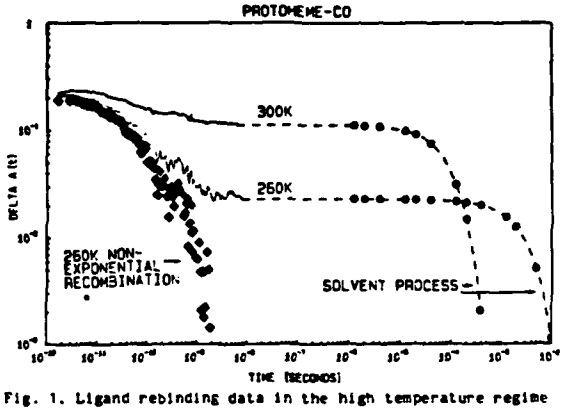

Fig. 1. Ligand rebinding data in the high temperature regime

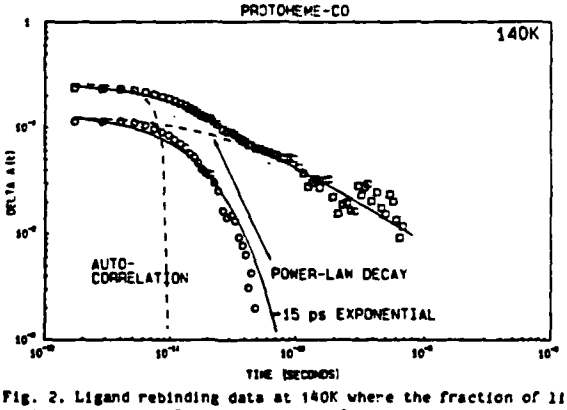

Fig. 2. Ligand rebinding data at 140K where the fraction of ligands that rebind via process I is equal to the fraction that rebind via process I^{e}.

Figure 3 summarizes the temperature dependence of ligand rebinding via these three processes. At the lowest temperatures studied, process I^{e} dominates. As the temperature increases, the fraction of ligands rebinding via process I increases until 240K. At that point the solvent process increases in importance.

In [2], process I was interpreted to arise from recombination of ligands trapped within the solvent cage. The barrier for this process is a property of the heme, and probably arises as a consequence of the transition from the unbound S=2 domed heme structure to the bound S=0 planar structure. The

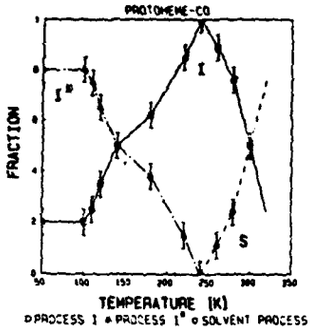

Fig. 3. Relative fraction of ligand rebinding to protoheme via the *three processes*

rebinding is nonexponential because this barrier possesses distributed activation enthalpy. In the β-chain of hemoglobin, process I becomes nearly exponential above ca. 250K, because the protein structure relaxes significantly on the timescale (1 ns) of the rebinding [1]. In protoheme, this conformational relaxation does not occur on the faster timescale (50 ps) of the rebinding.

The observed (linear) temperature dependence and the large rate of process I* at low temperatures suggest that it does not occur by classical over-the-barrier motion. The exponential time dependence shows that the height of the barrier is not distributed. Process I* may involve recombination to an S=1 heme which has not domed. At 140K, the rebinding rate of $7E10/s$ is a factor of ~40 slower than kT/h, the frequency of collision between the ligand and the heme. The reduction of the recombination rate can be caused by entropy, friction, and nonadiabatic barrier crossing [1].

This research was supported in part by the National Science Foundation, Solid State Chemistry, grant DMR 84-15070 (DDD), the U. S. Department of Health and Human Services under Grant GM 18051, and the National Science Foundation under Grant DMB 82-09616 (HF), and the National Science Foundation, grant CHE 83-14105 (JDM).

References

1. Frauenfelder, H., Wolynes, P. G., Science, 229, 337 (1985).
2. Alberding, N., Austin, R. H., Chan, S. S., Eisenstein, L., Frauenfelder, H., Gunsalus, I. C., Nordlund, T. M., J. Chem. Phys. 65, 4701 (1976).
3. Ansari, A., DiIorio, E. E., Dlott, D. D., Frauenfelder, H., Iben, I.E.T., Langer, P., Roder, H., Sauke, T. B., Shyamsunder, E., Biochemistry (in press).

PRESSURE STUDIES OF LARGE-SCALE PROTEIN MOTIONS

Robert D. Young
Departments of Physics
University of Illinois at Urbana-Champaign
1110 West Green Street
Urbana, IL 61801
and
Illinois State University
Normal, IL 61761
USA

INTRODUCTION

Protein motions are studied using the binding of carbon monoxide (CO) to myoglobin (Mb) as probe. A number of experimental tools have been used to study this simple protein reaction (1,2), but the most detailed information has come from flash photolysis experiments over wide ranges in time, temperature, viscosity, and pressure (3,4).

Here I describe the results of flash photolysis experiments using "pressure titration" to probe large-scale protein motions (5,6). In a pressure titration experiment, an ensemble of proteins is prepared in different nonequilibrium states by using different paths in the pressure-temperature plane to reach a given pressure and (low) temperature. In the case of CO binding to Mb the relaxation of the recombination kinetics between two nonequilibrium states of the protein ensemble at the same temperature and pressure probes large-scale protein motions. These motions have been previously denoted as EF1 (equilibrium fluctuations) and FIM1 (functionally important motions) (5,7). The pressure titration experiments imply that the EF1 must be described by a distribution of activation energies ranging between 70 to 85 kJ/mol.

HIERARCHICAL PROTEIN MODEL

The principal features of the hierarchical model of proteins are (7): (i) A globular protein exists in a large number of conformational substates (CS) separated by barriers, some of which become effectively infinitely high below about 160 K (CS1). (ii) Transitions among the substates are equilibrium fluctuations (EF); nonequilibrium transitions from one protein state, say MbCO, to another state, say deoxyMb, involve functionally important motions (FIMs). (iii) Substates and equilibrium fluctuations possess hierarchies. In Mb four different tiers of substates and motions are observed. (iv) The different tiers of substates are described by distributions of relaxation rates.

The pressure titration experiments probe equilibrium fluctuations (EF1) in tier 1 of the hierarchy of conformational substates (CS1). The EF1 most likely involve large-scale motions in the protein and possibly include the hydration layer and part of the solvent. FIM1 may be the motion that permits ligands to enter and leave the protein.

PRESSURE TITRATION EXPERIMENTS

Below about 180 K, Mb rebinds CO after photodissociation, but the kinetics follow a power law in time. This means that the protein cannot be in a unique state but must exist in a large number of conformational substates (CS1) with different barriers for recombination from the heme pocket. The fraction N(t) of proteins which have not rebound a ligand at time t after photodissociation is given by

$$N(t) = \int g(H) \exp(-k(H)t)dH \qquad (1)$$

where g(H)dH is the probability of a protein having a barrier with activation enthalpy between H and H + dH and k(H) is the rate coefficient. If rebinding is thermally activated then $k(H) = A\exp(-H/RT)$. The distribution g(H) and pre-exponential A are found from the experimentally measured N(t). Alternatively I use the model of Young and Bowne for the distribution g(H) which yields excellent fits to the low temperature kinetics (4,8).

Under pressure the binding of CO to Mb speeds up (6,9). The effect is particularly dramatic and relatively simple to interpret at low temperatures. The ensemble of proteins is prepared in different nonequilibrium states as follows: High pressure (2 kbar) is applied to the sample at high temperature (300 K) and the sample is then cooled to say 100 K before the pressure is released to 1 bar (state β'). The sample can also be cooled to low temperature (100 K) at atmospheric pressure (state β). Since CO binding is much faster at state β' than at state β, the two states are not in equilibrium and can be distinguished by measuring N(t). The g(H) for state β' has a similar shape as g(H) for state β but is simply shifted to smaller activation enthalpies.

The difference in the distributions g(H) is explained simply in terms of the conformational substates of tier 1. At β the ensemble of proteins is in a distribution of CS1 characteristic of 1 bar while at β' the distribution of CS1 is characteristic of 2 kbar. Transitions between states β' and β correspond to EF1. The EF1 are induced as follows: Starting in state β' at say 100 K and 1 bar, the recombination kinetics N(t) are measured. The temperature is then

increased to T_m, left there for 600s (the annealing time, t_a), cooled again to 100 K and N(t) measured. This procedure is repeated with increasing T_m until N(t) has relaxed to follow the curve corresponding to state β. The result is definitive: Up to T_m = 160 K, N(t) for β' is unrelaxed but at T_m = 200 K N(t) has completely relaxed to the kinetics corresponding to β.

Since the distributions g(H) for β and β' have the same shape, the states β and β' are characterized by the minimum activation enthalpy H_{min} of the distributions (8). The extent of relaxation is characterized by the fractional shift $\Delta(t_a,T_m)$ of $H_{min}(t_a,T_m)$ from $H_{min}(\beta)$: $\Delta(t_a,T_m) = [H_{min}(t_a,T_m)-H_{min}(\beta)]/[H_{min}(\beta')-H_{min}(\beta)]$. Assuming that the relaxation β' → β is described by a distribution of activation energies, $\Delta(t_a,T_m)$ is given by

$$\Delta(t_a,T_m) = \int \rho(E_1)\, \exp(-k_1 t_a)\, dE_1 \qquad (2)$$

where $\rho(E_1)dE_1$ is the probability of finding a barrier between E_1 and $E_1 + dE_1$. I fit the data with $k_1 = A_1 \exp(-E_1/RT)$ and a box distribution,

$$\rho(E_1) = \begin{cases} (E_{max}-E_{min})^{-1}, & E_{min} < E_1 < E_{max} \\ 0, & \text{otherwise} \end{cases} . \qquad (3)$$

A good fit to the relaxation of N(t) parameterized by H_{min} is obtained for $A_1 = 10^{19.3}\ s^{-1}$, E_{min} = 70 kJ/mol, and E_{max} = 85 kJ/mol.

DISCUSSION

The pressure titration experiments on CO rebinding to Mb after photodissociation show that at 1 bar the EF1 set in at 160 K and extend over a range of about 40 K. The resulting distribution of relaxation rates is reminiscent of glassy relaxation processes (10,11,12). It is possible that the hydration layer and solvent strongly influence the motions of tier 1. Additional evidence for EF1 has also come from Raleigh scattering of Mössbauer radiation (13) and microwave absorption in the hydration shell (14). However we are only at the beginning of the study of EF1 and FIM1. Clearly more theory is needed and more experiments are required to explore the properties of EF1 and FIM1, to study the role of the hydration layer and solvent (15), and to determine the connection between EF1 and unfolding.

ACKNOWLEDGEMENTS

This work was supported in part by Grant PCM82-09616 from the U.S. National Science Foundation and Grant PHS GM 18051 from the U.S. Department of Health and Human Services. I thank E. Shyamsunder, who performed the experiments, for many informative discussions.

REFERENCES

1. Antonini, E. and Brunori, M. (1971) in Hemoglobin and Myoglobin in the Reactions with Ligands, North-Holland, Amsterdam.
2. Lever, A. and Gray, H. (1983) in Iron Porphyrins, Parts I and II, Addison-Wesley, Reading.
3. Austin, R. H., Beeson, K. W., Eisenstein, L., Frauenfelder, H. and Gunsalus, I.C. (1975) Biochem. 14, 5355.
4. Ansari, A., Di Iorio, E., Dlott, D., Frauenfelder, H., Iben, I., Langer, P., Roder, H., Sauke, T. and Shyamsunder, E. (1986) Biochemistry, in press.
5. Frauenfelder, H. (1985) in Structure and Motion: Membranes, Nucleic Acids, and Proteins (Clementi, E., Corongui, G., Sarma, M. and Sarma, R., eds.), p. 205, Adenine, Press, New York.
6. Shyamsunder, E. (1986) Ph.D. Dissertation, University of Illinois at Urbana-Champaign.
7. Ansari, A., Berendzen, J., Bowne, S., Frauenfelder, H., Iben, I., Sauke, T., Shyamsunder, E. and Young, R. (1985) Proc. Natl. Acad. Sci. USA 82, 5000.
8. Young, R. and Bowne, S. (1984) J. Chem. Phys. 81, 3730.
9. Sorensen, L. (1980) Ph.D. Dissertation, University of Illinois at Urbana-Champaign.
10. Goldanskii, V., Krupyanskii, Yu. and Fleurov, V. (1983) Doklady Akad. Nauk SSSR 272, 978.
11. Singh, G., Schink, H., Lohneysen, H. v., Parak, F. and Hunklinger, S. (1984) Z. Phys. B55, 23.
12. Stein, D. (1985) Proc. Natl. Acad. Sci. USA 82, 3670.
13. Krupyanskii, Yu., Parak, F., Engelman, D., Mössbauer, R., Goldanskii, V. and Suscheliev, I. (1982) Z. Naturforsc. C. 37, 57.
14. Singh, G., Parak, F., Hunklinger, S. and Dransfield, K. (1981) Phys. Rev. Lett. 47, 685.
15. Doster, W., Bachleitner, A., Dunau, R., Hiebl, M. and Lüscher, E. (1986) Technische Universität München preprint.

Protein Dynamics and Ligand Binding

1. STATES, MOTIONS, AND FUNCTIONS

Proteins are dynamic systems that wriggle and breathe. During the past few years it has become clear that their motion is essential to their function.[1-9] In this Comment we describe some features of protein motions, concentrating on concepts and ideas. One main point must be emphasized. To investigate the importance of protein motions for protein function, we must look at a protein in action.

Before discussing a simple biological process, the binding of oxygen (O_2) or carbon monoxide (CO) to myoglobin (Mb),[10,11] we introduce some concepts that will be important in later sections.

States and Substates. Two equilibrium states are involved in the binding of CO to Mb, deoxy-Mb and MbCO. Each of these states can exist in a large number of *conformational substates*, denoted by *CS*.[12] The CS have the same overall structure, but differ in detail; they perform the same function, but possibly with different rates.

Equilibrium Fluctuations and FIMs. Thermodynamics predicts that a small system such as a protein does not have sharp values of internal energy, entropy, and volume; these quantities fluctuate

Comments Mol. Cell. Biophys.
1986, Vol. 3, No. 5, pp. 347–372
0143-8123/86/0305-0347/$25.00/0

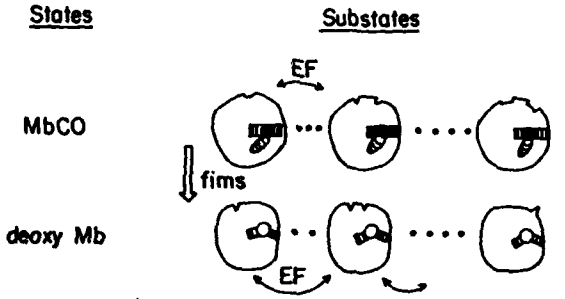

FIGURE 1 Schematic representation of states, substates, equilibrium fluctuations (EF), and functionally important motions (FIMs) in Mb.

about their mean values.[13] A resting protein at physiological temperature does not remain in one CS, but fluctuates from one CS to another. We denote these *equilibrium fluctuations* by *EF*. Figure 1 shows two different states (MbCO and deoxy-Mb) with corresponding CS. The equilibrium fluctuations are transitions among the various CS of a given state. The protein action—the transition from MbCO to deoxy-Mb, or the inverse transition—is performed through *functionally important motions*, *FIMs*. In order to fully understand the working of a particular protein, we must not only study and understand EF, but also FIMs. It may appear that EF and FIMs are unrelated and that the studies of EF in proteins would not be useful for understanding the functional aspects of protein reactions. There exists, however, a powerful connection that can facilitate the task of understanding protein reactions.

2. THE CONNECTION BETWEEN FLUCTUATIONS AND DISSIPATION

The fluctuation of a protein at rest about its mean structure is an equilibrium phenomenon and the magnitude, but not the time dependence, of the fluctuations is given by equilibrium thermodynamics.[14] Protein reactions, in contrast, are often dissipative and lead to a state of lower energy; they are not governed by equilibrium thermodynamics. Fortunately, the *fluctuation–dissipation theorem* provides a connection between the rates of EF and FIMs. Einstein[15] provided the first connection between an equilibrium and nonequilibrium property in his theory of Brownian motion where he wrote down the relation between the diffusion coefficient D and the friction coefficient f as $D = k_B T/f$. Here T is the temperature in Kelvin and k_B the Boltzmann constant. Another connection between an equilibrium fluctuation, the voltage fluctuation across a resistor (Johnson noise), and a transport coefficient, the resistance, was derived by Nyquist.[16] A general relation between equilibrium fluctuations and dissipative processes was formulated by Callen and Welton[17] and generalized by Kubo and others.[18–21]

A simple example of a fluctuation–dissipation theorem concerns a molecule that exists in either one of two states of equal energy.[22] The two states are represented by the two potential wells labelled L and R in Fig. 2. An ensemble of N molecules will occupy both wells equally at equilibrium, with $\langle L \rangle = \langle R \rangle = N/2$. The instantaneous values, $L(t)$ and $R(t)$, undergo equilibrium fluctuations about the mean value with rate $2k$ as shown in Fig. 2(a). If all molecules initially are in one well, say L, then the ensemble is in a nonequilibrium state and will approach the equilibrium state exponentially with a rate $2k$ as shown in Fig. 2(b). This example demonstrates that the rate of equilibrium fluctuations is the same as the rate for exponential decay from a state far from equilibrium to the equilibrium state.

A word of caution is in order here. Close to equilibrium, the fluctuation–dissipation theorem has been proven in considerable generality.[17–21] Far from equilibrium, the connection is no longer so easy and calculations are based on specific models.[23] From the experimental point of view, EF and FIMs can only be related if the two types of motions explore the same, or at least similar, substates.

3. MODELS OF LIGAND BINDING

The binding and the dissociation of a small ligand to a monomeric heme protein, for instance Mb,

$$\mathrm{Mb} + \mathrm{CO} \rightleftarrows \mathrm{MbCO} \qquad (1)$$

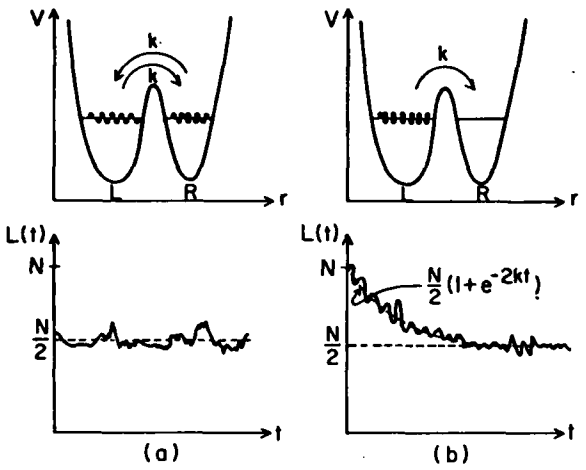

FIGURE 2 Fluctuation–dissipation theorem. Left: equilibrium fluctuations. The characteristic rate of EF can be obtained from the autocorrelation function of $L(t)$. Right: approach to equilibrium from a state far from equilibrium. The characteristic rate of EF can be obtained from the exponential time dependence of $L(t)$.

appears to be a simple one-step process.[9] Experimental and theoretical studies of the binding process have, however, resulted in a picture of increasing complexity. As in any other many-body system, such as a nucleus, a glass, or a plasma, it is not possible to start the theoretical description with a model that incorporates all features of reality. Success in understanding comes through a series of models, each describing some aspects particularly well and neglecting others. We present here some of the models for ligand binding.

We sketch in Fig. 3 the actual situation, namely the path of a CO molecule from the solvent S to the binding site A at the heme iron. The CO molecule executes a Brownian motion in the solvent, moves into the protein matrix M, migrates through the matrix into the heme pocket B and finally binds covalently to the heme iron.

In the *one-particle model*,[12] we assume that the protein forms

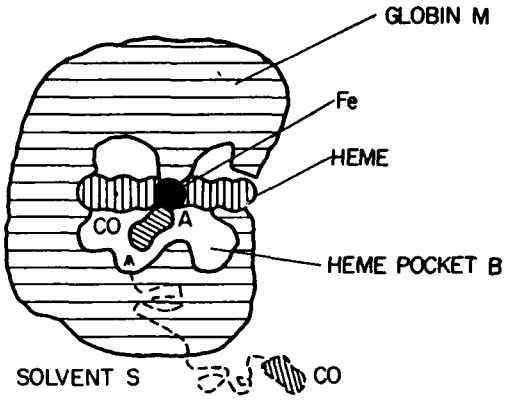

FIGURE 3 Schematic cross section through the active center of Mb with the CO bound to the heme iron. The heme pocket B, globin matrix M, and solvent S are also shown.

an effective potential in which the small ligand moves. The experiments to be discussed in the following sections demonstrate that the potential seen by the CO is as in Fig. 4. The general features of the "single-particle potential" are the same in all heme proteins that we have studied, but the details can differ. The details are, of course, important for the biological function and their understanding in terms of the protein composition and structure is one major goal of the work on heme proteins. While the features of Fig. 4 are easy to comprehend, the calculation of the motion of the ligand in such a potential is not trivial. The ligand will perform a complicated random walk; it may visit a particular site, for instance the heme pocket (well B), many times before finally binding.

The single-particle model in Fig. 4 is necessary for an understanding of ligand binding, but it is *static* and does not take the motions of the protein into account. In a second model we use ligand binding as a perturbation that induces protein motions and look at these motions alone. The perturbation caused by ligation or deligation leads to a chain of events with many similarities to

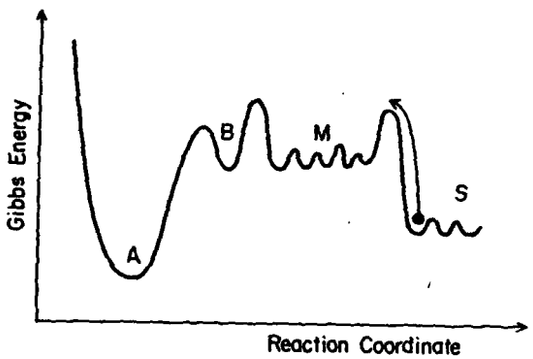

FIGURE 4 "Single-particle" potential for ligand binding. The bullet represents the ligand moving through the potential caused by the protein. The letters A, B, M, and S represent the wells A, B, M, and S, respectively, of the text.

an earthquake: A stress is relieved at the focus. The released strain energy is dissipated in the form of waves and through the propagation of deformations. Fortunately, in an earthquake the ratio of the released energy to the total gravitational binding energy of the earth is very small. The situation in Mb is shown in Fig. 5. Upon

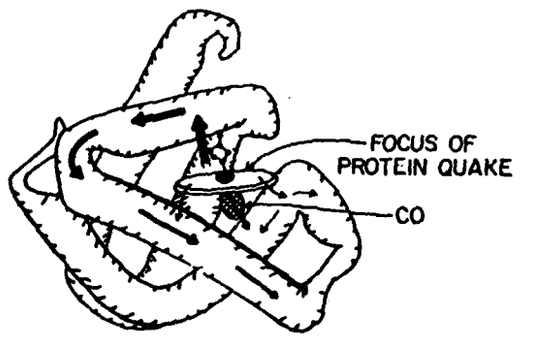

FIGURE 5 Proteinquake. Binding or dissociation of a ligand at the heme iron causes a "proteinquake."

binding of a ligand, the protein is stressed; upon photodissociation, the stress is relieved. In either case, the protein finds itself in a state far from equilibrium.[24] Return to equilibrium occurs through a *proteinquake*[25]: The released strain energy is dissipated through waves and through the propagation of a deformation. The propagation can be studied through suitable markers, and we thus obtain information on the dynamic motions that accompany ligand binding. We expect many protein reactions to exhibit features similar to a proteinquake.

The two models we have sketched are extremes. In the single-particle model, the protein produces the static potential in which the ligand moves. In the quake model, the ligand excites protein motions but then no longer interacts with the protein. In a unified model, the motions of the protein and the ligand would be considered together. At present, not enough is known about the dynamics of the protein and the interaction of the ligand with the protein to formulate such a model.

4. FLASH PHOTOLYSIS STUDIES OF LIGAND BINDING

The main features of the "single-particle" potential shown in Fig. 4 are deduced from flash photolysis experiments performed over very wide ranges in time (from ps to ks), temperature (from 2 to 300 K), and pressure (from 0.1 to 200 MPa).[12,25,26] In flash photolysis, the sample of liganded protein (MbCO, for instance) in a solvent saturated with the ligand is placed in a cryostat and brought to the appropriate pressure and temperature. The protein–ligand sample is photolyzed by a laser pulse. The rebinding, Mb + CO → MbCO, is followed optically by monitoring the Soret line at about 436 nm. Since the extinction coefficients of the liganded and photodissociated protein differ significantly in the Soret region, the absorbance change yields the fraction $N(t)$ of proteins that have not rebound a ligand at time t after the flash. Figure 6 displays the prominent features of $N(t)$ for the rebinding of CO to a separated beta chain (β^A) of normal adult hemoglobin.

$N(t)$ exhibits three processes denoted by I, M, and S in Fig. 6. These processes can be understood by reference to Figs. 3 and 4. A ligand coming from the solvent (well S), migrates through the globin matrix (well M) to the heme pocket (well B). From well B,

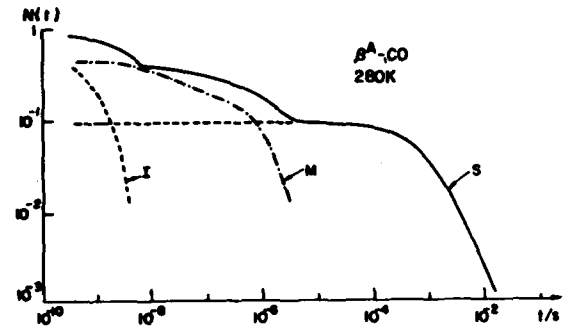

FIGURE 6 Rebinding of CO to the separated beta chain of human hemoglobin at 280 K. The solid line represents the experimental data. I is the internal rebinding from the pocket, M the rebinding from the matrix, and S the binding from the solvent.

the ligand either moves back into the globin or binds covalently to the heme iron (Fe). The covalently bound ligand is in well A. If the bond between the Fe and ligand is broken by a light flash, the ligand moves to well B. Rebinding from B depends on temperature. Below about 180 K, the ligand remains in the heme pocket and rebinds directly to the Fe (process I). Above about 180 K, some ligands move into the globin matrix before returning and binding (process M). At about 300 K, nearly all ligands pass through the globin matrix into the solvent. Any ligand in the solvent can then enter the globin matrix and ultimately bind to the Fe (process S).

5. LOW TEMPERATURE BINDING AND CONFORMATIONAL SUBSTATES

Below about 200 K, only process I is seen in the binding of CO to Mb (Fig. 7). We interpret process I by assuming that the photodissociated ligand remains in the heme pocket (well B) and rebinds from there. Figure 7 shows that process I is not exponential in time, but can be approximated by a power law

$$N(t) = (1 + t/t_0)^{-n}, \tag{2}$$

where t_0 and n are temperature-dependent parameters.[12]

Similar kinetics are observed in a variety of monomeric heme proteins including myoglobin,[12] separated α and β chains of normal adult hemoglobin,[27] β chains of mutant hemoglobin Zurich,[28,29] protoheme,[30] and soybean leghemoglobin.[31]

The interpretation of the power-law kinetics requires consideration of the immediate surroundings of the heme group.[11] Figure 3 gives a schematic view of a cross section through the active center of Mb or a separated chain of hemoglobin. Before photolysis, CO is covalently bound to the Fe, the heme group is nearly planar, and the Fe is displaced 0.02 nm from the mean heme plane towards the proximal histidine (HIS F8). The Fe has electronic spin equal to zero. After photodissociation, the ligand is in the heme pocket, the heme group is domed, and the Fe is displaced by 0.05 nm from the mean heme plane toward HIS F8. The Fe has electronic spin 2.[32] If the B → A transition is represented by a potential barrier with an activation enthalpy H_{BA}, the rate coefficient k_{BA} above about 40 K is given by an Arrhenius relation

$$k_{BA} = A_{BA} \exp(-H_{BA}/RT). \tag{3}$$

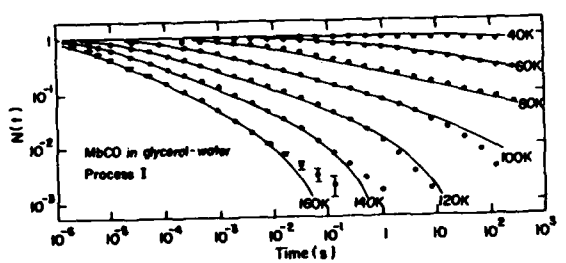

FIGURE 7 Time dependence of the binding of CO to Mb between 40 and 160 K. $N(t)$ is the fraction of Mb molecules that have not rebound a CO molecule at the time t after photodissociation.

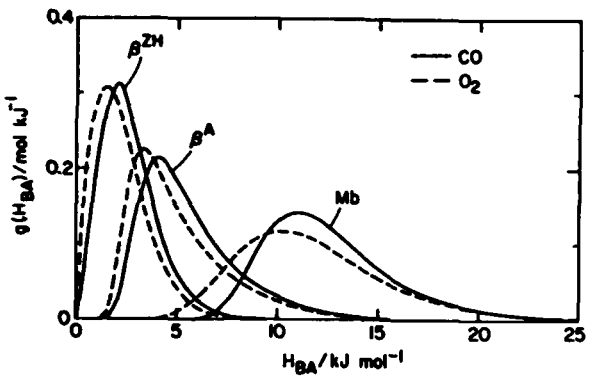

FIGURE 8 Activation enthalpy distributions for various monomeric heme proteins with O_2 and CO: Myoglobin (Mb), separated beta chain of normal adult hemoglobin (β^A), separated beta chain of mutant hemoglobin Zurich (β^{Zh}).

Below 40 K molecular tunneling can occur and modify Eq. (3).[33] If the barrier height H_{BA} is unique, then $N(t)$ is an exponential, $N(t) = \exp(-k_{BA}t)$, which is not observed.

The simplest explanation of the nonexponential time dependence postulates that at low temperatures different Mb molecules possess different activation barriers. If $g(H_{BA})dH_{BA}$ denotes the probability of finding a protein with activation enthalpy between H_{BA} and $H_{BA} + dH_{BA}$, the experimentally monitored fraction $N(t)$ becomes

$$N(t) = \int dH_{BA} g(H_{BA}) \exp(-k_{BA}t). \qquad (4)$$

Numerical inversion of Eq. (4) yields $g(H_{BA})$; if the inversion is performed at different temperatures, the pre-exponential A_{BA} in Eq. (3) can also be determined. The distributions $g(H_{BA})$ for various protein–ligand combinations are given in Fig. 8.

So far we have assumed without justification that different Mb molecules have different activation barriers at low temperatures. The construction of proteins leads to a plausible reason for this

inhomogeneity. A protein is created as a linear chain of amino acids which folds into the proper three-dimensional structure. Since the number of possible final states is very large, it is unlikely that a particular molecule can fold into the state of lowest Gibbs energy within the available time of the order of seconds or less. In fact, the idea of one lowest energy state is not meaningful—the protein will fold into one of a very large number of states that are close but not identical in structure. We call these conformational substates CS, a concept that we have already introduced in Section 1. At temperatures near 300 K, a protein will fluctuate among the CS. At temperatures below about 200 K, however, each protein will be frozen into a particular CS with corresponding barrier height H_{BA} and rebinding will be nonexponential in time.

The activation enthalpy distribution $g(H_{BA})$ as seen in Fig. 8 can arise in two distinct ways: (i) All proteins are identical and each can exhibit the full spectrum of activation enthalpies. This situation can occur if each protein possesses a number of sites in the heme pocket with different barrier heights for the B → A transition. The ensemble of proteins is then homogeneous, resulting in homogeneous broadening of the activation enthalpy spectrum. (ii) Below the freezing temperature, each protein exists in a different CS with a different barrier height for the B → A transition. The ensemble of proteins is then inhomogeneous, resulting in inhomogeneous broadening of the activation enthalpy spectrum. Fortunately, we can distinguish between the two cases by a multiple-flash experiment in which successive laser flashes are triggered before all protein molecules have rebound a ligand.[12,34–36] The results of the multiple-flash experiment are unambiguous: the data rule out identical proteins and support the concept of CS and inhomogeneous broadening of the activation enthalpy spectrum. In anticipation of the hierarchical model of protein states, we use the notation CS^1 for these conformational substates.

Our group has also studied the binding of CO to Mb at pressures from 0.1 to 210 MPa and temperatures from 60 to 160 K.[26,37] The pressure studies reveal additional properties of the CS^1. As pressure increases, the rate coefficient k_{BA} for the B → A transition increases for MbCO at low temperature. For example, the time at which $N(t) = 0.1$ can shift by a factor 50 in going from 0.1 MPa to 210 MPa at 100 K. The shift, however, depends on the path by

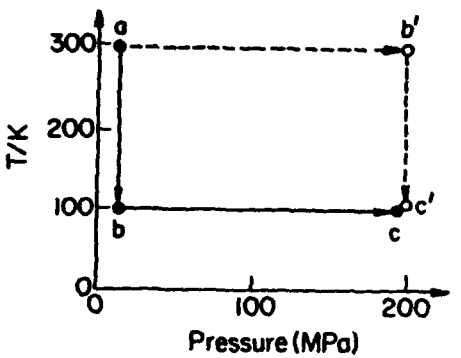

FIGURE 9 Pressure effect on the binding of CO to Mb. The MbCO system can be brought to a low-temperature, high-pressure state along the two pathways shown.

which the final state is reached (Figure 9). The sample is first cooled to, say, 100 K and then pressurized to 210 MPa (2 kbar). Alternatively, the sample is first pressurized and then cooled. The speed-up of the kinetics is significantly smaller in the first case ($a \rightarrow b \rightarrow c$) than in the second ($a \rightarrow b' \rightarrow c'$). At state c, the ensemble of proteins is in a distribution of CS^1 characteristic of 0.1 MPa, while at state c' the distribution of CS^1 is characteristic of 210 MPa. CO binding to Mb at 100 K is about 10 times faster in state c' than in state c. Such experiments can provide valuable information concerning the various reaction volumes involved in ligand binding and the change in distribution of CS^1 with pressure.

Studies of the transitions between states c and c' keeping pressure constant and changing temperature have been performed ("pressure titration").[26] The sample is first brought to c along the path $a \rightarrow b \rightarrow c$ and the fraction $N(t)$ is measured at 100 K and 190 MPa. Keeping pressure constant at 190 MPa, the temperature is increased to a value T', kept there for 60 s, cooled again to 100 K, and the fraction $N(t)$ is remeasured. This procedure is repeated until $N(t)$ follows the curve corresponding to state c'. The results displayed in Fig. 10 are dramatic: Up to $T' = 200$ K $N(t)$ is characteristic of state c, but at $T' = 220$ K $N(t)$ is characteristic of the

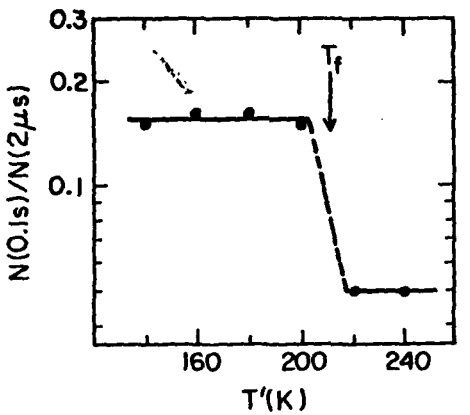

FIGURE 10 Pressure "titration" showing the onset of FIM 1 between 200 K and 220 K in MbCO.

curve for state c'. The transition $c \rightarrow c'$ consequently occurs between 200 and 220 K so the temperature T_f at which the ensemble of proteins is frozen into a particular distribution of CS^1 is between 200 and 220 K at 190 MPa.

The spatial distribution of CS for Mb has been obtained using x-ray diffraction data.[38-40] The Debye–Waller factor yields the mean-square displacement $\langle x^2 \rangle_x$ of every nonhydrogen atom in the protein. Protein crystals have large values of $\langle x^2 \rangle_x$ which were often attributed to crystal disorder. The existence of CS leads to a natural explanation of the large observed mean-square displacements. Additional information on the spatial distribution of CS in Mb comes from Mössbauer and Rayleigh scattering experiments.[41-45] The temperature dependence of the Debye–Waller factor implies that many atoms in proteins move on highly anharmonic potential surfaces.[38] The anharmonic potentials have been used to develop a model of the distribution of the CS^1 and their effect on the $B \rightarrow A$ transition, explaining the activation enthalpy distribution $g(H_{BA})$.[46]

6. BINDING AT PHYSIOLOGICAL TEMPERATURES

The complete explanation of the binding and relaxation processes at intermediate temperatures, with the protein undergoing EF and FIMs and the ligand entering the globin matrix or solvent after photodissociation, is very complicated and requires development of a detailed theory. However, the description of ligand binding from the solvent at about 300 K is simpler and independent of the details of a particular theory. Each protein rapidly moves from one substate to another and the ligand probes averaged barriers in the protein so that the single-particle model of Fig. 4 is appropriate.[12,28] The concentration-dependent binding from the solvent is exponential in time and can be written as

$$N(t) \simeq N_S \exp(-\lambda_{on} t), \tag{5}$$

Here, λ_{on} is a pseudo-first-order rate coefficient that is proportional to ligand concentration, and N_S is the fraction of photodissociated proteins whose ligands have migrated to the solvent. The association coefficient λ_{on} is given by

$$\lambda_{on}(c,T) = \bar{k}_{BA} P_B(c,T) N_S \tag{6}$$

where $P_B(c,T)$, the pocket occupation factor, is an equilibrium coefficient between the heme pocket and solvent at ligand concentration c. The term $\bar{k}_{BA}$ is the average rate coefficient for the B → A transition. Equation (6) is valid under very general conditions.[47] The factorization of λ_{on} as in Eq. (6) expresses the fact that the barrier between the heme pocket and the binding site at the Fe is still present at physiological temperatures and that the main control of ligand binding occurs at the heme.[28] The average rate coefficient $\bar{k}_{BA}$ is given by

$$\bar{k}_{BA} = A_{BA} \int dH_{BA} g(H_{BA}) \exp(-H_{BA}/RT). \tag{7}$$

$\bar{k}_{BA}$ is then extrapolated to high temperature.[28,46] Since λ_{on} and N_S are directly measureable at high temperature, information about the pocket occupation factor $P_B(c,T)$ is obtained. If we write

$$P_B(c,T) = P_0(c) \exp(-H_B/RT), \tag{8}$$

then H_B is the enthalpy of state B relative to the ligand in the solvent. The enthalpy H_B of the ligand in state B relative to the gas phase can be found using Eqs. (7) and (8) with the method of Ref. 28. Then, $H_B \simeq 2 \pm 2$ kJ/mol for MbCO and $H_B \simeq 0 \pm 2$ kJ/mol for MbO_2. The factor $P_0(c)$ gives an estimate of the volume of the pocket as 20 Å^3 for MbCO and 30 Å^3 for MbO_2.

7. A PROTEINQUAKE IN MYOGLOBIN

So far we have treated the binding of CO to Mb in the single-particle model and have not used the dynamic features of the protein explicitly. Implicitly, however, dynamics is already involved: The nonexponential time dependence of ligand binding below 200 K has led us to introduce conformational substates. The exponential time dependence of binding at 300 K implies transitions among the CS and protein dynamics is thus inescapably linked to protein function. In the present section we show that the detailed observation of the proteinquake following photodissociation of MbCO forces us to postulate more than one tier of CS. We consequently arrive at a hierarchy of protein substates.[25]

After photodissociation of MbCO, the system is initially in a nonequilibrium state. The iron has changed spin from 0 to 2 and the bond between the iron and the CO is broken. These changes occur within less than 250 fs after the laser pulse.[48] The heme and the protein, however, are still in the liganded form. Two processes now compete. The heme and the protein relax towards the deoxy structure in a quake-like motion and CO rebinds. We have already discussed CO binding and concentrate on the proteinquake here.

Experimental observations to be discussed below suggest that the relaxation of MbCO after photodissociation occurs through at

least four sequential steps:

$$MbCO \xrightarrow{h\nu} Mb_4^* \xrightarrow{FIM\ 4} Mb_3^* \xrightarrow{FIM\ 3} Mb_2^* \xrightarrow{FIM\ 2} Mb_1^* \xrightarrow{FIM\ 1} \text{deoxy-Mb}. \quad (9)$$

Mb_4^* to Mb_1^* are intermediate states. The discussion of the sequence in Eq. (9) requires both experimental data from many different techniques and guidance from theory. In the relevant theoretical work, Karplus and collaborators[49,50] start from high-resolution x-ray structures for hemoglobin and Mb and minimize the conformational energy. They find that an *allosteric core*, composed of the heme, HIS F8, the FG corner, and part of the F helix, plays a crucial role. The allosteric core appears to have two stable structures, one corresponding to the liganded and the other to the unliganded species. The unliganded geometry fits without strain into the unliganded globin, and the liganded geometry fits without strain into the liganded globin.

The proteinquake, Eq. (9), starts with the allosteric core and the globin still in the liganded structure, but with the iron in a high-spin state and the iron–ligand bond broken. The first phase,

$$Mb_4^* \xrightarrow{FIM\ 4'} Mb_3^*,$$

is very fast. Martin *et al.* have shown that a deoxy-like optical spectrum appears within 350 fs at 300 K after photodissociation with femtosecond laser pulses.[48] At 3 K, we have seen deoxy-like features at 1 μs after photodissociation. The activation energy for FIM 4 consequently is less than 0.4 kJ/mol. Resonance Raman experiments by Rousseau and Argade[51] and magnetic susceptibility measurements by Roder *et al.*[32] give more information on FIM 4. At 4 K, the Raman spectrum after photodissociation is close to the spectrum for deoxy-Mb, the iron has spin 2, and the heme core is expanded. These observations suggest that in Mb_3^*, which is metastable at 4 K, the heme is already domed, but the iron is constrained by the unrelaxed globin from moving fully into its deoxy position. The fact that FIM 4 occurs within less than 1 ps is supported by molecular dynamics calculations of Henry, Levitt and Eaton.[52]

In the second phase of the quake,

$$Mb_3^* \xrightarrow{FIM\ 3} Mb_2^*,$$

the iron probably moves completely into the deoxy position and the heme contracts to the deoxy structure. Raman experiments indicate that near 300 K FIM 3 starts at about 25 ps and is finished at 10 ns.[51,53] In steady-state Raman experiments, Mb_2^* is reached at 50 K.[51] While Mb_2^* has properties close to that of deoxy-Mb, small differences remain, as is seen particularly clearly in the position of a near-infrared band.[54] At about 20 K, the peak of the near-infrared band is at 758 nm in deoxy-Mb and at 766 nm in Mb_2^*. These observations can be interpreted by assuming that in the intermediate state Mb_2^*, which is metastable at 20 K, the globin has not yet relaxed.

The third phase of the proteinquake,

$$Mb_2^* \xrightarrow{FIM\ 2} Mb_1^*,$$

can be studied experimentally by determining the position of the "760 nm" near-infrared band as a function of temperature and time after photodissociation.[25,55] Below about 40 K, FIM 2 is too slow to be observed. Between 40 and 160 K, FIM 2 can be studied in detail and three remarkable features stand out: the band shifts without appreciably broadening; no isosbestic point exists; and the shift is nonexponential in time. It is not yet clear which residues of the protein are involved in FIM 2, but the work of Karplus and collaborators[49,50] suggests that the residues of the allosteric core must move to accommodate the unliganded geometry.

The third phase of the protein quake,

$$Mb_1^* \xrightarrow{FIM\ 1} \text{deoxy-Mb},$$

corresponds to the final rearrangement of the protein structure, including the hydration shell. Details of this motion are still unclear but its existence is assured by the result of the pressure titration experiment[26,37] shown in Fig. 10. The present knowledge of the rates for the four FIMs is summarized in Fig. 11.[25] Note in particular that FIM 2 is nonexponential in time and consequently

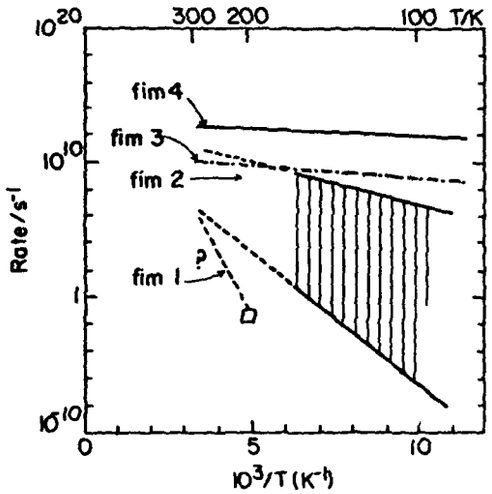

FIGURE 11 Relaxation rates for FIM 1 to FIM 4 as a function of $10^3/T$. For FIM 2, the range of rates is indicated. See text for discussion.

cannot be characterized by one rate. At each temperature, FIM 2 covers a wide range of rates.

8. THE HIERARCHY OF PROTEIN SUBSTATES

The observation of four different phases of the proteinquake or four different FIMs has consequences for the structure of CS in Mb. Even if the fluctuation–dissipation theorem does not hold rigorously, connections between fluctuations and dissipative motions must exist. Four different phases of the proteinquake call for four different tiers of CS. We thus arrive at the hierarchical model of protein substates given in Fig. 12.[23] A given state, for instance MbCO, shown at the top of Fig. 12 as a single potential well, is subdivided into a large number of conformational substates (CS^1),

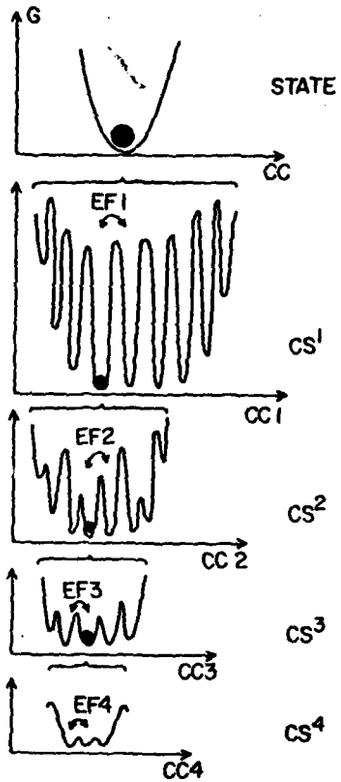

FIGURE 12 Hierarchical arrangement of substates in myoglobin showing the Gibbs free energy for four tiers of substates as a function of conformational coordinates CC1 to CC4.

separated by barriers with heights greater than about 80 kJ/mol. Each of these substates is in turn split into a large number of subsubstates (CS^2) with barriers between 12 and 40 kJ/mol. Each valley in the second tier furcates into a few subsubsubstates (CS^3) with barriers less than a few kJ/mol. Each of these CS^3 again branches into a few CS^4 with barriers less than 0.4 kJ/mol.

The equilibrium fluctuations (EF) that can occur in the protein characterized by the substate hierarchy of Fig. 12 depend crucially on temperature. Below about 10 K, the only motions are fluctuations in the CS^4. As the temperature increases, EF3 set in and at about 40 K they are so fast that all CS^3 (and CS^4) are in equilibrium and only the next tier has to be considered. At about 40 K, EF2 among the CS^2 set in. These EF2 also become faster with increasing temperature. Finally, above about 200 K, EF1 among the substates (CS^1) of the first tier begin. At physiological temperatures, the EF in a protein will be complex. In addition to the four tiers of EF with characteristic barrier heights for each tier, EF in one tier do not occur with one rate, but most likely span a range of rates as indicated in Fig. 11.

So far we have used only the evidence from FIMs for the construction of the hierarchical protein model of Fig. 12. Additional evidence comes from studies of the EF.[25] We will only give one example, the determination of the specific heat of metmyoglobin crystals below 4 K by Singh *et al.*[56] Their data, given in Fig. 13, show that the specific heat approaches a $T^{1.3}$ dependence below 0.4 K. Such a behavior is typical for glasses and implies the existence of tunnel states.[57,58] The barriers separating these tunnel states may extend up to a few kJ/mol and we identify the corresponding energy valleys with the substates CS^4 in Fig. 12.

9. SUMMARY AND OUTLOOK

Ligand Binding. The work of the past decade has resulted in a deeper, but also more complex, picture of ligand binding to heme proteins. The early model of ligand binding as taking place in a single step described by the association and dissociation coefficients λ_{on} and λ_{off} has been replaced by the more complicated single-particle model of Figs. 3 and 4. While most of the features of the single-particle model have been established,[12,27-31] signifi-

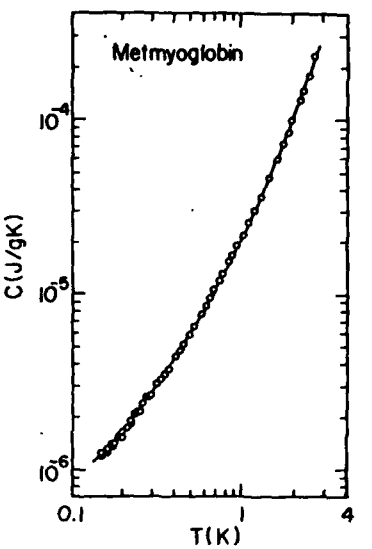

FIGURE 13 Specific heat C of metmyoglobin crystals as a function of temperature T. Solid line indicates a fit to the data (after Ref. 56).

cant work remains to be done on some aspects of the model. We mention only the following: (i) The extrapolation of the rate coefficient k_{BA} from low temperature to physiological temperature needs additional study.[12,28] (ii) Further work needs to be done on the adiabaticity of the covalent binding step B → A.[59] (iii) A complete mathematical formulation of the single-particle model including process M needs to be developed. (iv) The detailed features of the single-particle potential should be explained in terms of protein structure. While some aspects are clear,[12,28-31] we are still far from predicting what would be the result of a particular change in the amino-acid sequence.

The Hierarchical Protein Model. Figure 12 describes the structure of protein substates in terms of a hierarchical arrangement of tiers of CS, with different ranges of barrier heights. This model

must be verified with additional experiments and the characteristics of the barriers in the various tiers must be explored in more detail. Even in Mb, there could be more tiers. The explanation of the various substates in terms of structure remains to be found. So far, the hierarchical structure has only been studied for Mb. Do other proteins have similar hierarchies? Can the model be extended to nucleic acids? A number of such experimental and theoretical questions are unanswered.

FIMs and BUMs. The question of which of the observed motions in proteins are functionally important and which are not is easy to answer in principle but difficult to answer in practice. In principle a specific protein motion can be affected by changing the protein environment, altering the protein structure perhaps by genetic engineering, or employing suitable allosteric molecules. If the protein motion also changes without changing the protein function, then the protein motion is not a FIM and can, following a suggestion of Tony Crofts, be classified as a *BUM* (biologically unimportant motion). In practice, the classification of protein motions as FIMs or BUMs requires sophisticated and detailed studies which have not yet been performed. We consequently can only speculate about the functional importance of the motions observed so far in myoglobin and which part of the protein the motions involve: FIM 1 most likely involves large scale motions in myoglobin and may include the hydration shell and part of the solvent. FIM 1 may be the motion that permits ligands to enter and leave the protein and may transmit information from the protein surroundings to the active center. FIM 2 may permit relaxation of the allosteric core and motion of the ligand between the heme pocket and the globin matrix. FIM 3 does not as yet have a function assigned to it even speculatively. It may, however, be necessary that FIM 3 occurs prior to FIM 2 so that its function is to prepare the protein for FIM 2. FIM 4, the rapid motion immediately after photodissociation, may also allow the ligand to move away from the active center. If the iron stayed fixed near the center of the heme plane, then rebinding might be so fast that the ligand could never escape from the pocket before rebinding.

In connection with this tentative discussion of the functional importance of the four motions, FIM 1 to FIM 4, it should be

pointed out that the reaction pathway for the ligand–protein system after photodissociation can be different than the reaction pathway after thermal dissociation. In photodissociation the system starts in the liganded structure denoted MbCO. In thermal dissociation the protein can thermally change to a state where dissociation is favored before the actual dissociation of the ligand from the heme iron. Part of the proteinquake pathway therefore can already be travelled when thermal dissociation occurs so that the quake following thermal dissociation can be somewhat different than the quake following photodissociation.

Proteins and Glasses. The results discussed here suggest that proteins have many similarities with glasses and amorphous solids: They possess a hierarchical structure,[60] show nonergodic behavior,[61] and may be ultrametric.[62] The hierarchical arrangement of the CS is shown in Fig. 12. The nonergodic behavior can be stated as follows: Below about 200 K, a protein in a particular substate (CS^1) will remain in that substate for a very long time compared to any measurement time and will therefore not explore all possible substates. The ultrametric property can be explained with Fig. 12. Assume that the protein fluctuates from a CS^3 in one substate (CS^1) to another CS^3 that is a member of a different substate (CS^1) of the first tier. The barriers of the second and third tier then are not important and the fluctuation is dominated by the highest barrier between the initial and final CS^3. The similarity between glasses and proteins may be accidental or it may be based on the construction of proteins. Further work on the experimental and theoretical aspects of this problem are required. It may well turn out that proteins are excellent systems for testing glass theories and that glass theories may be useful in describing proteins and protein reactions.[63-65]

Theories of Protein Motions. Figures 11 and 12 raise some questions about how protein fluctuations, motions, and reactions can be represented theoretically. Molecular dynamics calculations[66] may not at present have the time range to describe motions of the first or second tier.[25,45] Moreover, the initial conditions may be such that the "theoretical protein" is caught in a particular CS^1 (or even CS^2) so that the calculations are ergodic only within such

a substate.[25] A second problem arises with respect to protein reactions and proteinquakes. Most calculations performed so far deal only with one state and thus with equilibrium fluctuations. The extension of theory to proteinquakes and to protein reactions is essential for a full understanding of proteins.

Acknowledgments

We thank the members of our biomolecular physics group at the University of Illinois, A. Ansari, J. Berendzen, S. F. Bowne, B. Cowen, D. Fung, I. E. T. Iben, T. E. Sauke, E. Shyamsunder, and P. Steinbach, for contributions to the research described in this Comment and for many illuminating discussions. This work was supported in part by National Science Foundation Grant PCM 82-09616 and Department of Health and Human Services Grant PHS GM10851.

HANS FRAUENFELDER
Department of Physics,
University of Illinois at Urbana-Champaign,
1110 West Green Street,
Urbana, Illinois 61801

ROBERT D. YOUNG
Department of Physics,
Illinois State University,
Normal, Illinois 61761

References

1. *Structure and Dynamics: Nucleic Acids and Proteins*, eds. E. Clementi and R. H. Sarma (Adenine Press, New York, 1983). This reference and Refs. 2 and 3 are conference proceedings which provide surveys and contain citations of other reviews and many seminal papers.
2. *Structure and Motion: Membranes, Nucleic Acids and Proteins*, eds. E. Clementi, G. Corongiu, M. H. Sarma and R. H. Sarma (Adenine Press, Guilderland, NY, 1985).
3. *Structure, Dynamics, Interactions, and Evolution of Biological Macromolecules*, ed. C. Hélène (Reidel, Dordrecht, 1983).
4. G. Careri, P. Fasella and E. Gratton, Ann. Rev. Biophys. Bioeng. **8**, 69 (1979).
5. A. Cooper, Sci. Prog. Oxford. **66**, 473 (1981).
6. P. Debrunner and H. Frauenfelder, Ann. Rev. Phys. Chem. **33**, 283 (1982).
7. J. A. McCammon, Rep. Prog. Phys. **47**, 1 (1984).
8. G. A. Petsko and D. Ringe, Ann. Rev. Biophys. Bioeng. **13**, 331 (1984).
9. E. Antonini and M. Brunori, *Hemoglobin and Myoglobin in Their Reactions with Ligands* (North-Holland, Amsterdam, 1971). This book contains early work on the binding of small ligands to hemoglobin and myoglobin.
10. L. Stryer, *Biochemistry*, Second Edition (W. H. Freeman, San Francisco, 1981), Chs. 2 and 3.

11. R. E. Dickerson and I. Geis, *Hemoglobin* (Benjamin/Cummings, Menlo Park, CA, 1983), Ch. 2.
12. R. H. Austin, K. W. Beeson, L. Eisenstein, H. Frauenfelder and I. C. Gunsalus, Biochem. **14**, 5355 (1975).
13. A. Cooper, Proc. Natl. Acad. Sci. USA **73**, 2740 (1976).
14. H. B. Callen, *Thermodynamics* (Wiley, New York, 1962); L. D. Landau and E. M. Lifshitz, *Statistical Physics* (Pergamon, London–Paris, 1980).
15. A. Einstein, Ann. Physik **17**, 549 (1905).
16. H. Nyquist, Phys. Rev. **32**, 110 (1928).
17. H. B. Callen and T. A. Welton, Phys. Rev. **83** (1951).
18. R. Kubo, Rep. Prog. Phys. **29**, 255 (1966).
19. M. Suzuki, Prog. Theor. Phys. **56**, 77 (1976).
20. M. Lax, Rev. Mod. Phys. **32**, 5 (1960).
21. F. Schlögl, Z. Phys. B **33**, 199 (1979).
22. H. Frauenfelder and E. Gratton, *Methods in Enzymology* (in press).
23. See, for example, the papers and discussions in G. Nicolis, G. Dewel and J. W. Turner (Eds.), *Order and Fluctuations in Equilibrium and Nonequilibrium Statistical Mechanics* (Wiley-Interscience, New York, 1981).
24. L. A. Blumenfeld, Q. Rev. Biophys. **11**, 251 (1978); L. A. Blumenfeld, *Problems of Biological Physics* (Springer-Verlag, Berlin, 1981).
25. A. Ansari, J. Berendzen, S. F. Bowne, H. Frauenfelder, I. E. T. Iben, T. E. Sauke, E. Shyamsunder and R. D. Young, Proc. Natl. Acad. Sci. USA **82**, 5000 (1985).
26. L. Eisenstein and H. Frauenfelder, *Frontiers in Biological Energetics*, Vol. 1 (Academic, New York, 1978), p. 680.
27. N. Alberding, S. Chan, L. Eisenstein, H. Frauenfelder, D. Good, I. C. Gunsalus, T. Nordlund, M. F. Perutz, A. Reynolds and L. Sorensen, Biochem. **17**, 417 (1978).
28. W. Doster, D. Beece, S. Bowne, E. Dilorio, L. Eisenstein, H. Frauenfelder, L. Reinisch, E. Shyamsunder, K. Winterhalter and K. T. Yue, Biochemistry **21**, 4831 (1982).
29. D. Dlott, H. Frauenfelder, P. Langer, H. Roder and E. E. Dilorio, Proc. Natl. Acad. Sci. USA **80**, 6239 (1983).
30. N. Alberding, R. Austin, S. Chan, L. Eisenstein, H. Frauenfelder, I. C. Gunsalus and T. Nordlund, J. Chem. Phys. **65**, 4701 (1976).
31. F. Stetzkowski, R. Banerjee, M. Marden, D. Beece, S. Bowne, W. Doster, L. Eisenstein, H. Frauenfelder, L. Reinisch, E. Shyamsunder and C. Jung, J. Biol. Chem. **260**, 8803 (1985).
32. H. Roder, J. Berendzen, S. Bowne, H. Frauenfelder, T. Sauke, E. Shyamsunder and M. Weissman, Proc. Natl. Acad. USA **81**, 2359 (1984).
33. N. Alberding, R. Austin, K. Beeson, S. Chan, L. Eisenstein, H. Frauenfelder and T. Nordlund, Science **192**, 1002 (1976).
34. H. Frauenfelder, *Methods in Enzymology*, Vol. I IV (Academic, New York, 1978), pp. 506–532.
35. H. Frauenfelder, *Dynamic Aspects of Protein Reactions*, in Ref. 1 (1983), p. 369.
36. W. Breinhl, J. Friedrich and D. Haarer, Chem. Phys. Lett. **106**, 487 (1984).
37. N. Alberding, Ph.D. Dissertation, University of Illinois at Urbana-Champaign (1978); L. Sorensen, Ph.D. Dissertation, University of Illinois at Urbana-Champaign (1980).
38. H. Frauenfelder, G. Petsko and D. Tsernoglu, Nature **280**, 558 (1979).
39. H. Frauenfelder and G. Petsko, Biophys. J. **10**, 465 (1980).

40. H. Hartmann, F. Parak, W. Steigemann, G. Petsko, D. Ringe Ponzi and H. Frauenfelder, Proc. Natl. Acad. Sci. USA 79, 4967 (1982).
41. H. Keller and P. G. Debrunner, Phys. Rev. Lett. 45, 68 (1980).
42. F. Parak, E. N. Frolov, R. L. Mössbauer and V. I. Goldanskii, J. Mol. Biol. 145, 824 (1981).
43. E. R. Bauminger, S. G. Cohen, I. Nowik, S. Ofer and J. Yariv, Proc. Natl. Acad. Sci. USA 80, 736 (1983).
44. Yu. Krupyanskii, F. Parak, D. Engelman, R. L. Mössbauer, V. I. Goldanskii and I. Suszcheliev, Z. Naturforsch 37b, 57 (1982).
45. F. Parak and E. W. Knapp, Proc. Natl. Acad. Sci. USA 81, 7088 (1984).
46. R. D. Young and S. F. Bowne, J. Chem. Phys. 81, 3730 (1984). See also, N. Agmon and J. J. Hopfield, J. Chem. Phys. 79, 2042 (1983).
47. R. D. Young, J. Chem. Phys. 80, 554 (1984).
48. J. L. Martin, A. Migus, C. Puyart, Y. Lecarpentier, R. Astier and A. Antonetti, Proc. Natl. Acad. Sci. USA 80, 173 (1983).
49. B. R. Gelin and M. Karplus, Proc. Natl. Acad. Sci. USA 74, 801 (1977).
50. B. R. Gelin, A. W. Lee and M. Karplus, J. Mol. Biol. 171, 489 (1983).
51. D. L. Rousseau and P. V. Argade, Proc. Natl. Acad. Sci. USA (in press).
52. E. R. Henry, M. Levitt and W. A. Eaton, Proc. Natl. Acad. Sci. USA 82, 2034 (1985).
53. C. Johnston, G. Dalickas, D. Gupta, T. Spiro and R. Hochstrasser, Biochemistry (submitted).
54. T. Iizuka, H. Yamamoto, M. Kotani and T. Yonetani, Biochem. Biophys. Acta 371, 126 (1974).
55. H. Frauenfelder, *Ligand Binding and Protein Dynamics*, in Ref. 2, p. 205.
56. G. P. Singh, H. J. Shink, H. V. Lohneysen, F. Parak and S. Hunklinger, Z. Phys. B 55, 23 (1984).
57. P. W. Anderson, B. I. Halperin and C. M. Varma, Philos. Mag. 25, 1 (1972).
58. W. A. Phillips, J. Low Temp. Phys. 7, 351 (1972).
59. H. Frauenfelder and P. G. Wolynes, Science 229, 337 (1985).
60. *M. Mezard, G. Parisi, N. Sourlas, G. Toulouse and M. Virasoro*, Phys. Rev. Lett. 52, 1156 (1984).
61. R. G. Palmer, Adv. Phys. 31, 669 (1982).
62. B. A. Huberman and M. Kerszberg, J. Phys. A 18, 331–336 (1985).
63. V. I. Goldanskii, Yu. F. Krupyanskii and V. N. Fleurov, Doklady AN SSSR 272, 978 (1983).
64. R. G. Palmer, D. L. Stein, E. Abrahams and P. W. Anderson, Phys. Rev. Lett. 53, 958 (1984).
65. D. Stein, Proc. Natl. Acad. Sci. USA 82, 3670 (1985).
66. M. Karplus and J. A. McCammon, CRC Crit. Rev. Biochem. 9, 293 (1981).

Submitted to Biophysical Chemistry

ILL-(EX)-87-#14
February 1987

REBINDING AND RELAXATION IN THE MYOGLOBIN POCKET[#]

Anjum Ansari, Joel Berendzen, David Braunstein, Benjamin R. Cowen,

Hans Frauenfelder, Mi Kyung Hong, Icko E. T. Iben, J. Bruce Johnson,

Pál Ormos[†], Todd B. Sauke, Reinhard Scholl, Alfons Schulte,

Peter J. Steinbach, Joseph Vittitow, and Robert D. Young[*]

Department of Physics, 1110 West Green Street
and
Department of Biophysics, 505 South Mathews Street
University of Illinois at Urbana-Champaign, Urbana, IL 61801 USA

Keywords: Myoglobin, CO stretching bands, hierarchy of substates and motions, protein relaxation, protein dynamics, control mechanisms

[#]Dedicated to Manfred Eigen on the occasion of his 60th Birthday.

[†]Permanent address: Institute of Biophysics, Biological Research Center, Hungarian Academy of Sciences, Szeged H-6701 HUNGARY.

[*]Permanent address: Department of Physics, Illinois State University, Normal, IL 61761 USA

PACS Indices: 87.15.By; 87.15.He
33.20.Ea; 82.20.-w

Typed by Mary Ostendorf

ABSTRACT

The infrared stretching bands of carboxymyoglobin (MbCO) and the rebinding of CO to Mb after photodissociation have been studied in the temperature range from 10 to 300K in a variety of solvents. Four stretching bands imply that MbCO can exist in four substates, A_0 to A_3. The temperature dependences of the intensities of the four bands yield the relative binding enthalpies and entropies. The integrated absorbances and the pH dependences of the bands permit identification of the substates with the conformations observed in the X-ray data [Kuriyan et al., J. Mol. Biol. 192 (1986) 133]. At low pH, A_0 is hydrogen-bonded to His E7. The substates A_0 to A_3 interconvert above about 180K in a 75% glycerol-water solvent and above 270K in buffered water. No major interconversion is seen at any temperature if MbCO is embedded in a solid poly(vinyl)alcohol matrix. The dependence of the transition on solvent characteristics is explained as a slaved glass transition.

After photodissociation at low temperature the CO is in the heme pocket B. The resulting CO stretching bands which are identified as B substates are blue-shifted from those of the A substates. At 40K, rebinding after flash photolysis has been studied in the Soret, the near-IR, and the integrated A and B substates. All data lie on the same rebinding curve and demonstrate that rebinding is nonexponential in time from at least 100 ns to 100 ks. No evidence for discrete exponentials is found.

Flash photolysis with monitoring in the IR shows four different pathways within the pocket B to the bound substates A_j. Rebinding in each of the four pathways B → A is nonexponential in time to at least 10 ks and the four pathways have different kinetics below 180K. From the time and temperature dependence of the rebinding, activation enthalpy distributions $g(H_{BA})$ and preexponentials A_{BA} are extracted. No pumping from one A substate to another,

or one B substate to another, is observed below the transition temperature of about 180K.

If MbCO is exposed to intense white light for 10 to 10^3s before being fully photolyzed by a laser flash, the amplitude of the long-lived states increases. The effect is explained in terms of a hierarchy of substates and substate symmetry breaking.

The characteristics of the CO stretching bands and of the rebinding processes in the heme pocket depend strongly on the external parameters of solvent, pH, and pressure. This sensitivity suggests possible control mechanisms for protein reactions.

1. INTRODUCTION

The binding of small ligands such as carbon monoxide (CO) to heme proteins at first appears to be a simple one-step process[1], but a closer look over extended ranges in temperature, time, and wavelength reveals a surprising complexity. Binding is governed by a sequence of barriers rather than a single one.[2] After photodissociation, rebinding occurs at temperatures as low as a few K[3] and is nonexponential in time below 180K in a 75% glycerol-water solvent.[2,4,5] Below about 40K, binding no longer proceeds by classical over-the-barrier motion, but through quantum-mechanical tunneling.[6,7] The behavior of the photodissociated CO within the heme pocket, followed by IR spectroscopy, turns out to be complicated.[8,9]

In the present paper we investigate processes within the heme pocket of myoglobin (Mb) in more detail. Mb has been called the hydrogen atom of biology; it is a globular protein of about 18 kdalton that stores dioxygen (O_2) in muscles.[10] O_2 or CO binds reversibly to the central iron atom of the heme group in Mb. Since Mb is sturdy and very well explored, it offers a nearly ideal system for more sophisticated studies.

The impetus for the present work came from two directions: (1) At low temperatures, CO bound to Mb shows a number of stretching bands.[8,9] During our earlier work we had noticed that the different bands rebind with different rates after photodissociation. A rate difference has also been noticed by Gerwert et al.[11] and M. Chance et al.[12] Such a rate variation suggests a control mechanism and calls for more studies. (2) Nonexponential kinetics below 180K has been seen in all protein-ligand systems that have been studied. In general, nonexponential time dependences can be explained either by homogeneous or inhomogeneous processes. By using a sequence of laser flashes repeated before all the Mb molecules have rebound a CO ("hole burning in

time") we have demonstrated that pumping from short-lived to long-lived states at 60 and 70K is very small and that the nonexponential kinetics results predominantly from inhomogeneities among Mb molecules and cannot be explained by multiple states within one protein molecule.[5,13,14] In view of these results it is surprising that B. Chance et al. recently claimed evidence for a bi- or triexponential time course and considerable pumping from short- to long-lived components in the binding of CO to Mb at 40K.[15] The difference between their interpretation and ours is fundamental. B. Chance et al. assume that the different lifetimes are caused by different pathways or sites within the same molecule. We postulate a large number of structurally different conformational substates (CS), with each molecule remaining in a given CS at temperatures where the solvent is frozen.[5,16] Our interpretation leads to the concept of a hierarchy of substates[17] and to connections between proteins and (spin) glasses.[18] We will discuss the concept of CS and of the hierarchy of CS in Subsection 4.5.

Here we report on expanded low-temperature experiments.[19] The new experiments verify our earlier experiments and also yield surprising results that open new windows on phenomena in the heme pocket.

2. EXPERIMENTAL APPROACH

The primary experimental technique is low-temperature flash photolysis. An MbCO sample at a controlled temperature is photodissociated with a light pulse and rebinding is monitored through optical absorption measurements. We have observed rebinding at many different wavelengths, as indicated in Fig. 1, thus monitoring the rebinding process(es) at different locations in the heme pocket.[20,21] In the Soret and the α and β bands, changes in the electronic structure of the heme on binding are seen. The near-IR band (band III, near 760 nm) is a charge-transfer band and involves both the iron atom and the heme. In the IR, the bands near 1950 cm^{-1} result from the stretching mode of the bound CO[22,23] and the ones near 2100 cm^{-1} result from the stretching mode of the photodissociated CO within the pocket.[8,9] If only one simple rebinding process were to occur, all of these markers would give the same time course.

Four different systems were used for the experiments, a nanosecond (ns) visible-wavelength flash photolysis system, a conventional dispersive visible-near-IR spectrophotometer, an FTIR spectrophotometer and a microsecond mid-IR flash photolysis system. Samples were prepared from lyophilized sperm whale Mb from Sigma (St. Louis, MO) dissolved in buffer solution. Buffers used were: 0.4M citrate-phosphate buffer for the pH 5.0 sample, 0.4M carbonate-bicarbonate buffer for pH 9.0 samples, 0.1M HEPES buffer for the pH 7.0 poly(vinyl)alcohol (PVA) samples, and 0.5M sodium phosphate buffer for all of the other samples. Solvents were water, 75% (volume/volume) glycerol-water, and PVA. The Soret data were taken on 10-14 μM samples placed in a 1 cm × 1 cm cuvette and the near-IR experiments were done on a 1.5 mM sample in a 1 cm by 0.1 cm cell.[17] FTIR and fast-IR measurements were performed on 15-20 mM samples held between two CaF_2 windows with a 75 μm mylar spacer.

The ns system employed a 30 ns pulse from a frequency-doubled, Q-switched Nd^{+}-glass laser (530 nm, 300 mJ). Rebinding was monitored with the light from a tungsten lamp passed through a monochromator. Monitor beam intensities were kept small (< 10^{-3} photons/s absorbed per protein molecule). The photomultiplier (Hamamatsu 928) signal was digitized with a LeCroy TR8818 transient digitizer from 10 ns to 300 μs and with a logarithmic time-base digitizer from 2 μs to 300 s. A storage cryostat (Janis 10-DT) permitted temperature control.

Our OLIS-Cary 14 spectrophotometer is interfaced to an IBM PC/AT computer. Kinetics data obtained from this instrument extend from 60 to 3×10^{4}s.

The FTIR experiments were performed on a Mattson Sirius 100 FTIR spectrometer. All spectra were taken at 1 or 2 cm^{-1} resolution. Low temperatures were produced with a closed-cycle helium refrigerator, CTI model 21. Photolysis in the kinetics experiments was achieved with a 500 ns, 0.3 J, 590 nm pulse from a Phase-R DL2100C dye laser using rhodamine 6G dye. Absolute absorbance spectra were obtained by subtracting the solvent background spectrum from the MbCO spectrum. The difference absorption spectra in the kinetics experiments were obtained by referencing the photolyzed spectrum to the unphotolyzed background spectrum.

The fast kinetics of the CO stretching bands was measured in a separate mid-IR flash photolysis system. The infrared monitoring light was produced by a Spectra-Physics/Laser Analytics tunable-diode laser and directed through the protein solution and monochromator onto a LN_2-cooled IR-Associates HgCdTe detector. Photolysis was induced by the same laser used in the FTIR experiments. For times between 100 ms and 100 s the diode laser current was modulated at 10 kHz and the signal was amplified by a PAR 5101 lock-in amplifier.

3. RESULTS AND DATA EVALUATION

A coherent picture of the low-temperature binding emerges after the data obtained with the different instruments and in the different wavelength regions are pieced together.

3.1 IR Measurements of MbCO

(i) The A Substates. The stretching bands of the bound CO are superb probes. We have measured the "dark" or bound-state IR spectrum of MbCO at temperatures between 15 and 300K in 75% glycerol-water (Fig. 2), in water (Fig. 3), and in solid poly(vinyl)alcohol (PVA) (Fig. 4).

The spectra shown in Figs. 2-4 can be decomposed into Gaussian superpositions of Lorentzians, called Voigtians.[24,25] Two such decompositions are shown in Fig. 5. Four different IR bands can be distinguished. We denote the bands in order of decreasing wavenumbers by A_0 ($\approx$ 1966 cm^{-1}), A_1 ($\approx$ 1946 cm^{-1}), A_2 ($\approx$ 1941 cm^{-1}), and A_3 ($\approx$ 1930 cm^{-1}). (Because of the new band A_2 the nomenclature differs from the one we used earlier.[8]) The fits yield the center positions ν_{CO}, the full-width at half maximum Γ, and the areas of the four bands. Since the band A_2 is difficult to extract unambiguously, we shall discuss only the other three.

(ii) Temperature Dependence of the A Bands. In order to characterize the temperature dependence of the individual bands in glycerol-water, we select the most intense band, A_1, as standard and plot in Fig. 6 the logarithm of the intensity ratios A_0/A_1 and A_3/A_1 as a function of $10^3/T$. The ratios A_i/A_1 in Fig. 6 show a different behavior for PVA and glycerol-water. For PVA, the ratios change very little. MbCO in 75% glycerol-water, in contrast, shows two regions. Above about 180K, the ratios change rapidly; below that temperature, the change is much slower. The behavior above 180K can be understood if the four bound substates A_0 to A_3 have different binding enthalpies and entropies

and may interconvert freely. Below 180K, the change may be explained by assuming that the proteins are frozen into particular substates and the extinction coefficients for the different A substates depend slightly differently on temperature. Above 180K, the ratios are given by

$$A_i/A_1 = \exp[S_i/R]\ \exp[-H_i/RT]\{\varepsilon_i(T)/\varepsilon_1(T)\} \qquad (1)$$

where S_i and H_i are the entropy and enthalpy of substate A_i with respect to substate A_1 and $\varepsilon_i(T)$ is the extinction coefficient of substate A_i at temperature T. Assuming as a first approximation that the ratio of extinction coefficients is unity, relative binding enthalpies and entropies have been extracted from the data in Fig. 6. The binding parameters for two values of pH are given in Table 1.

The total integrated area ΣA_i of the A bands of MbCO in 75% glycerol-water, given as a function of temperature in Fig. 7, shows a decrease of about 20% in going from 10 to 300K. Such a decrease can be explained by a change in the electron-nuclear coupling.[26]

The temperature dependence of the center frequency ν_{CO} is given in Fig. 8 for the bands A_0 and A_1 for two samples. The temperature dependence of the line width Γ is displayed in Fig. 9.

(iii) Nonequilibrium Behavior of the A Bands. The ratios A_0/A_1 and A_3/A_1 in Fig. 6 follow a van't Hoff behavior from 260K to 190K. Below 190K, they deviate from the van't Hoff line and become essentially temperature independent. We explain this temperature dependence by assuming that the A substates are not in dynamic equilibrium below about 180K in 75% glycerol-water. To verify this assumption we have measured the time dependence of the IR spectrum after the temperature was lowered from 195K to the measurement

temperature T. We denote with $A_j(t)$ the integrated absorbance of band A_j at the time t after lowering the temperature. $A_j(0)$ is the integrated absorbance at 195K, and $A_j(\infty)$ the equilibrium value at temperature T which would be reached after an extremely long (∞) time. We estimate $A_j(\infty)$ by extrapolating the van't Hoff line, obtained from 260 to 195K, to the temperature T. The fraction $n_j(t)$ of MbCO molecules that have not yet transferred to substate A_j at time t after the change in T is given by

$$n_j(t) = \{A_j(t)-A_j(\infty)\}/\{A_j(0)-A_j(\infty)\}. \qquad (2)$$

$n_0(t)$ at 190K is shown in Fig. 10. The data indicate that the approach to equilibrium is nonexponential in time. In addition we observe that the time to reach equilibrium is extremely long below 180K. The A substates are not in equilibrium below 180K.

(iv) External Influence on A Substates. Makinen et al.[22] and Brown et al.[27] have pointed out that external influences can change the relative intensities of the A substates. Such effects can be seen in Figs. 2-4. A_0 is much more intense in PVA and in ice than in glycerol-water. Pressure and pH also affect the ratio A_j/A_1. Fig. 11 shows that A_3 decreases while A_1 and A_0 increase with increasing pressure. Fig. 12 shows that A_0 increases at the expense of A_1 with decreasing pH. While the band intensities are affected strongly by solvent state, pressure, and pH, the band positions remain nearly unchanged.

The close coupling of the environment with the protein is supported by the data in Fig. 13. The IR spectrum of a 75% glycerol-water solvent exhibits a transition near 180K, essentially at the temperature where the substate exchange is frozen.

3.2 Overall Rebinding at 40K

Figure 1 shows that rebinding after photodissociation can be monitored at various locations in the heme-CO system. We have studied the rebinding at 40K over a wide range of times at various wavelengths. We selected 40K because B. Chance et al.[15] have claimed evidence for discrete exponentials at this temperature. The results of our measurements are shown in Fig. 14. The data correspond to four different spectral regions. The symbol ◇ indicates measurement at 440 nm, near the deoxy Soret peak; □ indicates the integrated absorbance of the "760 nm" charge transfer band III; ▽ refers to the integral over all A (bound) CO stretching bands; and the O shows the integrated magnitude of the absorbance change of the Soret band region from 400 to 450 nm.

The data in Fig. 14 are smooth over more than twelve orders of magnitude in time. No evidence for the bi- or triexponential behavior is visible. Within experimental uncertainties all of the above measurements give the same time course.

3.3 Rebinding to the A Substates

New features appear when the rebinding of each of the four A substates is monitored separately. Fig. 15 gives the rebinding of A_0, A_1, and A_3 at various temperatures. The data, taken at pH 6.8 in 75% glycerol-water, show the following features:

(i) At all temperatures, the four substates rebind with different kinetics.

(ii) Rebinding of each A substate is nonexponential in time up to 180K.

(iii) A_3 is always considerably slower than A_1.

We evaluate the nonexponential kinetics by assuming that each protein molecule is in a substate with barrier height H_{BA} for rebinding from the pocket state B to the covalently bound state A.[5] If $g(H_{BA})dH_{BA}$ denotes the probability of finding a barrier with height between H_{BA} and $H_{BA} + dH_{BA}$, the rebinding function is given by

$$N(t) = N(0) \int dH_{BA}\, g(H_{BA}) \exp\{-k_{BA}(H_{BA})t\}. \quad (3)$$

Here $k_{BA}(H_{BA})$ is the rate coefficient appropriate for a barrier of height H_{BA}. Below about 40K, $k_{BA}(H_{BA})$ is dominated by tunneling.[6,7] Above 40K, $k_{BA}(H_{BA})$ is related to H_{BA} by an Arrhenius relation,

$$k_{BA}(H_{BA}) = A_{BA}(T/T_0) \exp[-H_{BA}/RT]. \quad (4)$$

We have verified this form, with the overall preexponential factor proportional to T, for CO binding to the separated β chain of hemoglobin Zürich.[28] T_0 is an arbitrary reference temperature which we take to be 100K. The parameter A_{BA} consequently gives the preexponential factor at 100K. We further assume $g(H_{BA})$ to be given by the gamma distribution as in the model of Young and Bowne.[29] This distribution peaks at the activation enthalpy H_{peak}. The rebinding parameters are found by fitting the experimental data to Eq. (3), with $g(H_{BA})$ given by the gamma distribution and k_{BA} by Eq. (4). We have used this technique for many heme protein-ligand systems.[5,28,30] The barrier parameters for binding to the A substates are given in Table 2. For comparison, we also list the parameters obtained by monitoring at 440 nm.

3.4 The B Substates

Since we observe four discrete CO-bound substates, A_0-A_3, we also expect four discrete stretching frequencies in the photodissociated state B. We observe, however, only three bands, as shown in Fig. 1b. In an earlier paper we have discussed these bands in detail.[8] B_2 at 2119 cm^{-1} is an intermediate that decays to B_1 at temperatures above 15K. For the treatment of rebinding above about 15K, we are left with only B_0 and B_1. At pH 5.6 and 6.8, B_1 is much more intense than B_0, and it decays with the same time dependence as A_1,

while B_0 shows the same time dependence as A_3. B_1 therefore must bind to substate A_1 and B_0 to substate A_3.

The fact that we cannot see the B substates that bind to A_0 and A_2 is not surprising. The integrated extinction coefficients of the B bands are small (1.4 ± 0.1 $mM^{-1}cm^{-2}$) and a sufficiently sensitive measurement of the spectrum is difficult. Moreover, the intensities of A_0 and A_2 are much smaller than that of A_1. We consequently expect the B substates that bind to A_0 and A_2 to be much smaller than B_1 and therefore to be hidden.

3.5 Rebinding Observed Between 350 and 800 nm

The different kinetics for the various A substates raises the question of whether similar differences can also be seen over the interval 350 to 800 nm, where the spectral features are dominated by the heme group. The time range from 100 ns to 300 s was scanned with our flash photolysis system at the wavelengths indicated in Fig. 1a. Times from 60 s to about 30 ks were monitored with the OLIS-Cary spectrometer where the entire wavelength region was scanned. While small differences were observed, no major variations in the time course as a function of wavelength were found at pH 6.8. The fastest rebinding was observed around the maximum of the CO bound spectrum, the slowest around the peak of deoxymyoglobin. The average rates at 421 and 440 nm differ by a factor of 2.2 at 60K and 1.6 at 80K. The kinetics at 440 nm, where we normally monitor rebinding, agrees well with that of the integrated A substates. The result is reassuring. Observations in the Soret region yield information about the average rebinding behavior.

3.6 Transitions Among A Substates?

We have shown in Subsection 3.1 that the A substates are frozen when the protein is embedded in a solid matrix. This observation leaves open the possibility that even below 180K transitions among B substates can take place.

Transitions among the A substates could then be induced by light, for instance through the chain $A_i \rightarrow B_j \rightarrow B_k \rightarrow A_\ell$. To study this possibility, we have performed a number of additional experiments.

(i) MbCO After Illumination. If transitions among the B substates occur the ratios A_i/A_1 measured after cooling in the dark and after illumination should in general differ below 180K. We have performed such experiments at 160K, 140K, and 120K. The change in relative intensities after illumination is less than 1% for A_1 and less than 5% for A_0 and A_3. The B substates do not exchange significantly with each other below 180K.

(ii) Rebinding Under Illumination. As a second test, we measured the IR spectrum as a function of time during exposure of the MbCO sample to constant illumination. Under the assumption that each A substate communicates only with one B substate and that neither A nor B substates exchange with each other, the rate $A \rightarrow B$, denoted by k_L, is determined by the intensity of illumination. Rebinding $B \rightarrow A$ is characterized by the rate k. The absorbance change $\Delta A_i(t)$ in the band A_i is then given by

$$\Delta A_i(t) = \Delta A_i\{k_L/(k_L+k)\}\{1-\exp[-(k_L+k)t]\}, \qquad (5)$$

where ΔA_i is the maximum absorbance change of band A_i, corresponding to complete photodissociation. If the rebinding rate k is given by a distribution, Eq. (5) must be generalized.

For $k_L \gg k$, Eq. (5) predicts two features: (i) The approach to the steady state at $t = \infty$ is given by k_L. (ii) The steady-state value of the absorbance change, $\Delta A_i(\infty)$, is equal to ΔA_i. At 40K both of these predictions are correct to within about 3%. All A and B bands approach the steady state

with the same kinetics, given by k_L and the steady state values agree with the values shown in Fig. 2. This result verifies that no transitions $A_i \rightarrow A_j$ or $B_i \rightarrow B_j$ take place at 40K. Data at 60K give the same result. At 70K and above, however, A_1 approaches equilibrium much slower than predicted by Eq. (5). The data can be explained if a small fraction of the A_1 substates are pumped into longer-lived states. Observations of all A and B substates rule out transitions from A_1 to other A substates. We discuss an explanation of the observed effect in Subsection 4.5.

(iii) Multiple-flash Experiments. As a third test, we have performed multiple-flash experiments at various temperatures. In these experiments[5,13,14], photodissociation is repeated before all Mb molecules have rebound a ligand. Monitoring of the separate A lines can reveal if pumping from one A substate to another occurs. At 40K, flashes were repeated every 3000 s. No pumping from one A substate to another is observed over the course of 4 flashes.

(iv) Photodissociation After Illumination. In the earlier multiple-flash experiments (monitored in the visible), flashing is repeated at intervals of length τ on the order of 20 times.[5] If transitions from one substate to a longer-lived one occurred with a small probability, say 10^{-3}, or only at times longer than τ, they would not be detected. A different experiment permits the search for such rare transitions: We expose the sample to an intense white light ($k_L \approx 10\ s^{-1}$) for a time t_L varying between 10 s and 10^3s. The light continuously re-photolyzes the rebound CO. At 80K and above more than 50% of the CO molecules rebind within less than 0.1 s and will therefore be re-photolyzed between 10^2 and 10^4 times. At the end of the illumination, the sample is completely photolyzed by a laser pulse and rebinding is measured. Results of such experiments at 30K, 40K, 92K and 139K are given in Fig. 16.

At 30K, a very small increase in long-lived states is seen for t_L = 1100 s. At 40K, pumping is still small. At higher temperatures, rebinding at short times remains unaltered; at 139K, >90% of the photolyzed CO rebind without change in rate. The change in the rebinding curve at long times, however, is dramatic; long-lived substates are greatly enhanced.

In a second set of experiments, a second laser pulse was applied with a delay, t_D, after the end of the illumination. Data at 92K, given in Fig. 17, prove that the protein relaxes toward the initial state after the illumination is terminated. The relaxation is slow, however, and is not finished at time $t_D = t_L$. We interpret these results in terms of a hierarchy of substates in Subsection 4.5.

4. SUMMARY AND INTERPRETATION

The experiments reported in Section 3 answer the main questions raised in the introduction, but also reveal new problems and point to new avenues of investigation. We summarize here the main results and interpret some of the new data.

4.1 Conformational Substates

One of the motivations for the present work was the question raised by the work of B. Chance et al.[15]: Is rebinding bi- or triphasic as originally claimed by Iizuka et al.[31] or is it characterized by a power law?[5] The result of the present work, displayed in Figs. 14 and 15, is unambiguous: Regardless of where rebinding is monitored, the kinetics is smooth and nonexponential over more than 12 orders of magnitude in time. The original reason for introducing the concept of conformational substates is consequently still valid.

The observation of pumping into long-lived states (Figs. 16 and 17) raises, however, the question of whether the arguments rejecting all models with only sequential[32] rather than parallel barriers are still valid. The answer is yes. The multiple-flash technique, described in detail elsewhere[13,14,33] is very sensitive to the difference between homogeneous and inhomogeneous systems and shows that the main components of the system must be inhomogeneous. We will show below in Subsection 4.5 (iv) that the pumping experiments lead to a generalization of our model which can explain all data.

4.2 The Substates in the Heme Pocket

(i) The A Substates. It has been known for a considerable time that CO binds to the heme iron in more than one conformation.[22,23,27,34] Indeed, Fig. 5 shows four different stretching bands and implies four substates, A_0 to A_3. The reversible exchange among the substates down to about 180K, shown in Fig. 6, implies that all bands correspond to folded, undenatured proteins and

can occur within the same molecule. The main properties of the A substates are given in Table 1 and Figs. 6-9.

The spectroscopic data in Section 3 together with the X-ray structure obtained at 260K by Kuriyan et al.[35] permit a tentative structural assignment of A_0 through A_3. Kuriyan et al. find four different orientations ("conformations A, B, C, D") of the bound CO molecule with respect to the heme group, and they refine two of the four. Their conformation C has an occupation of 78% and can therefore be identified with our substate A_1 which has an occupation of 70% at about pH 6 and 260K. With this identification, A_1 has an angle Θ(Fe-C-O) of 141° and points toward C1D, the carbon atom 1 of pyrrole D of the heme group. (The nomenclature is defined in Fig. 2 of Kuriyan et al.[35]) Their conformation D has an occupation of 22%. Fig. 5 shows that A_3 has a fractional intensity of about 25%. We therefore identify D with A_3. A_3 then has an angle Θ = 120° and points in the direction of C4B, a considerable distance away from A_1.

We identify A_0 and at the same time solve an old problem by considering the effect of pH on A_0. Watson and Kendrew[36] pointed out that a water molecule bound to the iron in metMb would be within hydrogen-bonding distance of the distal His 64(E7). Since CO is not very different from a water molecule in size, a hydrogen bond between the oxygen of the CO and His E7 could be expected. Neutron diffraction data by Hanson and Schoenborn[37], however, show no hydrogen bond in MbCO. If A_0 is identified with conformation A of Kuriyan et al., the following picture emerges: Of the four substates, A_0 is closest to His E7 and can form a hydrogen bond with N^{ϵ} if His E7 is protonated. If His E7 is the heme-linked protonation group with pK = 5.7 observed in optical and NMR measurements[38,39] we expect CO in the substate A_0 to be fully hydrogen-bonded to His E7 well below pH 5.7 and the hydrogen bond

to be absent well above pH 5.7. The data in Table 1 and in Fig. 9 support this expectation. At pH 5, substate A_0 is more tightly bound than A_1 by about 8 kJ/mol, and at pH 6.8 it is more tightly bound by about 4 kJ/mol. The difference, 4 kJ/mol, is consistent with a weak hydrogen bond. Additional evidence for the identification of A_0 comes from the angle $\theta = 154°$ for conformation A which is similar to the angle found in chelated protoheme-CO.[40] Heme carbonyls typically[41] have CO stretching frequencies near 1970 cm^{-1}, similar to the value for A_0. The fact that no hydrogen bond is seen in the neutron diffraction data is explained by the low intensity of substate A_0 at room temperature and the absence of protonated His E7 near neutral pH. To test the assignments directly, the intensities of the IR bands and the X-ray conformations should be measured on the same crystal at a pH for which A_0 is sufficiently populated. Moreover, additional pH studies are needed to determine whether the four bands correspond to four distinct orientations or two bands correspond to the protonated and deprotonated forms of a single orientation.

We summarize the complete assignment in Table 3 where we also include the van der Waals energies calculated by Kuriyan et al.[35] Table 3 shows that the calculated binding energies are close to the relative enthalpies found here but are generally larger. In reality, the difference in occupation is determined as much by the relative entropies as by the binding enthalpies.

(ii) Interpretation of the B Substates. The IR spectrum of the CO stretching modes in the photodissociated state B is shown in Fig. 1b. Above 20K only two bands, B_0 and B_1, are unambiguously observed. B_0 binds to substate A_3 and B_1 to A_1. At present, no X-ray diffraction data are available on the photodissociated CO, so no steric interpretation of the B substates can be given. The fact that no exchange among B_0 and B_1 is observed below about 180K suggests that each is sterically close to the corresponding A substate.

4.3 CO Binding at Low Temperatures

(i) Binding Pathways. Each Mb molecule possesses four different pathways within the pocket for CO binding. In 75% glycerol-water, there is no exchange among the four channels below about 170K; above 180K transitions $A_i \rightarrow A_j$ and presumably $B_i \rightarrow B_j$ occur. The kinetics of each of the four pathways is nonexponential in time below about 180K, as shown in Figs. 14 and 15. Each is governed by different barrier parameters as given in Table 2.

The data provide no evidence for discrete way-stations or "docking" within the heme pocket as postulated by B. Chance et al.[42] The substate B_2 decays quickly to B_1 at 20K and above[8], long before any appreciable rebinding occurs. B_1 binds to substate A_1 with essentially the same kinetics as observed in the visible. Above 20K, no intermediate substates appear in either the bound or the photodissociated CO bands.

(ii) Reaction Theory. The data in Table 2 imply that both entropic and enthalpic factors control the binding reaction at the heme iron. A_0 and A_1 both have about the same peak activation enthalpy H_{peak}; the faster binding rate of A_0 relative to A_1 is caused by the larger preexponential factor, A_{BA}. A_3 has a slightly larger preexponential than A_1, but has a slower binding rate owing to a much larger peak activation enthalpy. An explanation of these characteristics in terms of the pocket structure and of specific residues will require detailed studies of binding rates as a function of pH and with modified myoglobins.

The parameters listed in Tables 1 and 2 show a Brønsted correlation[43]: The most tightly bound substate, A_0, binds fastest and the most weakly bound, A_3, binds slowest. The same correlation is found for different heme proteins where the one with the most tightly bound ligand has the smallest activation enthalpy barrier.[44] Such a correlation is expected for an "overcoupled"

transition, where an increase in the well depth for the covalently bound state A leads to a decrease in the barrier between the pocket state B and A. The experimental result consequently demonstrates that CO binding to many heme proteins, in particular Mb, is "overcoupled" and not "undercoupled".[45]

4.4 Influence of the Environment and Control

From the biological point of view, the most important feature of our data is the exquisite sensitivity of the occupation of the substates in the pocket to external parameters such as pH (Fig. 12), pressure (Fig. 11), and solvent state (Figs. 2-4).[22,27] Earlier we found that the association rate of CO to Mb increases with decreasing pH and follows a Henderson-Hasselbalch equation with pK = 5.7.[46] The present data provide more insight into the pH dependence; a change in pH can not only affect the kinetics of an individual pathway, but can also shift the system from one pathway to another. Such shifts also occur on changes in pressure and solvent state. Three conclusions may be drawn from these experiments: (i) Processes in the heme pocket are extremely responsive to external influer es. (ii) IR observation of ligand binding is a tool well suited for the investigation of the effect of external parameters. (iii) The sensitivity of the processes in the heme pocket to external parameters may be used in vivo for the control of protein reactions, for example in membrane proteins through changes in membrane viscosity and composition, and in hemoglobin through quaternary changes. In all processes, entropy may play a more important role than enthalpy, as is suggested by Table 2.

4.5 Protein Dynamics and Models

The sensitivity of the IR stretching bands to the conformation of the protein makes them excellent probes for investigating protein dynamics and models. We sketch the background for such investigations and describe the conclusions that emerge from the experiments reported in Section 3.

(i) The Hierarchy of Conformational Substates (CS). A model with a single set of CS is not capable of explaining all experiments. On the one hand, rebinding in a 75% glycerol-water solvent is nonexponential up to at least 170K[28], and pressure titration experiments prove that transitions among the CS responsible for the nonexponential kinetics occur only above about 180K.[47] On the other hand, evidence for slow transitions among substates even at 80K comes from X-ray diffraction: The Debye-Waller factor of many atoms changes appreciably down to 80K.[48,49] Studies of the rearrangement of the protein structure after photodissociation ("proteinquake") demonstrate that a hierarchy of motions exists and that protein conformations can be classified into a hierarchy of substates.[17,50] We draw in Fig. 18 the hierarchy of CS as modified by the results of the present work.

Figure 18 represents the conformational energy of MbCO drawn for various tiers as function of a conformational coordinate (cc). The energy valley in the top diagram represents MbCO. The observation of four CO stretching bands implies that MbCO can exist in four distinct substates of the zeroth tier (CS^0), A_0 to A_3. The nonexponential rebinding kinetics observed for each band suggests that the actual energy surface for each CS^0 consists of a large number of conformational substates of the first tier, CS^1. Each of these again is subdivided into a large number of substates of the second tier, CS^2. The furcation continues, but the lower tiers are not relevant for the present discussion.

At rest, a protein will not remain in one CS, but equilibrium fluctuations (EF) will move the protein from CS to CS. The rates of the EF depend strongly on temperature and environment. In 75% glycerol-water, only EF2 (and EF3...) take place below about 170K, but each protein remains frozen in a particular CS^1. Above about 180K, EF1 occur and the protein fluctuates

rapidly from one CS^1 to another. After photodissociation of MbCO, proteins relax from one state (MbCO) to another (Mb) through a sequence of functionally important motions (fims).[17]

(ii) Relaxation of the A Substates. In a 75% glycerol-water solvent, the behavior of the A substates undergoes a change near 180K. The CS^0 no longer interconvert (Fig. 6), the band frequency ν_{CO} shifts, and the linewidth changes. We interpret these features in terms of the CS^1. If the large-scale motions of the proteins are absent, the controlling sidechains within the pocket may be prevented from fluctuating, thereby stopping transitions among the CS^0. This explanation also accounts for the large change in the linewidth Γ of band A_0 in Fig. 9. At pH 5 almost all of the His E7 are protonated and therefore most of the CO in state A_0 are hydrogen bonded. Below about 180K, the motion of His E7 and therefore also the motion of the CO is restricted, leading to a narrow band. Above 180K, the sidechain motion may also force the CO to large excursions, leading to a large Γ. At pH 6.8, approximately 10-20% of the CO are hydrogen bonded to His E7 and these may account for the smaller increase in Γ above 180K.

(iii) Slaved Glass Transition. Mb in 75% glycerol-water possesses a remarkable transition between about 180 and 200K as discussed in (ii). The transition occurs in an interval of about 20K (Figs. 6 and 8) and approach to equilibrium is nonexponential in time (Fig. 10). These characteristics are similar to the ones observed in glass and spin glass transitions. Glasses (amorphous solids)[51,52,53] and spin glasses[54] are disordered and frustrated[55] systems that are believed to have a highly degenerate (many-valley) ground state.[56] The transition to the glass or spin-glass state occurs in a finite temperature range and is nonexponential in time.[57,58] Because proteins are disordered and most likely frustrated systems[18] with many energy valleys

(Fig. 18) we expect a transition similar to a glass or spin-glass transition. The transition near 180K satisfies all the requirements.

This transition manifests one property not encountered in glasses: It depends crucially on the solvent surrounding the protein. In 75% glycerol-water, the transition is at approximately 180K (Fig. 8). The solvent undergoes a glass transition at essentially the same temperature (Fig. 13).[59,60] In water, the transition is near 260K, close to the melting point of the buffered solvent (Fig. 6). In solid PVA, no transition in MbCO is apparent up to at least 300K, although the ratio A_3/A_1 decreases gradually above 100K. The observations imply that the EF1, the fluctuations of the CS^1, are suppressed when the protein surrounding is frozen or solid. The motions of the first tier thus are "slaved" to the motions of the solvent and we consequently call the transition a "slaved glass transition."

The slaved glass transition is not a property of the protein alone; protein and solvent together must be considered as one system. The hydration shell of the protein most likely plays a crucial role both in the glass transition and in the function of the protein.[27,61,62] Studies of the hydration water in Mb solutions and crystals by calorimetry and IR spectroscopy show a broad glass transition between 180 and 270K which depends on the degree of hydration.[63]

(iv) Pumping and Substate Symmetry Breaking. The results in Figs. 16 and 17 appear at first to call for a new explanation of the nonexponential kinetics. We show here, however, that an extension of our earlier model explains the pumping into long-lived states. In that model[5] we ascribe the nonexponential kinetics to a distribution of activation enthalpies, characterized by the probability density $g(H_{BA})$ as given for the binding of CO to Mb in Fig. 19a. Each substate CS^1 of the first tier in Fig. 18 is characterized

by a unique H_{BA}. Different CS^1 thus have different properties: the energy valleys of the first tier are not identical and we call this property "substate symmetry breaking". At this level of substate symmetry breaking the substates of the second tier, CS^2, have no effect on the activation energy for covalent bond formation. Experiments suggest that this assumption may be incorrect. The nonexponential relaxation in tier 2 seen in the proteinquake experiment[17] and the temperature dependence of the Debye-Waller factor below 180K[48,49] imply that different CS^2 have different physical properties. The substate symmetry thus is also broken in the second tier, and we assume that different CS^2 have different barriers for the binding step B → A. The CS^1 determine the barrier crudely, while the CS^2 fine-tune the barrier. We represent the situation in Fig. 19b. Within each CS^1, the CS^2 determine a range of activation enthalpies. The distribution of the barriers within a given CS^1 is indicated by the solid curves, and the overall distribution as determined by the CS^1 is given by the dashed envelope.

A possible explanation of the pumping observed in Figs. 16 and 17 is now straightforward. Since the CS^1 are frozen below 180K, we only have to consider a given CS^1. Fig. 20 gives a schematic representation of the barriers for the binding step B → A as a function of a conformational coordinate cc2 of the second tier. The two coordinates have a very different meaning. The conformational coordinate cc2 describes the protein structure within a given CS^1; shown are three substates of the second tier, labelled by a, b, and c. The reaction coordinate rc describes the transition of the CO from the pocket (B) to the covalently bound state at the iron (A). The potentials along the reaction coordinate for fixed cc2 are drawn as dashed lines. If the system is initially in a, the lowest CS^2, photodissociation will move it to a'. The system can now either rebind, B → A, without change

in cc2, or it can relax to another CS^2 of lower Gibbs energy, for instance b'. We have studied the relaxation to lower CS^2 through fim 2 in detail and have found that it is nonexponential in time and extends over extremely large ranges in time.[17] In states b' and c', the barrier B → A may either be higher or lower than in a'. If it is lower, the system will rapidly return to b and from there relax to a. If it is higher, the system will stay longer in B and this behavior appears as pumping. The shift to longer rebinding times is caused by a relaxation in the protein coordinate[64] and not by a longer-lived intermediate state between B and A. The model explains both the pumping seen in Fig. 16 and the relaxation in Fig. 17. Relaxation occurs if the system is first pumped into long-lived CS^2, some of which rebind in the dark from, say, c' to c. From there it will relax toward a, the lowest CS^2. A flash at a later time explores the degree of relaxation.

A theory of pumping remains to be constructed, but simple estimates indicate that the relaxation times and enthalpies observed are consistent with our earlier experiments.[17] Consider the pumping observed at 30K in Fig. 16. The absorbance scale is greatly expanded. The rate at N(t) = 0.95 changes by a factor of 2 after illuminating for 1100 s. This rate change corresponds to a shift of $\delta H_A^B \approx RT \ln 2 \approx 0.17$ kJ/mol. Since $g(H_{BA})$ extends from 5 to 25 kJ/mol, such a small shift is not even visible in Fig. 19 and it is reasonable to attribute it to substates of the second tier. At 139K, the largest time-shift in Fig. 16 corresponds to an enthalpy shift of $\delta H_{BA} \approx 8$ kJ/mol. This shift will change the distribution, but is still reasonable. Times and temperatures seen in pumping experiments are also consistent with fim 2 values. Recent measurements on fim 2 (unpublished) indicate that it starts already at 30K and extends to much longer times than shown in ref. 17.

4.6 Remarks and Outlook

(i) The IR Bands as Tools. The experiments described and evaluated here demonstrate that IR spectra, when studied as a function of time, temperature, solvent, and pressure, provide a powerful tool for studies of protein dynamics and protein function. Nearly all investigations here mark a beginning, and extensions to shorter times, other systems, and other solvents are likely to yield even richer information.

(ii) The Chance Experiment. B. Chance et al.[15] have made two claims, that CO rebinding to Mb is bi- or triexponential at 40K and that they can pump short-lived into long-lived states. Fig. 14 proves that the first claim is incorrect; data extended to 10^5s show no evidence for individual components. The second claim has to be discussed in more detail because of our new evidence for a small amount of pumping at 40K in Fig. 16. Chance et al. use a very weak pump light, adjusted so that on the average about 50% of the MbCO are photolyzed. Fig. 14 shows that N(t) at 40K drops 50% by about $5 \cdot 10^4$s. Thus in the Chance experiment, equilibrium can occur only for illumination times much greater than $5 \cdot 10^4$s. Owing to the large distribution of flashoff rates k_L through the thick sample, a time-dependent, nonequilibrium distribution of recombination rates is established in the sample. In the Chance et al. experiment, the relative amplitude of the slow components is enhanced by up to a factor of two resulting in apparent pumping. Their result, therefore, can be explained without pumping in a straightforward way; it is caused by the combination of weak pump light, thick sample, nonexponential kinetics, and adjustment to about 50% photolysis. A computer simulation of this combination, based on the generalization of Eq. (5), reproduces the apparent pumping.

(iii) Theories. A goal of protein dynamics studies is a theory that classifies and describes protein states and protein motions. Remarkable progress toward this goal has been made with molecular dynamics computations, particularly by Karplus and collaborators.[65] Elber and Karplus[66] have verified the existence of multiple energy valleys with a 300 ps simulation. One unsolved question in such calculations concerns the level of substates that are reached. Comparison of the timescales simulated with the ones involved in the various tiers of substates[17] suggests that molecular dynamics explores many of the substates of tier 2, but cannot yet reach tier 1.

A second theoretical approach is based on ultrametricity.[56] We have proposed that the arrangement of the substates as shown in Fig. 18 suggests ultrametricity.[17] Elber and Karplus have approached this problem with molecular dynamics[66] and find no evidence for ultrametricity. Since they investigate the distance matrix and we propose ultrametricity in the space of conformational energy, no disagreement between the two models exists yet. One possible problem regarding ultrametricity is raised by Fig. 18: We have assigned the zeroth tier, CS^0, to the four A substates. Such an assignment is certainly correct below the glass temperature where no exchanges among the A substates take place. Above the glass temperature, however, both the CS^0 and CS^1 interchange, and it is no longer clear how to classify and order these substates. Additional investigations, both experimental and theoretical, may shed new light on these aspects of protein states and motions.

ACKNOWLEDGMENTS

We gratefully acknowledge the technical assistance of Stanley Luck and Rahul Pandharipande. Neil Alberding, Sam Bowne, Al Reynolds, and Erramilli Shyamsunder conducted some of the preliminary FTIR experiments. We thank Jim Alben, Anders Ehrenberg, Joel Friedman, John Kuriyan, Greg Petsko, Denis Rousseau, Benno Schoenborn, Ken Suslick, and Peter Wolynes for illuminating discussions and advice. We thank Mary Ostendorf for her many efforts and technical assistance in preparing the manuscript. RDY wishes to thank Illinois State University for research support. This work was supported in part by the U.S. National Institute of Health grants GM 18051 and GM 32455, by the National Science Foundation grant DMB 82-09616, and by the Office of Naval Research grant N00014-86-K-00270.

REFERENCES

1. E. Antonini and M. Brunori, Hemoglobin and Myoglobin in Their Reactions with Ligands (North-Holland, Amsterdam, 1971).
2. R. H. Austin, K. Beeson, L. Eisenstein, H. Frauenfelder, I. C. Gunsalus, and V. P. Marshall, Phys. Rev. Letters 32 (1974) 403.
3. B. Chance, B. Schoener, and T. Yonetani, in: Oxidases and Related Redox Systems, eds T. E. King, H. S. Mason, and M. Morrison (Wiley, New York, 1965) p. 609.
4. R. H. Austin, K. Beeson, L. Eisenstein, H. Frauenfelder, I. C. Gunsalus, and V. P. Marshall, Science 181 (1973) 541.
5. R. H. Austin, K. W. Beeson, L. Eisenstein, H. Frauenfelder, Biochemistry 14 (1975) 5355.
6. N. Alberding, R. H. Austin, K. W. Beeson, S. S. Chan, L. Eisenstein, H. Frauenfelder, and T. M. Nordlund, Science 192 (1976) 1002.
7. J. O. Alben, D. Beece, S. F. Bowne, L. Eisenstein, H. Frauenfelder, D. Good, M. C. Marden, P. P. Moh, L. Reinisch, A. H. Reynolds, and K. T. Yue, Phys. Rev. Letters 44 (1980) 1157.
8. J. O. Alben, D. Beece, S. F. Bowne, W. Doster, L. Eisenstein, H. Frauenfelder, D. Good, J. D. McDonald, M. C. Marden, P. P. Moh, L. Reinisch, A. H. Reynolds, E. Shyamsunder, and K. T. Yue, Proc. Natl. Acad. Sci. USA 79 (1982) 3744.
9. F. G. Fiamingo and J. O. Alben, Biochemistry 24 (1985) 7964.
10. L. Stryer, Biochemistry (Freeman and Co., San Francisco, 1981).
11. K. Gerwert, R. Rodriguez-Gonzalez, and F. Siebert, in: Time-Resolved Vibrational Spectroscopy, eds. A. Laubereau and M. Stockburger (Springer, Berlin, 1985) p. 263.
12. M. Chance, B. Campbell, and J. Friedman, Biophys. J. 51 (1987) 291a.

13. H. Frauenfelder, in: Methods in Enzymology, Vol. 54, eds. S. Fleischer and L. Packer (Academic Press, New York, 1978) p. 506.

14. H. Frauenfelder, in: Structure and Dynamics: Nucleic Acids and Proteins, eds. E. Clementi and R. H. Sarma (Adenine, Guilderland, NY, 1983) p. 369.

15. B. Chance, L. Powers, Y.-H. Zhou, and A. Naqui, Bull. Am. Phys. Soc. 31 (1986) 386; B. Chance, L. Powers, C. Zhou, A. Naqui, and M. Chance, Biophys. J. 49 (1986) 537a; B. Chance, Y.-H. Zhou, K. S. Reddy, and L. Powers, Fed. Proc. 45 (1986) 1641.

16. H. Frauenfelder, G. A. Petsko, and D. Tsernoglou, Nature 280 (1979) 558.

17. A. Ansari, J. Berendzen, S. F. Bowne, H. Frauenfelder, I. E. T. Iben, T. B. Sauke, E. Shyamsunder, and R. D. Young, Proc. Natl. Acad. Sci. USA 82 (1985) 5000.

18. D. Stein, Proc. Natl. Acad. Sci. USA 82 (1985) 3670.

19. A. Ansari, J. Berendzen, D. Braunstein, B. R. Cowen, H. Frauenfelder, M. K. Hong, I. E. T. Iben, P. Ormos, T. B. Sauke, A. Schulte, P. J. Steinbach, and R. D. Young, Biophys. J. 51 (1987) 289a; two additional, related abstracts also appear in this issue of Biophys. J.

20. W. A. Eaton and J. Hofrichter, in: Methods in Enzymology, Vol. 76, eds. S. Colowick and E. Antonini (Academic Press, New York, 1981) p. 175.

21. M. W. Makinen and A. K. Churg, in: Iron Porphyrin Part One, eds. A. B. P. Leyer and H. B. Gray (Addison-Wesley, Reading, MA, 1982) p. 141.

22. M. W. Makinen, R. A. Houtchens, and W. S. Caughey, Proc. Natl. Acad. Sci. USA 76 (1979) 6042.

23. W. Caughey, H. Shimada, M. G. Choc, and M. P. Tucker, Proc. Natl. Acad. Sci. USA 78 (1981) 2903.

24. B. L. Roberts, R. A. J. Riddle, and G. T. A. Squier, Nuclear Instr. and Meth. 130 (1975) 559.

25. C. J. Batty, S. D. Hoath, and B. L. Roberts, Nuclear Instr. and Meth. 137 (1976) 179.

26. L. Cordone, A. Cupane, M. Leone, and E. Vitrano, Biophys. Chem. 24 (1986) 259.

27. W. E. Brown III, J. W. Sutcliffe, and P. D. Pulsinelli, Biochemistry 22 (1983) 2914.

28. D. D. Dlott, H. Frauenfelder, P. Langer, H. Roder, and E. E. DiIorio, Proc. Natl. Acad. Sci. USA 80 (1983) 6239.

29. R. D. Young and S. F. Bowne, J. Chem. Phys. 81 (1984) 3730.

30. F. Stetzkowski, R. Banerjee, M. C. Marden, D. K. Beece, S. F. Bowne, W. Doster, L. Eisenstein, H. Frauenfelder, L. Reinisch, E. Shyamsunder, and C. Jung, J. Biol. Chem. 260 (1985) 8803.

31. T. Iizuka, H. Yamamoto, M. Kotani, and T. Yonetani, Biochim. Biophys. Acta 371 (1974) 126.

32. M. Marden, Eur. J. Biochem. 128 (1982) 399.

33. K. T. Yue, Ph.D. Thesis, University of Illinois at Urbana-Champaign, USA (1983).

34. S. McCoy and W. S. Caughey, in: Probes of Structure and Function of Macromolecules and Membranes, Vol. 2, eds. B. Chance, T. Yonetani and A. S. Mildvan (Academic Press, New York, 1971) p. 289.

35. J. Kuriyan, S. Wilz, M. Karplus, and G. A. Petsko, J. Mol. Biol. 192 (1986) 133.

36. H. C. Watson and J. C. Kendrew, Nature 190 (1961) 670.

37. J. C. Hanson and B. P. Schoenborn, J. Mol. Biol. 153 (1981) 117.

38. Y. Hayashi, H. Yamada, and I. Yamazaki, Biochim. Biophys. Acta 427 (1976) 608.

39. G. N. La Mar, D. L. Budd, H. Sick, and K. Gersonde, Biochim. Biophys. Acta 537 (1978) 270.

40. A. Bianconi, A. Congiu-Castellano, M. Dell'Ariccia, A. Giovannelli, E. Burattini, P. J. Durham, G. M. Giacometti, and S. Morante, Biochim. Biophys. Acta 831 (1985) 114.

41. J. O. Alben and W. S. Caughey, Biochemistry 7 (1968) 175.

42. L. Powers, B. Chance, A. Naqui, Y.-H. Zhou, and M. Chance, Biophys. J. 51 (1987) 290a; B. Chance, Bull. Am. Phys. Soc. 32 (1987) 429.

43. L. I. Krishtalik, Charge Transfer Reactions in Electrochemical and Chemical Processes (Consultants Bureau, New York, 1986).

44. N. Alberding, S. S. Chan, L. Eisenstein, H. Frauenfelder, D. Good, I. C. Gunsalus, T. M. Nordlund, M. F. Perutz, A. H. Reynolds, and L. B. Sorensen, Biochemistry 27 (1978) 43.

45. R. F. Goldstein and W. Bialek, Comments Mol. Cell. Biophys. 3 (1986) 407.

46. W. Doster, D. Beece, S. F. Bowne, E. E. DiIorio, L. Eisenstein, H. Frauenfelder, L. Reinisch, E. Shyamsunder, K. H. Winterhalter, and K. T. Yue, Biochemistry 21 (1982) 4831.

47. L. Eisenstein and H. Frauenfelder, in: Frontiers of Biological Energetics: Electrons to Tissues, Vol. 1, eds. L. P. Dutton et al. (Academic Press, New York, 1979) p. 680.

48. H. Hartmann, F. Parak, W. Steigemann, G. A. Petsko, D. Ringe Ponzi, and H. Frauenfelder, Proc. Natl. Acad. Sci. USA 79 (1982) 4967.

49. F. Parak, H. Hartmann, K. D. Aumann, H. Reuscher, G. Rennekamp, H. Bartunik, and W. Steigemann, J. Mol. Biol., in press.

50. H. Frauenfelder and R. D. Young, Comments Mol. Cell Biophys. 3 (1986) 347.

51. J. M. Ziman, Models of Disorder (Cambridge University Press, Cambridge, 1979).

52. R. Zallen, The Physics of Amorphous Solids (John Wiley, New York, 1983).

53. J. Jäckle, Rep. Progr. Phys. 49 (1986) 171.

54. K. Binder and A. P. Young, Rev. Mod. Phys. 58 (1986) 801.

55. G. Toulouse, Commun. Phys. 2 (1977) 115.

56. R. Rammal, G. Toulouse, and M. A. Virasoro, Rev. Mod. Phys. 58 (1986) 765.

57. G. W. Scherer, Relaxation in Glass and Composites (John Wiley, New York, 1986).

58. O. Beckman, Festkörperprobleme 25 (1985) 233.

59. R. L. Bohon and W. T. Conway, Thermochimica Acta 4 (1972) 321.

60. P. L. Kuhns and M. S. Conradi, J. Chem. Phys. 77 (1982) 1771.

61. V. I. Goldanskii and Yu. F. Krupyanskii, in: Proceedings of the International Conference on the Applications of the Mössbauer Effect, Vol. 1 (Gordon and Breach, New York, 1985) p. 83.

62. G. P. Singh, F. Parak, S. Hunklinger, and K. Dransfeld, Phys. Rev. Lett. 47 (1981) 685.

63. W. Doster, A. Bachleitner, R. Dunau, M. Hiebl, and E. Lüscher, Biophys. J. 50 (1986) 213.

64. N. Agmon and J. J. Hopfield, J. Chem. Phys. 78 (1983) 6947.

65. M. Karplus and J. A. McCammon, Ann. Rev. Biochem. 52 (1983) 263.

66. R. Elber and M. Karplus, Science 235 (1987) 318.

TABLE 1

Relative binding parameters of the A substates.

R is the gas constant. Solvent: 75% glycerol/water.

Substate	H_A(kJ/mol)		S_A/R	
	pH 6.8	5.	6.8	5.
A_0	-4	-8	-5	-7
A_1	0	0	0	0
A_3	2	2	0	0

TABLE 2

Barrier parameters for CO binding to A Substates.

Substate	H_{peak} kJ/mol	$\log[A_{BA}(100K)/s^{-1}]$
A_0	10	10.8
A_1	9.5	9.3
A_3	18	9.8
Soret (440nm)	10.1	9.0

TABLE 3

The values for ν_{CO} refer to a 75% glycerol-water solvent, pH 6.8, and 240K. The conformations and their properties are from Kuriyan et al.[35], at 260K and pH 6. Φ and Θ characterize the CO conformation; Φ is the dihedral angle between the Fe-C-O and the Fe-C-NC planes; Θ is the angle Fe-C-O.[35]

Substate	ν_{CO} cm^{-1}	H_A kJ/mol	Conformation	E_{vdW}[35] kJ/mol	Φ	Θ
A_0	1966	-4	A	-12	20°	154°
A_1	1945	0	C	-12	60°	141°
A_2	1941	-	(B)	+25	93°	120°
A_3	1930	2	D	+4	-62°	120°

FIGURE CAPTIONS

1 The spectral range where rebinding is monitored. (a) shows the absorption spectra of Mb (dotted line) and MbCO (solid line) in the Soret, the α and β, and the near-IR regions. Arrows indicate where we have measured rebinding in the flash photolysis experiments. (b) gives the IR difference spectrum (Mb-MbCO).

2 Temperature-dependent IR spectrum of the CO stretching bands of MbCO. Solvent: 75% glycerol-water; pH 6.8.

3 Temperature-dependent IR spectrum of the CO stretching bands in MbCO. Solvent: water; pH 6.7.

4 Temperature-dependent IR spectrum of the CO stretching bands in MbCO. Solvent: solid poly(vinyl)alcohol (PVA); pH 7.0.

5 Voigtian decomposition of the MbCO IR spectrum into four A substates at 10K and 240K. Solvent: 75% glycerol-water; pH 6.8.

6 Plots of (a) (A_0/A_1) and (b) A_3/A_1 versus $10^3/T$. A_j/A_1 is the ratio of the areas of the stretching bands in the bound states A_j and A_1. Below 180K, the ratios change little.

7 Temperature-dependent area of the CO stretching bands in MbCO.

8 Temperature dependence of the peak frequency of the CO stretching bands A_0 and A_1 in 75% glycerol-water at pH 5.0 and pH 6.8.

9 Temperature dependence of the line widths (full width at half maximum) of the A substates. Solvent: 75% glycerol-water; pH 6.8.

10 Approach to equilibrium of substate A_0 after a change in temperature from 195K to 190K. $n_0(t)$ denotes the fraction of MbCO that have not reached equilibrium in substate A_0 at the time t after the temperature change.

11 The CO stretching frequencies of MbCO at 0.1 MPa, 50 MPa, 100 MPa (1 MPa = 9.9 atm). Solvent: 75% glycerol-water; 0.25 M Tris-HCl buffer; pH 6.1.

12 The CO stretching frequencies of MbCO in 75% glycerol-water at various values of pH.

13 IR spectrum of 75% glycerol-water solvent as a function of temperature.

14 Rebinding Mb + CO → MbCO at 40K. ◇ : 440 nm; ∇: Integrated areas of the A bands; O: Integrated area in the Soret region, 400-450 nm; □ : Integrated area of the 760 nm band. The individual rebinding curves have not been matched but have been normalized independently.

15 Rebinding to the substate (a) A_0, (b) A_1, and (c) A_3 as a function of time at various temperatures. ●: mid-IR flash photolysis data. ■ : FTIR data. The solid lines are the fits to the data using Eqs. (3) and (4) and a gamma distribution for $g(H_{BA})$. The fit parameters H_{peak} and A_{BA} are listed in Table 2. Solvent: 75% glycerol-water; pH 6.8.

16 Rebinding after illumination. The MbCO sample is illuminated by an intense white light for t_L seconds before being photodissociated by a laser flash. Note the expanded scale for the absorbance change in (a). In (b) the lines have been drawn through each data point. Marker symbols have been omitted to avoid clutter.

17 Photodissociation after a delay t_D following illumination for t_L = 1110s. Normal 92K rebinding kinetics (t_L = 0, t_D = 0) is included for comparison. Lines have been drawn through each data point. Solvent: 75% glycerol-water; pH 7.0.

18 Hierarchical arrangement of conformational substates (CS) in Mb. The conformational energy G is drawn as a function of a conformational coordinate. The two lowest tiers, CS^3 and CS^4, are omitted.

19 (a) Activation enthalpy distribution $g(H_{BA})$ determined entirely by conformational substates of the first tier. (b) The overall distribution, the dashed envelope, is determined by the substates of the first tier; the substates of the second tier provide the fine-tuning represented by the narrow solid distributions.

20 Rebinding within one conformational substate of the first tier. The diagram shows the energy surfaces as a function of the conformational coordinate cc2 and the reaction coordinate rc. Details are given in the text.

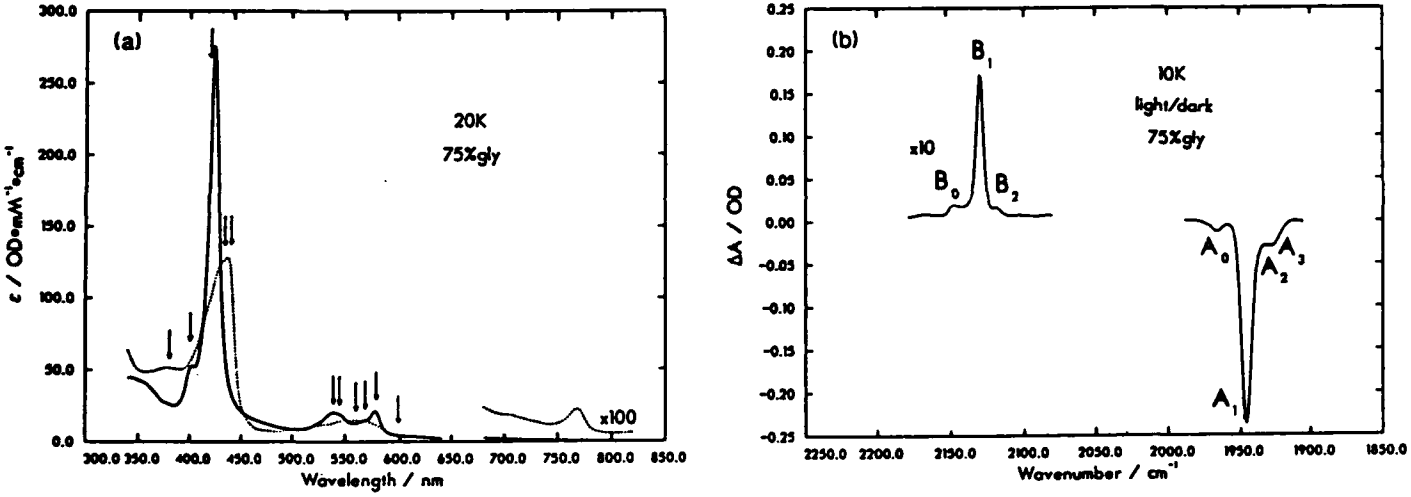
(a)
20K
75%gly
x100
ε / OD mM⁻¹ cm⁻¹
Wavelength / nm
(b)
B1
B0
B2
x10
10K
light/dark
75%gly
A0
A1
A2
A3
ΔA / OD
Wavenumber / cm⁻¹

Fig 1

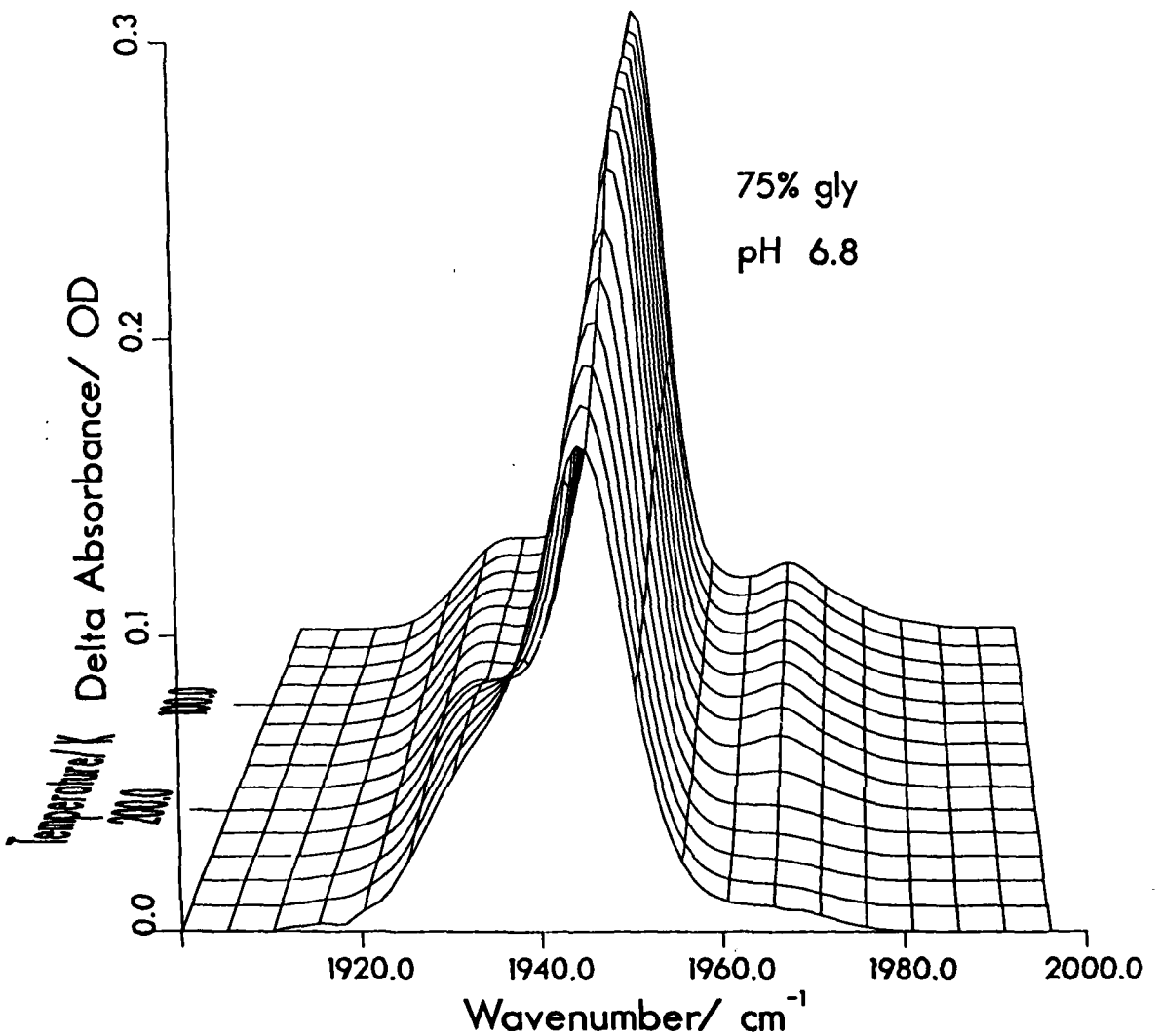
75% gly
pH 6.8
Delta Absorbance/ OD
0.0
0.1
0.2
0.3
1920.0
1940.0
1960.0
1980.0
2000.0
Wavenumber/ cm^{-1}

Fig. 2

Fig. 3

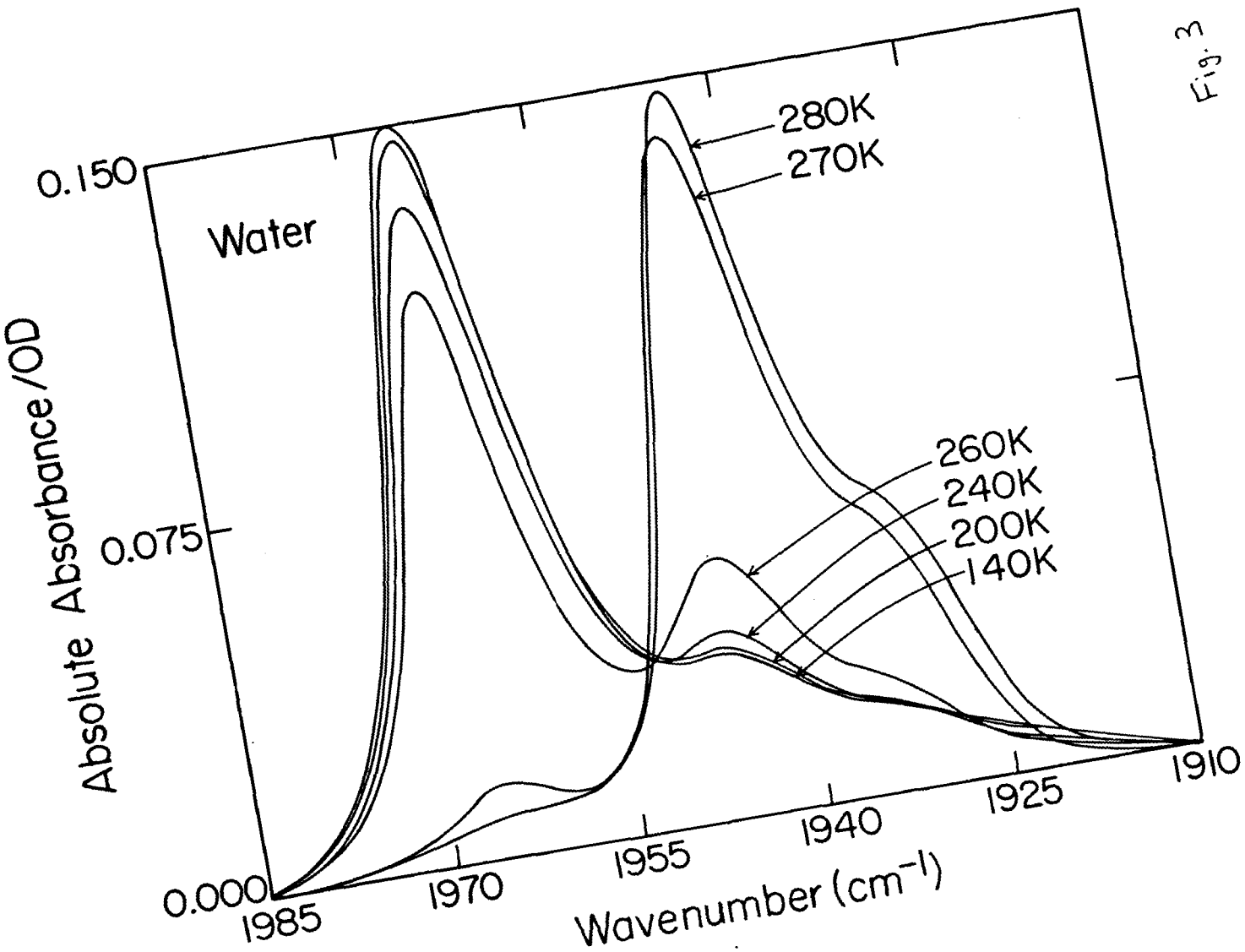
Water
280K
270K
260K
240K
200K
140K
0.150
0.075
0.000
Absolute Absorbance /OD
1985
1970
1955
1940
1925
1910
Wavenumber (cm⁻¹)

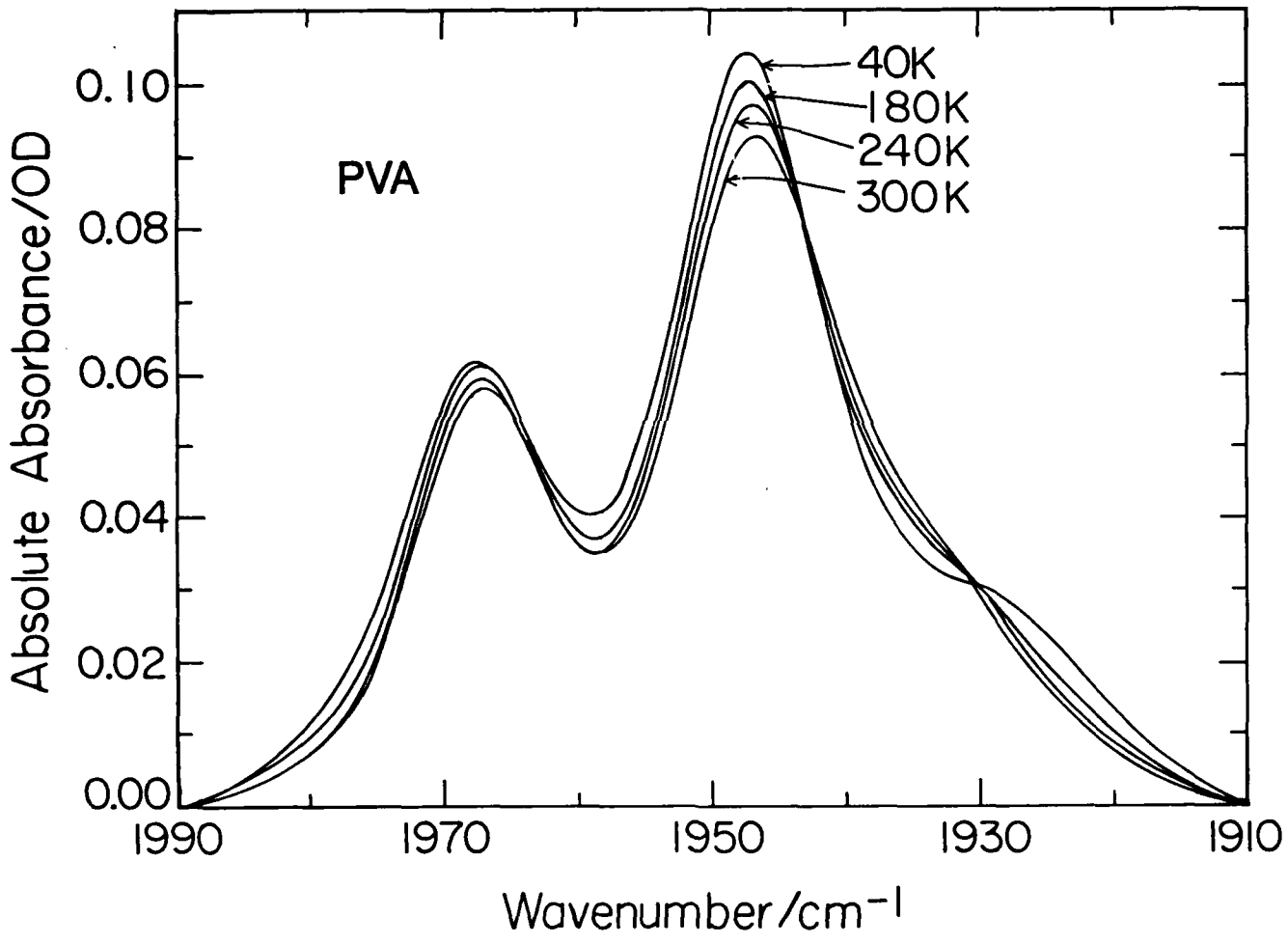
PVA
40K
180K
240K
300K
Absolute Absorbance/OD
0.10
0.08
0.06
0.04
0.02
0.00
1990
1970
1950
1930
1910
Wavenumber/cm⁻¹

Fig. 4

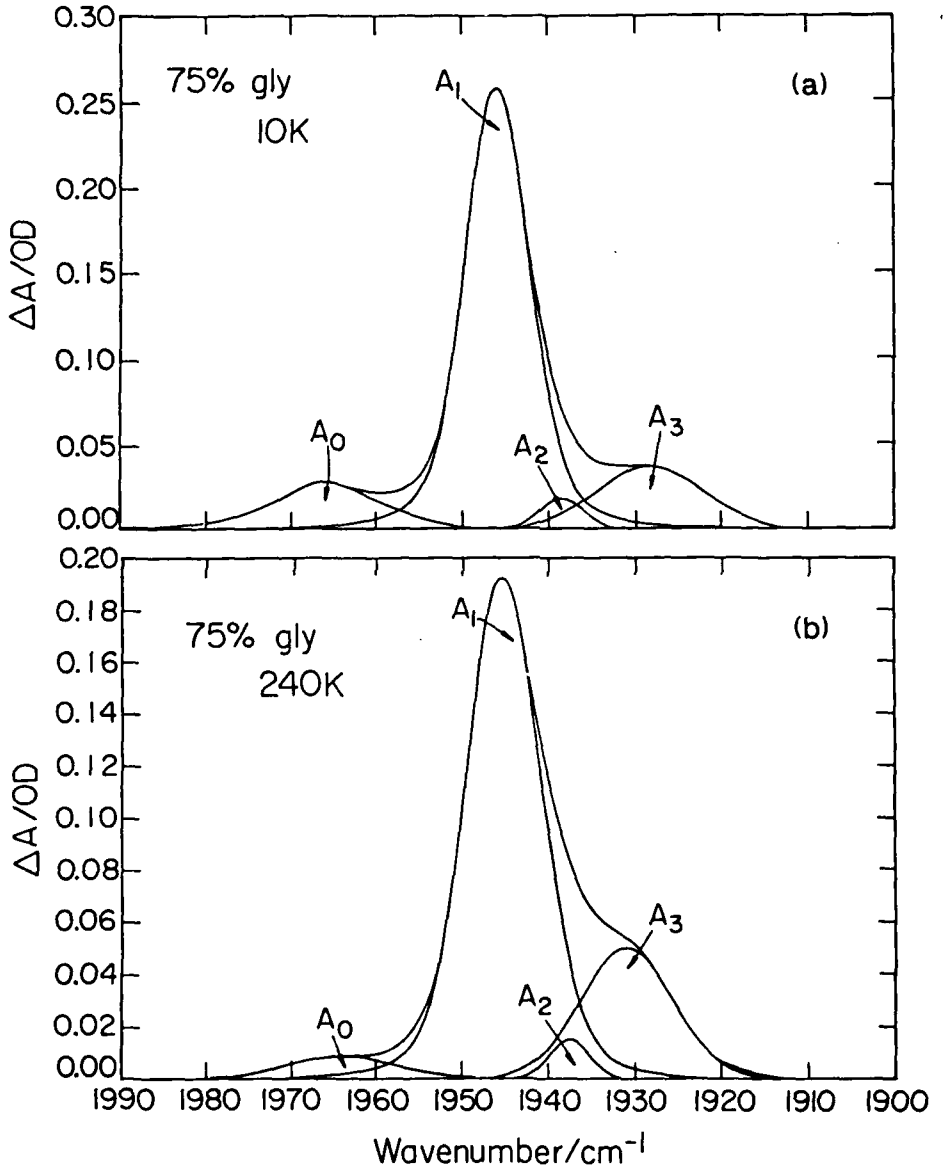
75% gly
10K
(a)
A1
A0
A2
A3
ΔA/OD
0.30
0.25
0.20
0.15
0.10
0.05
0.00
75% gly
240K
(b)
A1
A3
A2
A0
ΔA/OD
0.20
0.18
0.16
0.14
0.12
0.10
0.08
0.06
0.04
0.02
0.00
1990 1980 1970 1960 1950 1940 1930 1920 1910 1900
Wavenumber/cm-1

Fig. 5

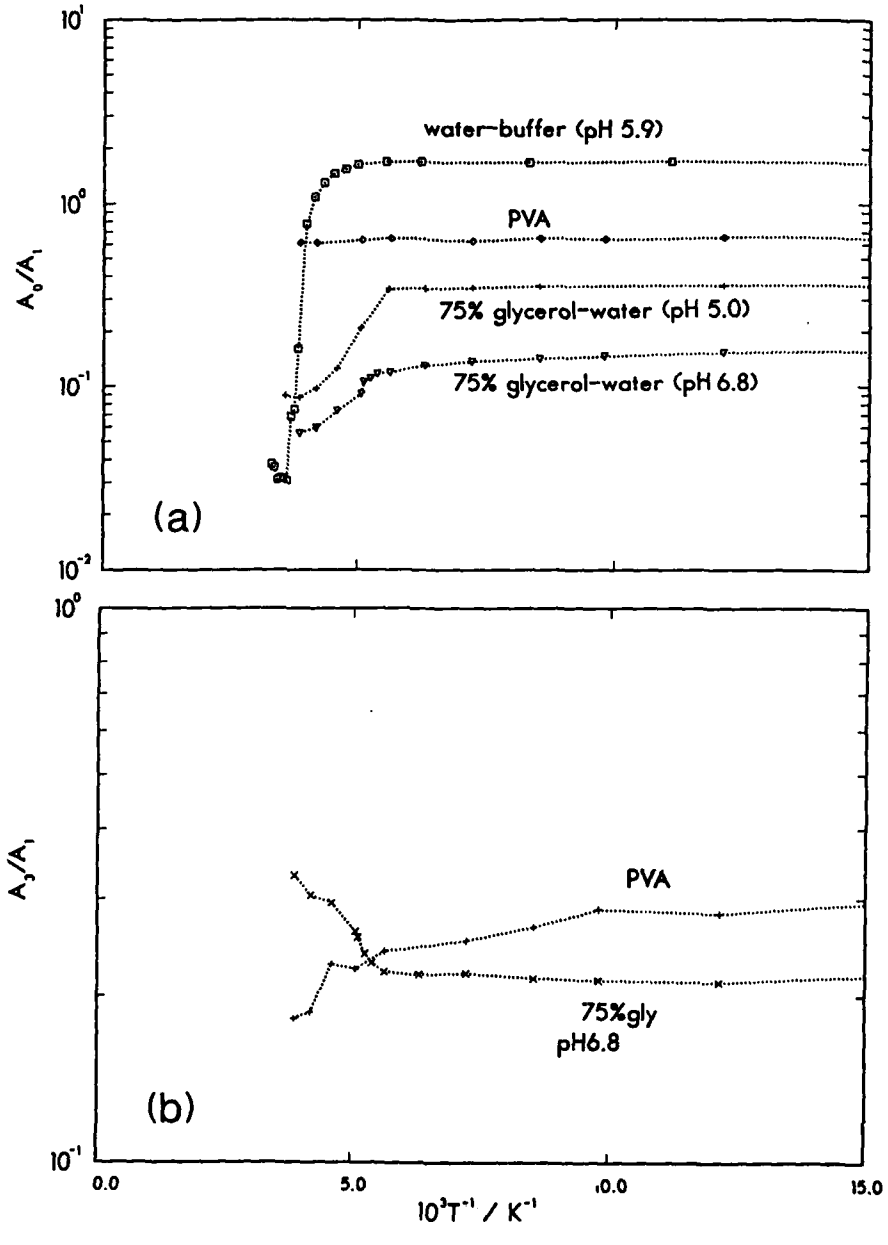
water-buffer (pH 5.9)
PVA
75% glycerol-water (pH 5.0)
75% glycerol-water (pH 6.8)
(a)
A_0/A_1
PVA
75%gly
pH6.8
(b)
A_3/A_1
10^3T^{-1} / K^{-1}

Fig. 6

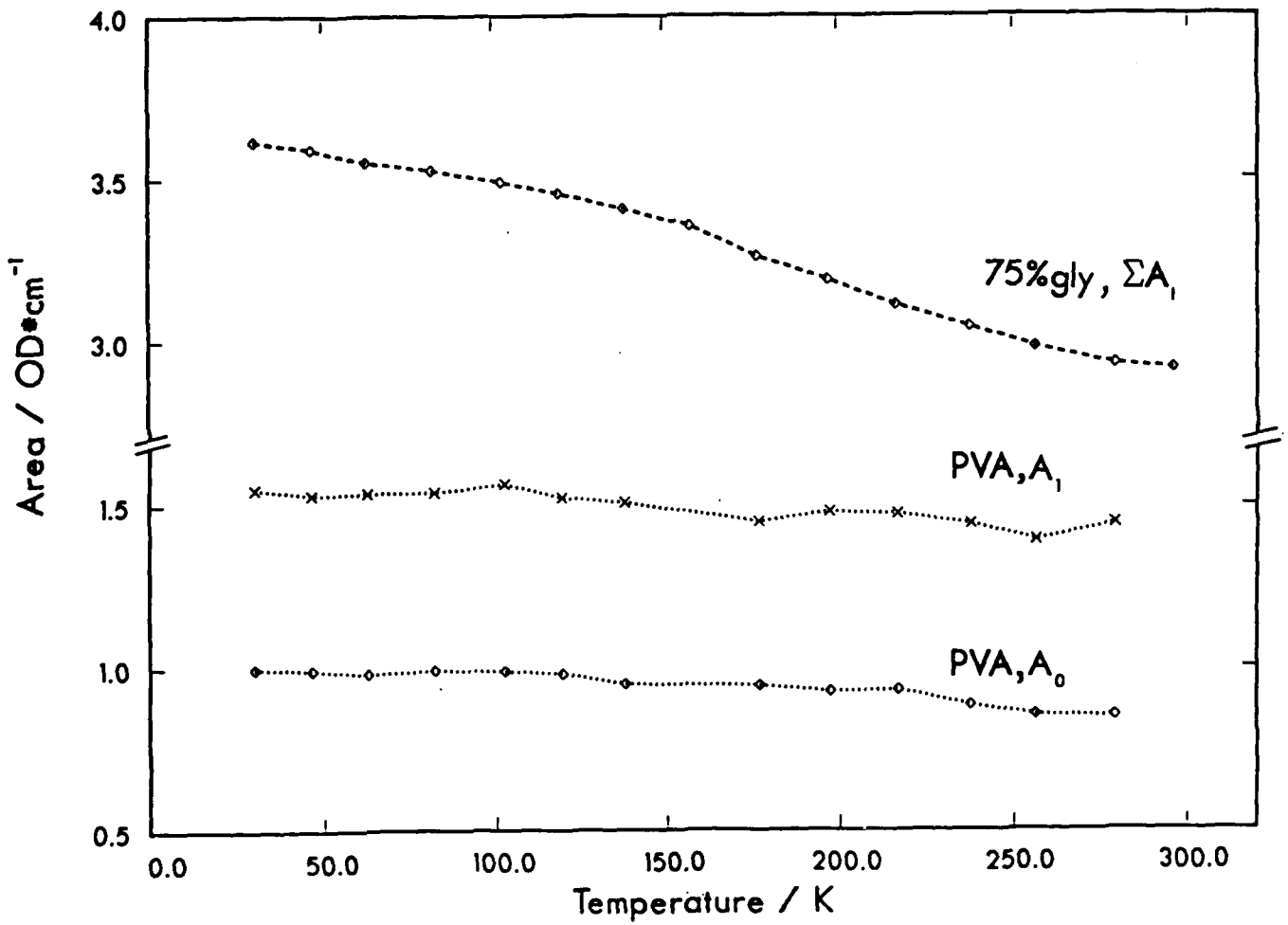
4.0
3.5
3.0
1.5
1.0
0.5
Area / OD•cm⁻¹
75%gly, ΣA1
PVA, A1
PVA, A0
0.0
50.0
100.0
150.0
200.0
250.0
300.0
Temperature / K

Fig. 7

Fig. 8

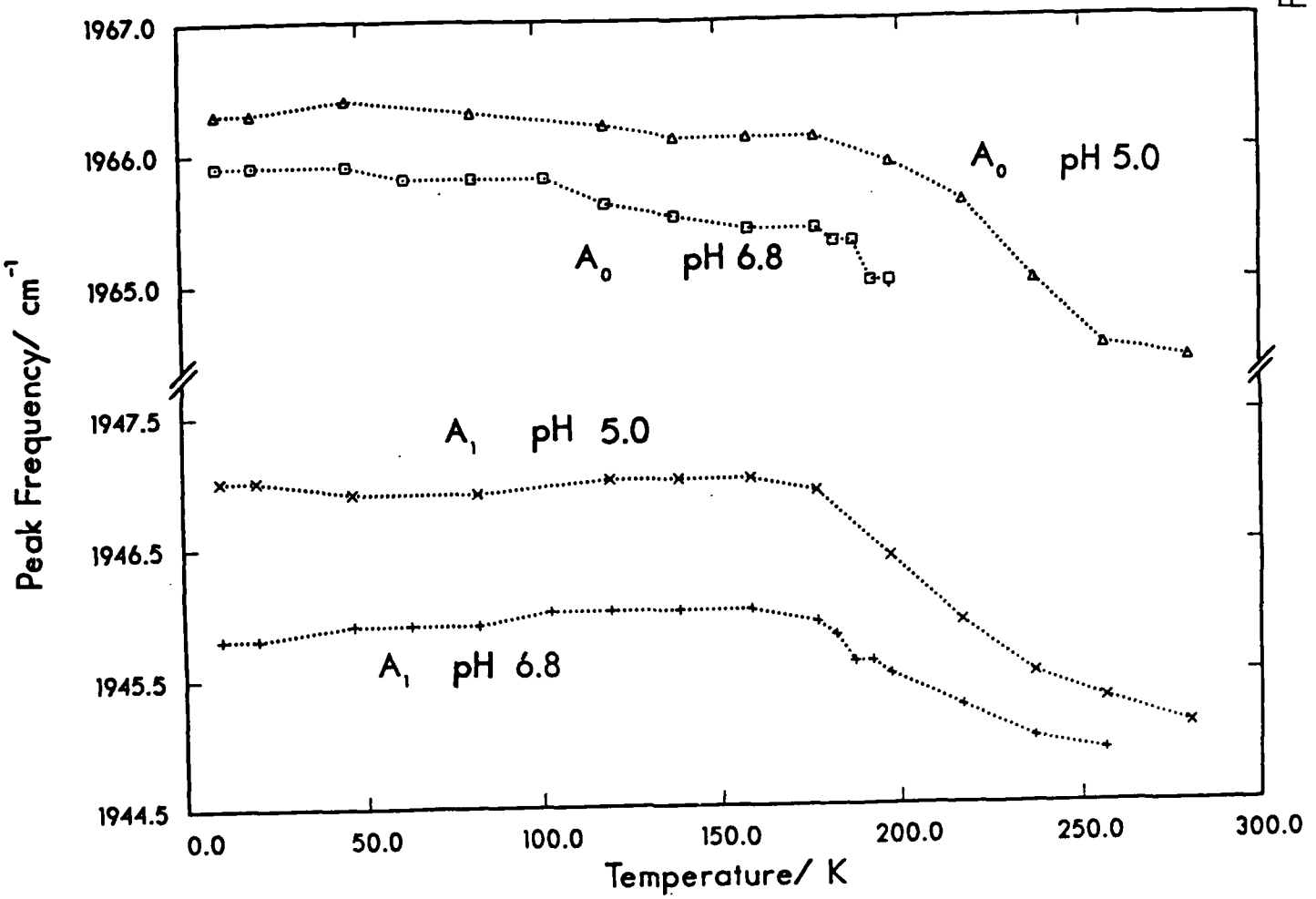
1967.0
1966.0
1965.0
1947.5
1946.5
1945.5
1944.5
Peak Frequency/ cm⁻¹
A₀ pH 5.0
A₀ pH 6.8
A₁ pH 5.0
A₁ pH 6.8
0.0
50.0
100.0
150.0
200.0
250.0
300.0
Temperature/ K

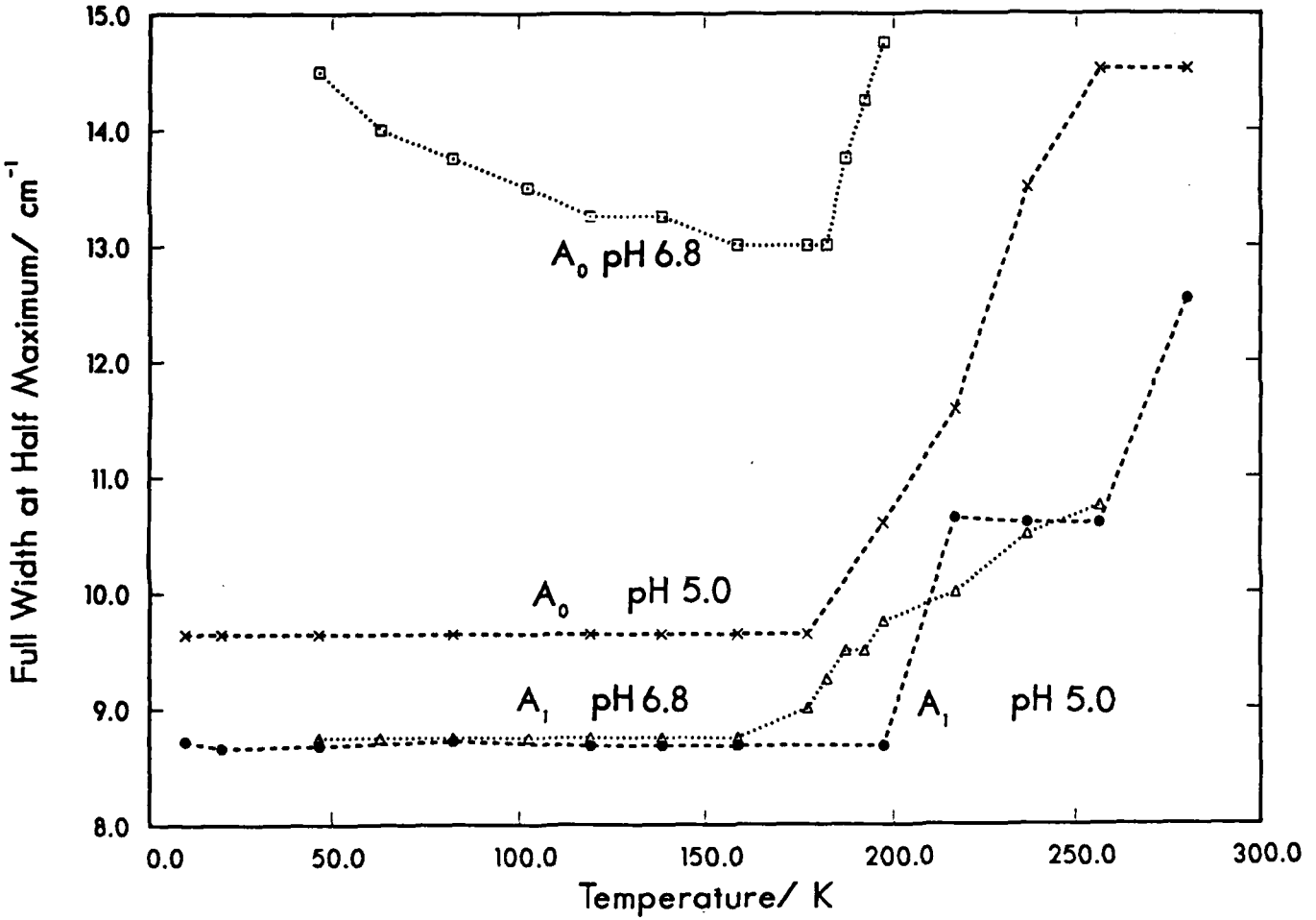
15.0
14.0
13.0
12.0
11.0
10.0
9.0
8.0
0.0
50.0
100.0
150.0
200.0
250.0
300.0
Full Width at Half Maximum/ cm⁻¹
Temperature/ K
A0 pH 6.8
A0 pH 5.0
A1 pH 6.8
A1 pH 5.0

Fig. 9

Fig. 10

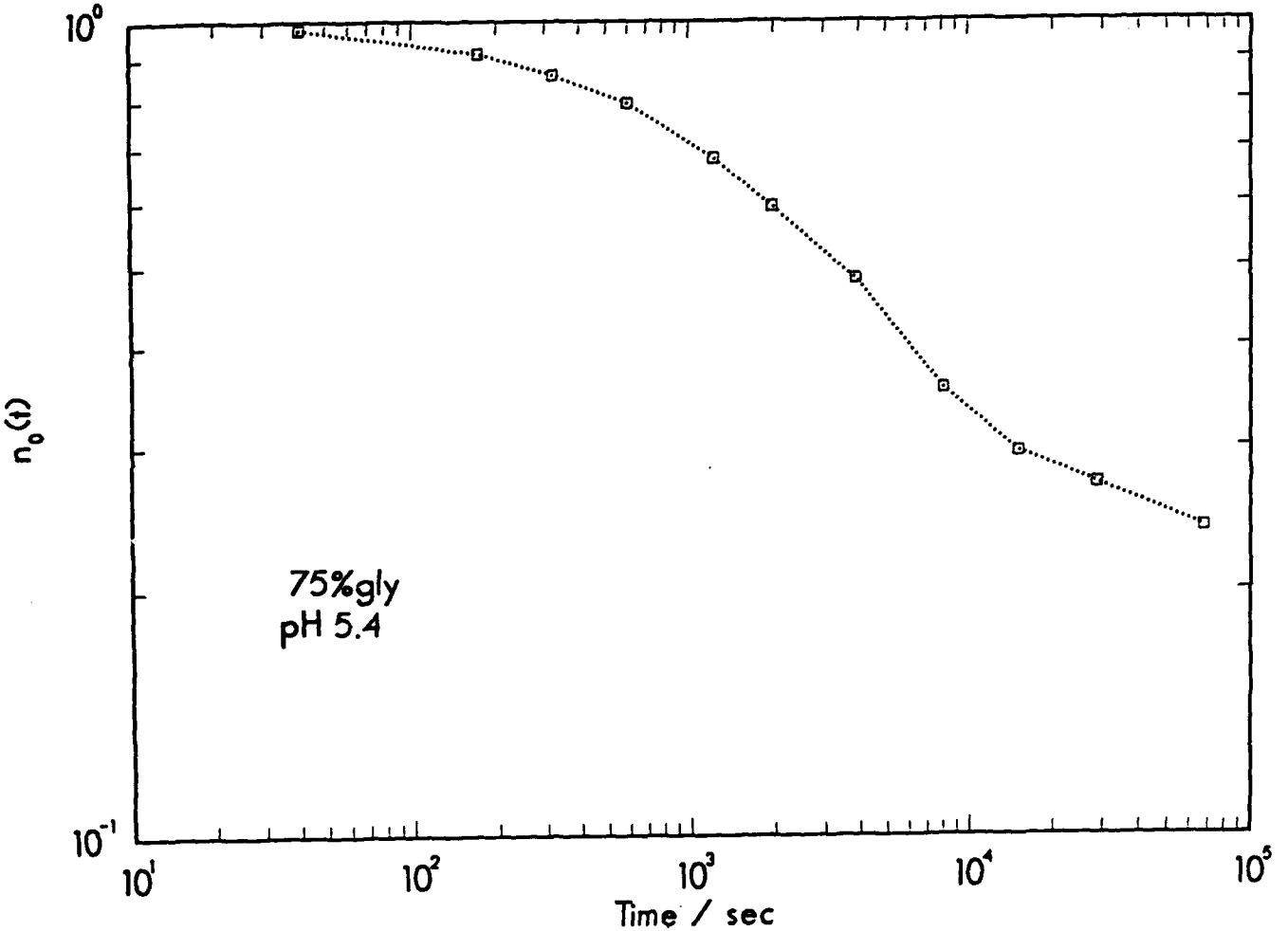

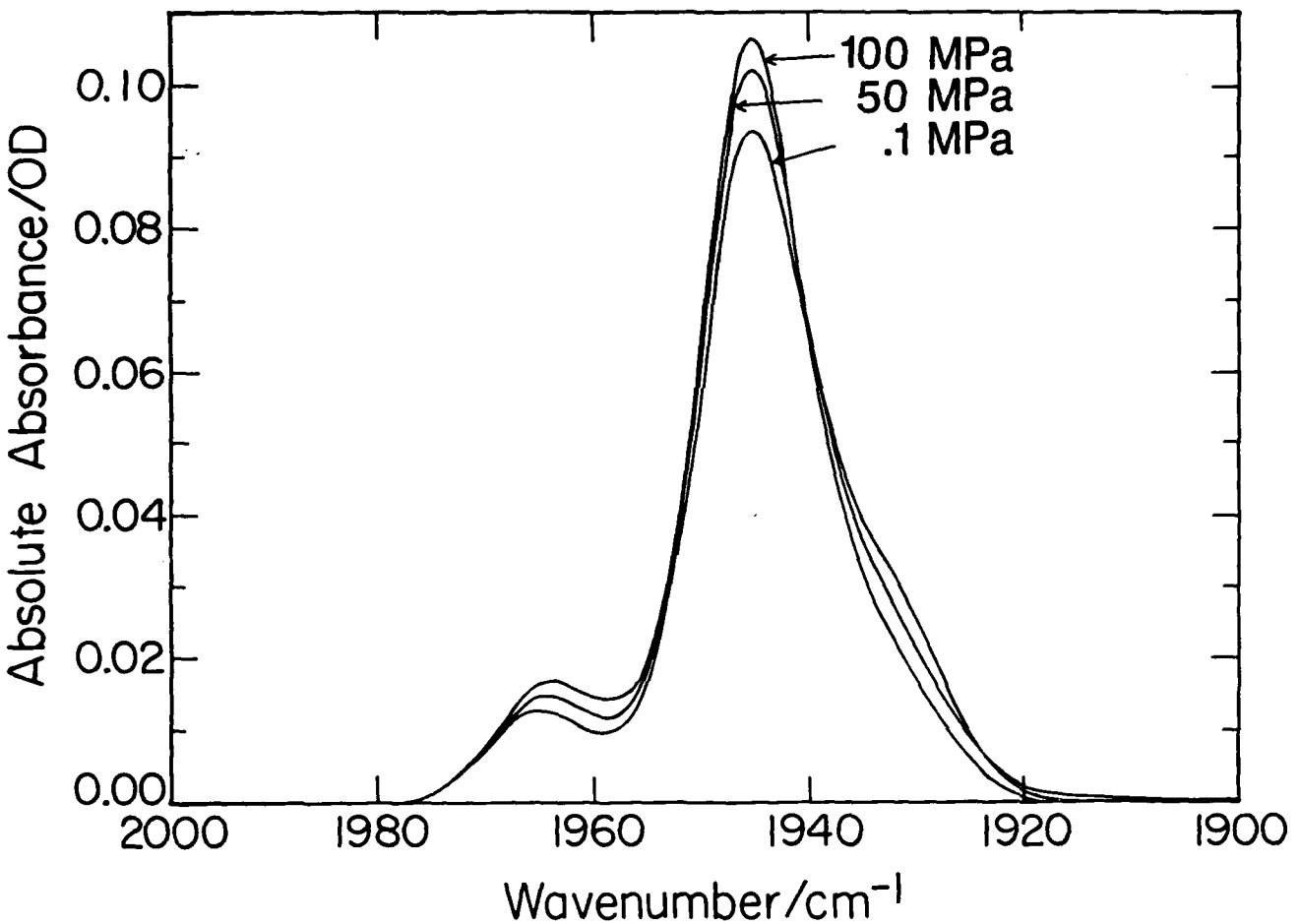
100 MPa
50 MPa
.1 MPa
Absolute Absorbance/OD
0.10
0.08
0.06
0.04
0.02
0.00
2000
1980
1960
1940
1920
1900
Wavenumber/cm⁻¹

Fig. 11

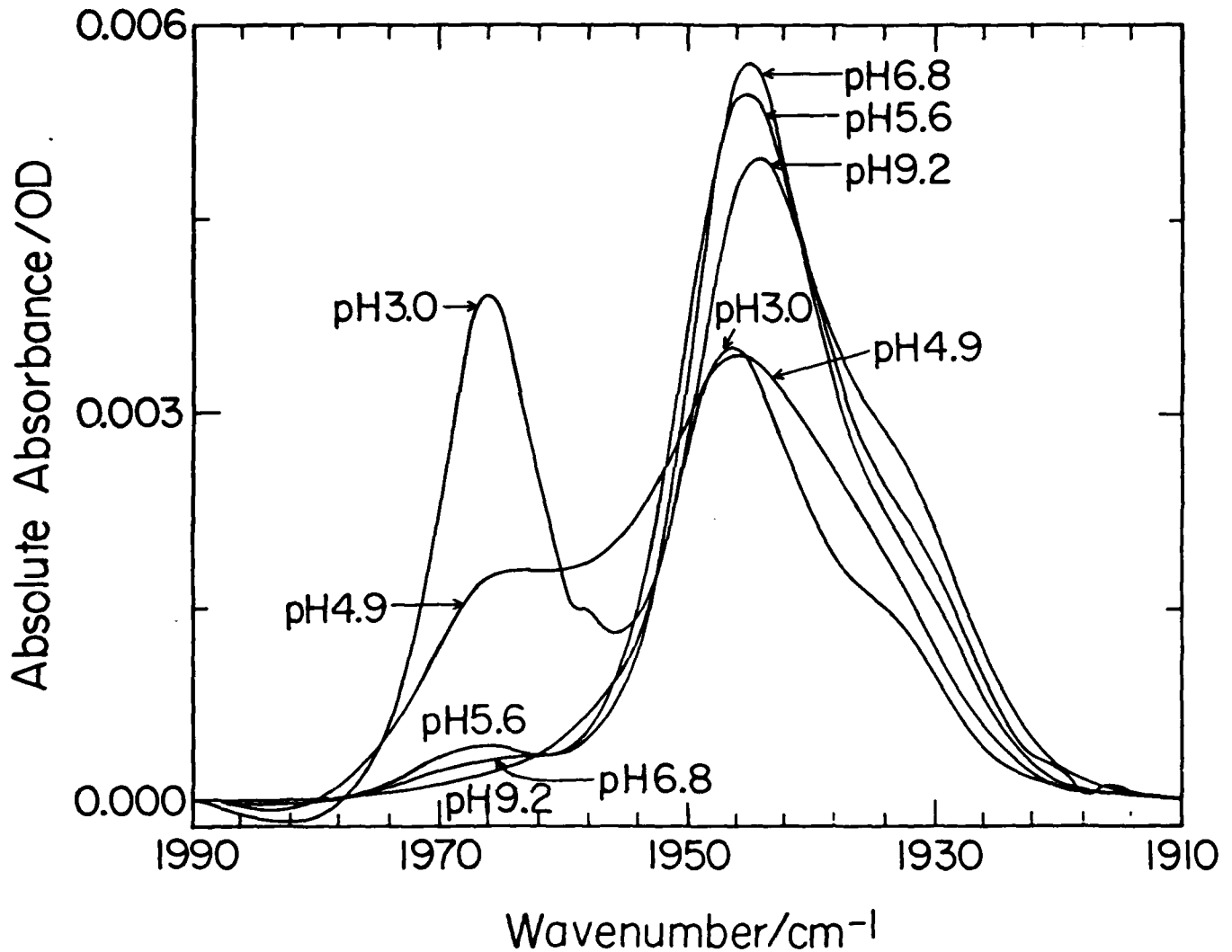
0.006
0.003
0.000
Absolute Absorbance/OD
pH6.8
pH5.6
pH9.2
pH3.0
pH3.0
pH4.9
pH4.9
pH5.6
pH6.8
pH9.2
1990
1970
1950
1930
1910
Wavenumber/cm⁻¹

Fig. 12

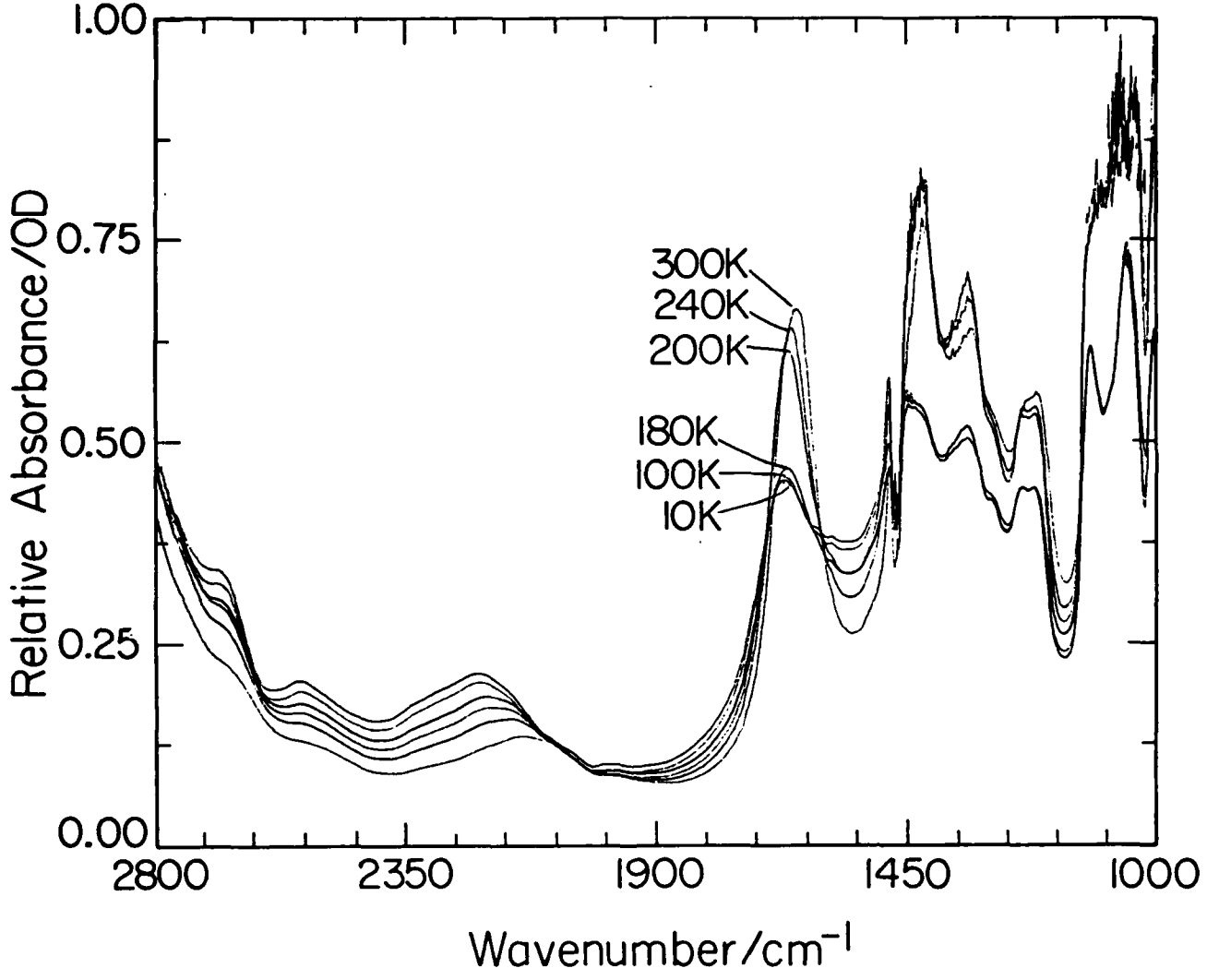
1.00
0.75
0.50
0.25
0.00
Relative Absorbance/OD
300K
240K
200K
180K
100K
10K
2800
2350
1900
1450
1000
Wavenumber/cm⁻¹

Fig. 13

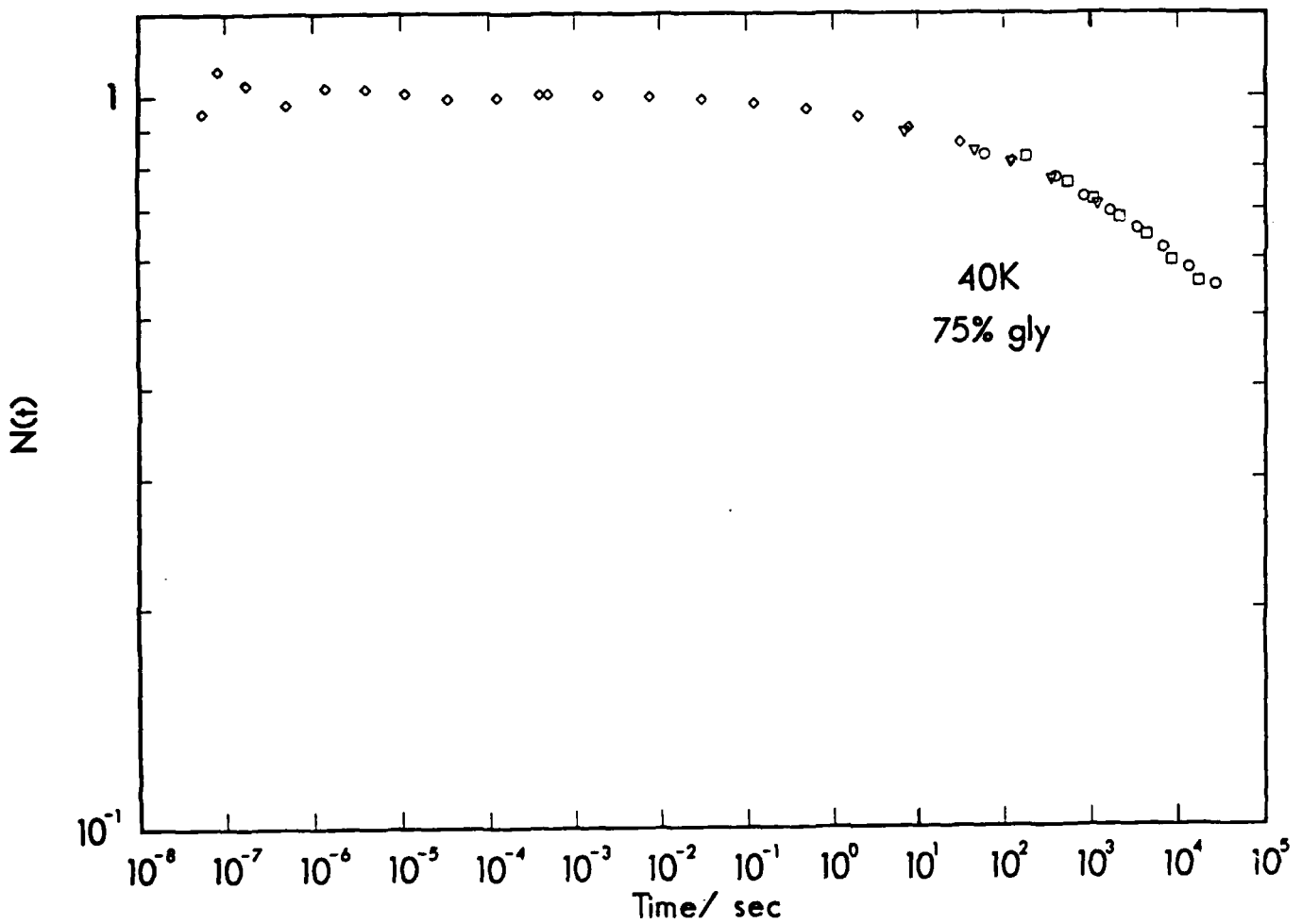
1
10^{-1}
N(t)
40K
75% gly
10^{-8} 10^{-7} 10^{-6} 10^{-5} 10^{-4} 10^{-3} 10^{-2} 10^{-1} 10^{0} 10^{1} 10^{2} 10^{3} 10^{4} 10^{5}
Time/ sec

Fig. 14

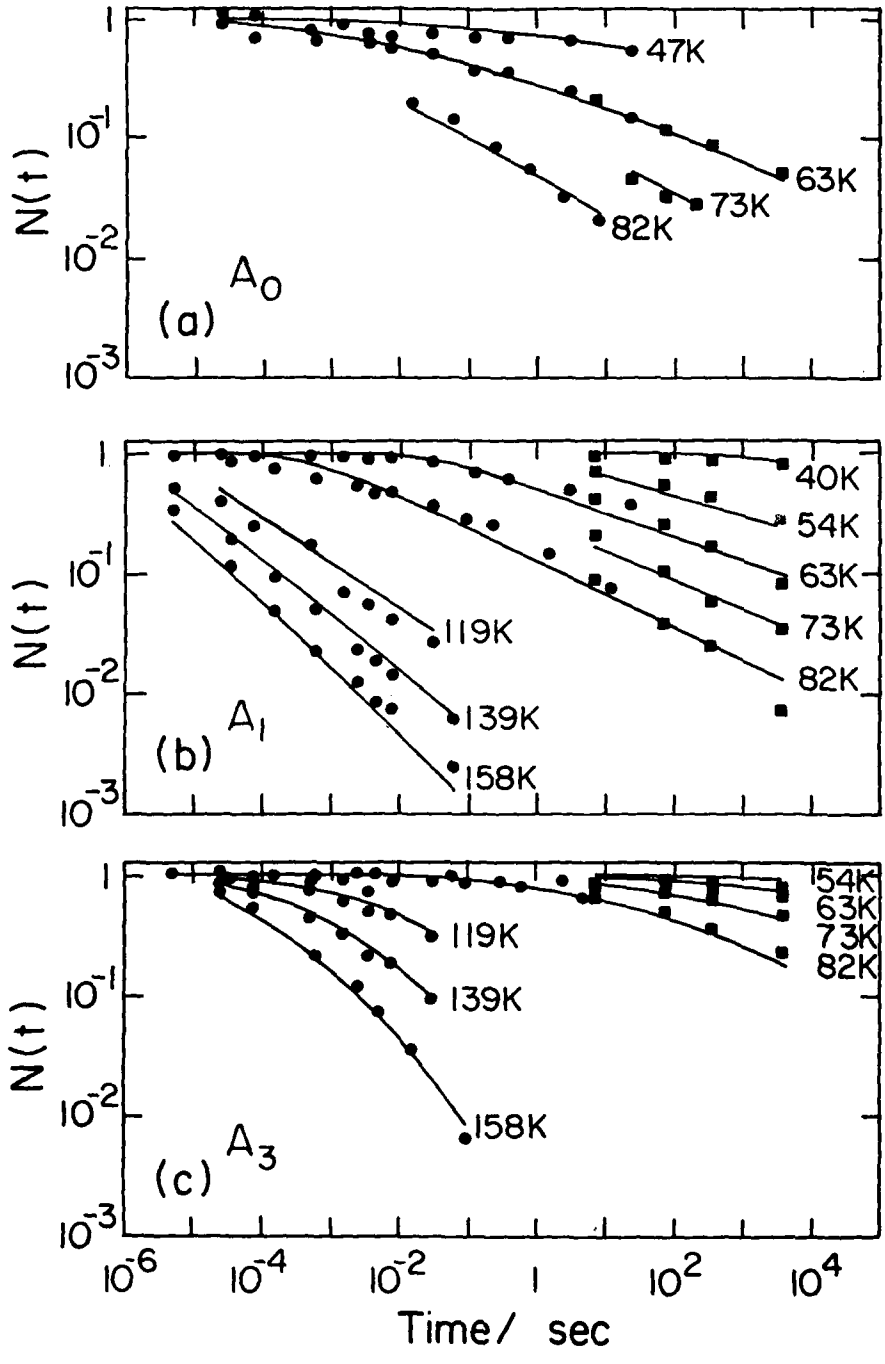
N(t)
1
10^{-1}
10^{-2}
10^{-3}
47K
63K
73K
82K
A_0
(a)
40K
54K
63K
73K
82K
119K
139K
158K
A_1
(b)
154K
63K
73K
82K
119K
139K
158K
A_3
(c)
10^{-6}
10^{-4}
10^{-2}
1
10^{2}
10^{4}
Time / sec

Fig. 15

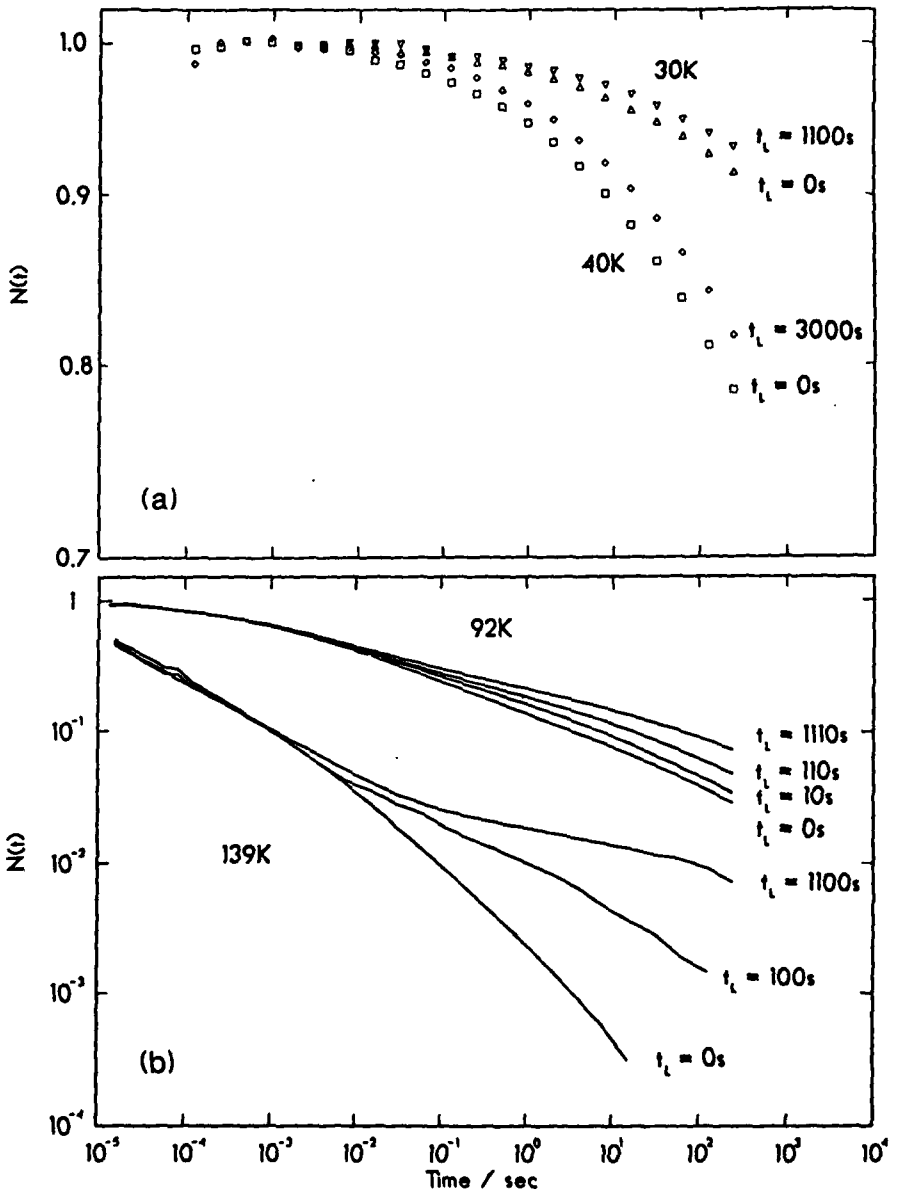
1.0
0.9
0.8
0.7
N(t)
30K
t_L = 1100s
t_L = 0s
40K
t_L = 3000s
t_L = 0s
(a)
1
10^{-1}
10^{-2}
10^{-3}
10^{-4}
92K
t_L = 1110s
t_L = 110s
t_L = 10s
t_L = 0s
139K
t_L = 1100s
t_L = 100s
t_L = 0s
(b)
10^{-5} 10^{-4} 10^{-3} 10^{-2} 10^{-1} 10^{0} 10^{1} 10^{2} 10^{3} 10^{4}
Time / sec

Fig. 16

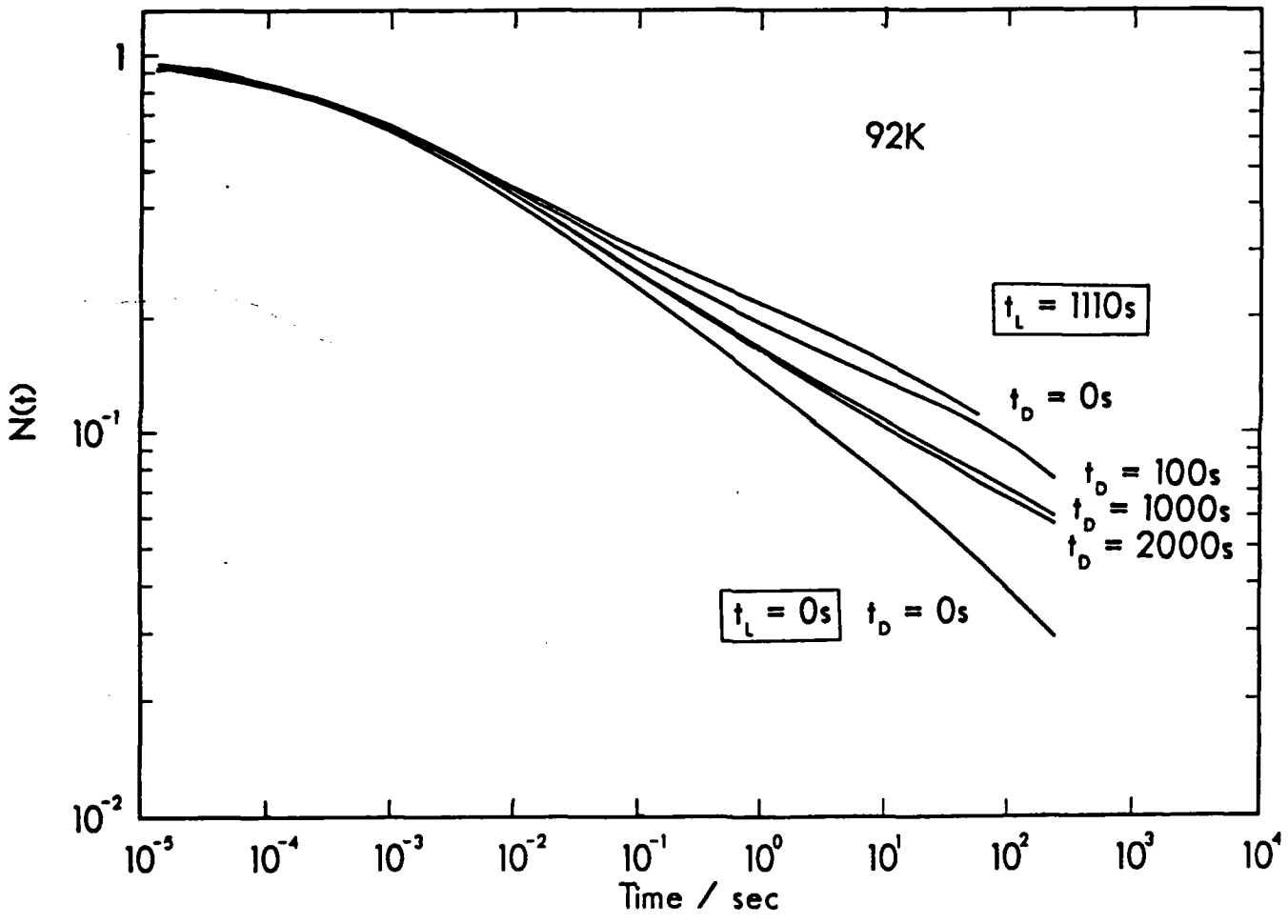
92K
t_L = 1110s
t_D = 0s
t_D = 100s
t_D = 1000s
t_D = 2000s
t_L = 0s
t_D = 0s
N(t)
1
10^{-1}
10^{-2}
10^{-5}
10^{-4}
10^{-3}
10^{-2}
10^{-1}
10^{0}
10^{1}
10^{2}
10^{3}
10^{4}
Time / sec

Fig. 17

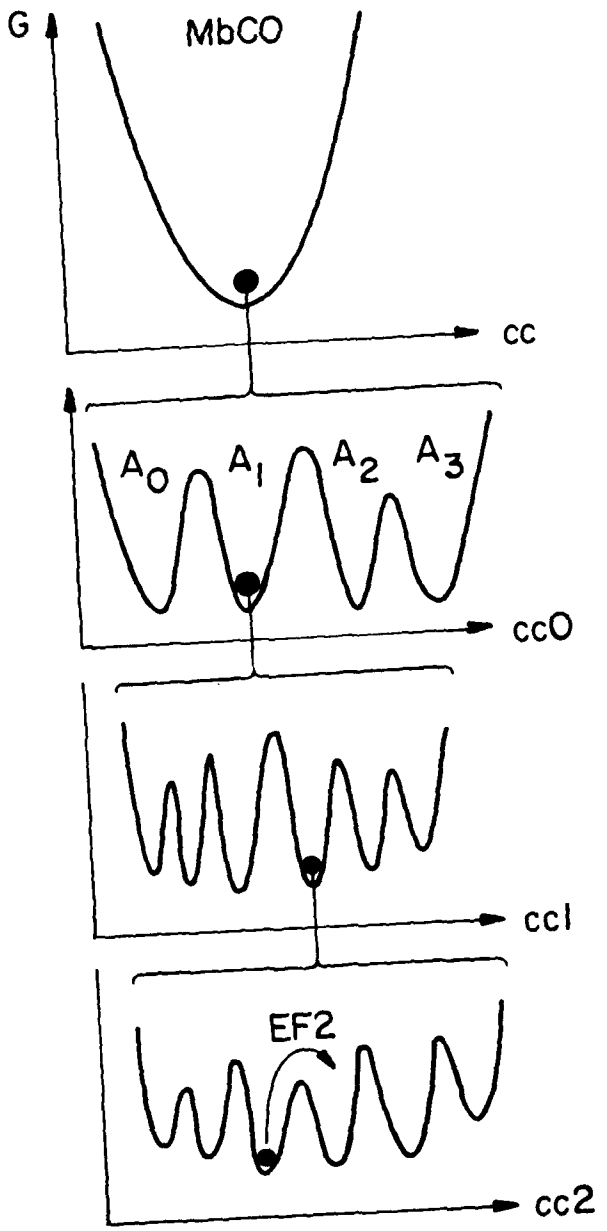

Fig. 18

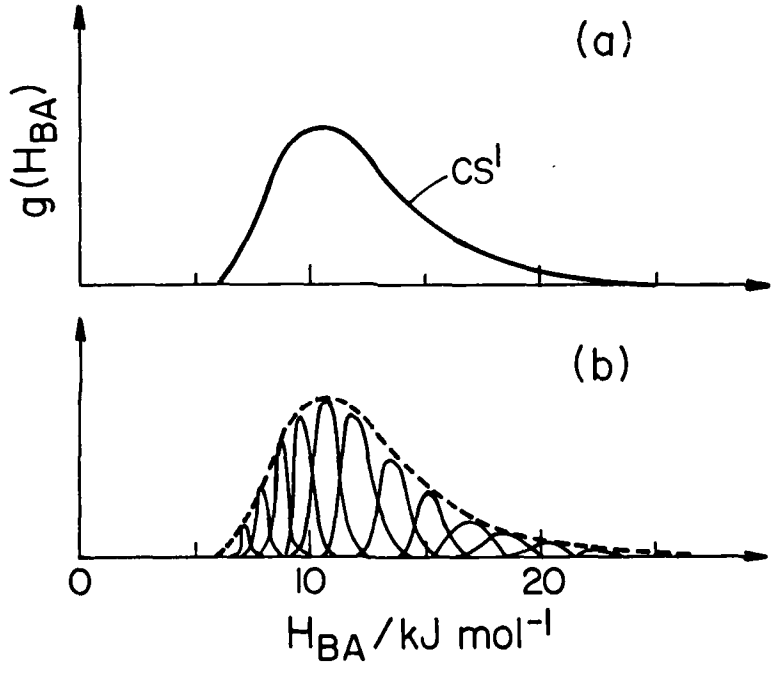

Fig. 19

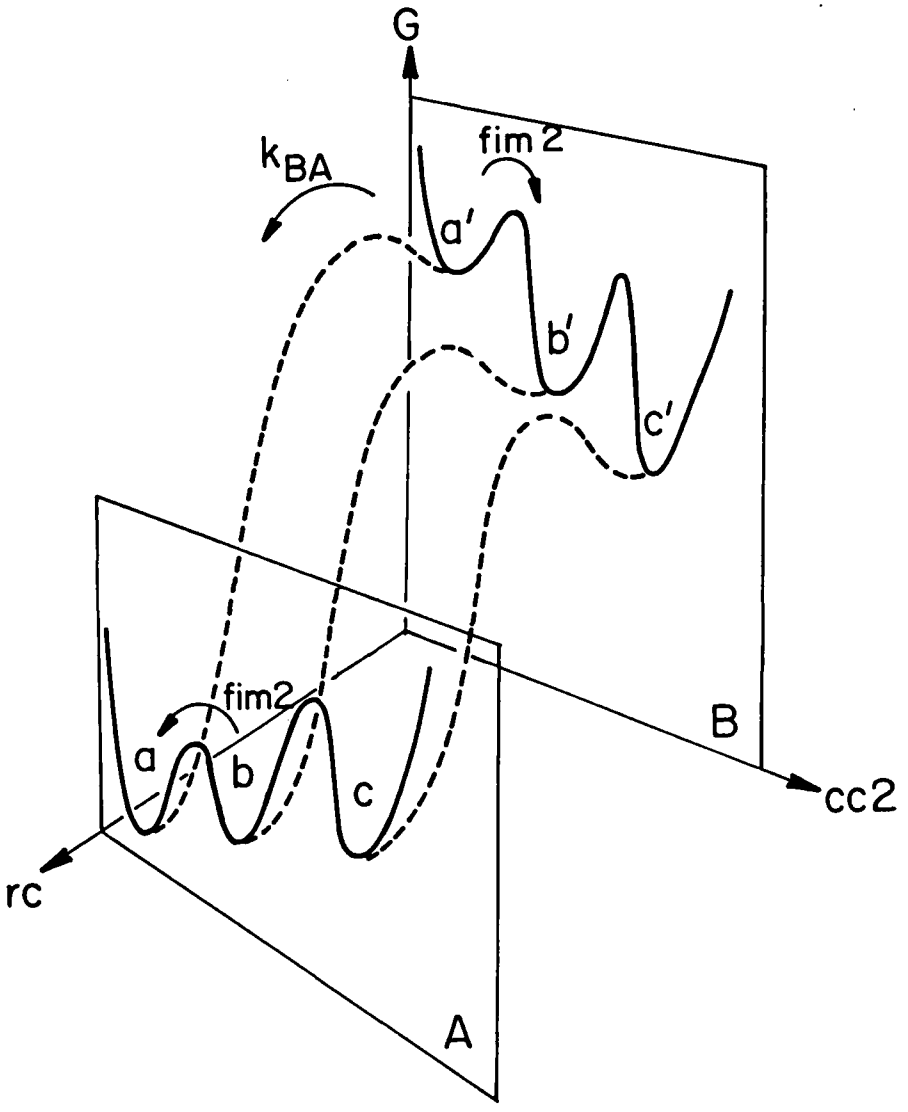

Fig. 20

DISTRIBUTION LIST MOLECULAR BIOLOGY PROGRAM

ANNUAL, FINAL, AND TECHNICAL REPORTS (One copy each except as noted)

Dr. Lewis F. Affronti
George Washington University
Department of Microbiology
2300 I ST NW
Washington, DC 20037

Dr. J. Thomas August
The Johns Hopkins University
School of Medicine
720 Rutland Avenue
Baltimore, MD 21205

Dr. Myron L. Bender
Chemistry Department
Northwestern University
Evanston, IL 60201

Dr. R. P. Blakemore
University of New Hampshire
Department of Microbiology
Durham, New Hampshire 03824

Dr. Ronald Breslow
Columbia University
Department of Chemistry
New York, NY 10027

Dr. James P. Collman
Department of Chemistry
Stanford University
Stanford, California 94305

Dr. Alvin Crumbliss
North Carolina Biotechnology Center
Post Office Box 12235
Research Triangle Park, NC 27709

Dr. Marlene Deluca
University of California, San Diego
Department of Chemistry
La Jolla, CA 92093

Dr. Bruce Erickson
Chemistry Department
University of North Carolina
Chapel Hill, NC 27514

Dr. Richard B. Frankel
Massachusetts Institute of Technology
Francis Bitter National Laboratory
Cambridge, MA 02139

Dr. Hans Frauenfelder
Department of Physics
University of Illinois
Urbana, IL 61801

Dr. Bruce Gaber
Naval Research Laboratory
Code 6190
Washington, DC 20375

Dr. R. W. Giese
Northeastern Univ
Section of Medicinal Chemistry
360 Huntington Ave
Boston, MA 02115

Dr. Barry Honig
Columbia University
Dept of Biochemistry and Molecular Biophysics
630 West 168th St
New York, NY 10032

Brochure 1/4

Dr. Alex Karu
Department of Plant Pathology
College of Natural Resources
University of California
Berkeley, CA 94720

Dr. Robert G. Kemp
University of Health Sciences
Chicago Medical school
Department of Biological Chemistry
3333 Green Bay Road
North Chicago, IL 60064

Dr. Ghobind H. Khorana
Massachusetts Institute of Technology
77 Massachusetts Avenue
Cambridge, MA 02139

Dr. Richard Laursen
Chemistry Department
Boston University
590 Commonwealth Avenue
Boston, MA 02215

Dr. Robert W. Lenz
Chemical Engineering Department
University of Massachusetts
Amherst, MA 01003

Dr. Harden M. McConnell
Stanford University
Department of Chemistry
Stanford, CA 94305

Dr. Kristin Bowman Mertes
University of Kansas
Department of Chemistry
Lawrence, Kansas 66045

Dr. Edgard F. Meyer
Texas A&M University
Department of Biochemistry and Biophysics
Box 3578
College Station, TX 77843

Dr. Jiri Novotny
Laboratory of Cellular and Molecular Research
Massachusetts General Hospital
Boston, MA 02114

Dr. Carl O. Pabo
Johns Hopkins Medical School
Department of Biophysics
Baltimore, MD 21205

Dr. Franklyn Prendergast
Mayo Foundation
200 First St. SW
Rochester, MN 55905

Dr. Naftali Primor
New York Zoological Society
New York Aquarium
Osborne Laboratory of Marine Science
Brooklyn, NY 11224

Dr. K. S. Rajan
Illinois Institute of Technology
Research Institute
10 W. 35th St.
Chicago, IL 60616

Dr. C. Patrick Reynolds
Naval Medical Research Institute
Transplantation Research Program Center
Bethesda, MD 20814

Biochem 4/4

Dr. Alexander Rich
Department of Biology
Massachusetts Institute of Technology
Cambridge, MA 02139

Dr. J. H. Richards
California Institute of Technology
Division of Chemistry and Chemical Engineering
Pasadena, CA 91125

Dr. J. S. Richardson
Duke University School of Medicine
Department of Anatomy
Durham, NC 27910

Dr. Richard Roblin
Genex Corporation
16020 Industrial Drive
Gaithersburg, MD 20877

Dr. Peter G. Schultz
Department of Chemistry
University of California
Berkeley, CA 94720

Dr. Michael E. Selsted
Department of Medicine
UCLA School of Medicine
37-055 CHS
Los Angeles, CA 90024

Dr. Michael Shuler
School of Chemical Engineering
Cornell University
Ithaca, New York 14853

Dr. David S. Sigman
UCLA School of Medicine
Department of Biological Chemistry
Los Angeles, CA 90024

Dr. John M. Stewart
University of Colorado Health Science Center
Department of Biochemistry
Denver, CO 80262

Dr. Dan W. Urry
Laboratory of Molecular Biophysics
University of Alabama
P. O. Box 311
Birmingham, AL 35294

Dr. J. Herbert Waite
College of Marine Studies
University of Deleware
Lewes, DE 19958

Dr. Gerald D. Watt
Battelle-C. F. Kettering Research Laboratory
150 East South College Street
P. O. Box 268
Yellow Springs, Ohio 45387

Dr. Jon I Williams
Allied Corporation
Columbia Rd and Park Ave.
Morristown, NJ 07960

Dr. Eli D. Schmell, Code 1141MB
Office of Naval Research
800 North Quincy Street
Arlington, VA 22217-5000

Dr. Michael T. Marron, Code 1141MB
Office of Naval Research
800 North Quincy Street
Arlington, VA 22217-5000

Biochem 3/4

Dr. Margo G. Haygood
Office of Naval Research
800 North Quincy Street
Arlington, VA 22217-5000

Adminstrator (2 copies, Enclose DTIC Form 50)
Defense Technical Information Center
Building 5, Cameron Station
Alexandria, VA 22314

ANNUAL AND FINAL REPORTS ONLY (One copy each)
Commander
Chemical and Biological Sciences Division
Army Research Office
P. O. Box 12211
Research Triangle Park, NC 27709

Directorate of Life Sciences
Air Force Office of Scientific Research
Bolling Air Force Base
Washington, DC 20332

Chemistry and Atmospheric Sciences Directorate
Air Force Office of Scientific Research
Bolling Air Force Base
Washington, DC 20332

Director
Biotechnology Division
CRDEC
Aberdeen Proving Grounds, MD 21010-5423

Administrative Contracting Officer
ONR Resident Representative
(Address varies - obtain from your business office)

Director, Code 12
Applied Research and Technology Directorate
Office of Naval Research
800 North Quincy Street
Arlington, VA 22217-5000

Director, Code 22
Support Technology Directorate
Office of Naval Technology
800 North Quincy Street
Arlington, VA 22217-5000

Director, Code 112
Environmental Sciences Directorate
Office of Naval Research
800 North Quincy Street
Arlington, VA 22217-5000

Director, Code 113
Chemistry Division
Office of Naval Research
800 North Quincy Street
Arlington, VA 22217-5000

FINAL AND TECHNICAL REPORTS ONLY
Director (6 copies)
Naval Research Laboratory
Attn: Technical Information Division, Code 2627
Washington, DC 20375

Brochen 4/4

END

DATE
FILMED

5-87